Max-Planck-Institut für Biogeochemie

TECHNICAL REPORTS
26

Setup of a CO_2 and CH_4 measurement system
in Central Siberia and modeling of its results

by
Jan Winderlich

MAX-PLANCK-GESELLSCHAFT

Technical Reports - Max-Planck-Institut für Biogeochemie 26, 2012

Setup of a CO_2 and CH_4 measurement system in Central Siberia and modeling of its results

Dissertation

zur Erlangung des

Doktorgrades der Naturwissenschaften

im Fachbereich Geowissenschaften

der Universität Hamburg

vorgelegt von

Jan Winderlich

aus Dresden

Hamburg

2012

Jan Winderlich

Max-Planck-Institut für Biogeochemie

Hans-Knöll-Str. 10

07745 Jena

Deutschland

Betreuung der Doktorarbeit durch:

Prof. Dr. Martin Heimann, *Max-Planck-Institut für Biogeochemie, Jena*

Dr. Christoph Gerbig, *Max-Planck-Institut für Biogeochemie, Jena*

Dr. Victor Brovkin, *Max-Planck-Institut für Meteorologie, Hamburg*

Als Dissertation angenommen vom Fachbereich Geowissenschaften der Universität Hamburg auf Grund der Gutachten von:

Prof. Dr. Martin Claußen, *Meteorologisches Institut, Universität Hamburg*

und

Prof. Dr. Martin Heimann, *Max-Planck-Institut für Biogeochemie, Jena*

Hamburg, den 29.11.2011

Prof. Dr. Jürgen Oßenbrügge

Leiter des Fachbereichs Geowissenschaften

Abstract / Kurzfassung

English: To improve the monitoring of the carbon cycle, an automated, low maintenance measurement system has been installed at the Zotino Tall Tower Observatory in Central Siberia (ZOTTO, 60°48' N, 89°21' E) in April 2009. A cavity ring-down spectroscopy (CRDS) analyzer continuously measures carbon dioxide (CO_2), methane (CH_4) and water vapor (H_2O) from six heights up to 301 m a.g.l. The measurement precision (accuracy) of 0.04 ppm (0.09 ppm) for CO_2 and 0.3 ppb (1.5 ppb) for CH_4 is compliant with the WMO recommendations. The data collected so far (until June 2011) reveals an increase of 2.62 ppm/yr and a seasonal cycle amplitude of 28.3 ppm for CO_2 at the 301m level. Buffer volumes in each air line allow continuous, near-concurrent measurements from all tower levels with only one analyzer. The gradients between the tower levels have been analyzed in combination with meteorological measurements to estimate diurnal cycles of local CO_2 and CH_4 fluxes for individual summer months, which compare well with previous studies. Finally, the CO_2 and CH_4 observations have been incorporated into an atmospheric transport inversion model to estimate fluxes for the boreal zone of Central Siberia of 0.04 ± 0.11 PgC through CO_2 and 8.4 ± 1.1 TgC through CH_4 in the year 2009.

Deutsch: Um die Überwachung des Kohlenstoffkreislaufes zu verbessern, wurde im April 2009 ein automatisiertes, wartungsarmes Messsystem am „Tall Tower Observatory" (ZOTTO, 60°48' n.B., 89°21' ö.L.) in Zentralsibirien installiert. Ein auf Cavity-Ring-Down-Spektroskopie (CRDS) basierendes Messgerät misst kontinuier-lich Kohlenstoffdioxid (CO_2), Methan (CH_4) und Wasserdampf (H_2O) von sechs Turmhöhen bis zu 301 m. Die Messgenauigkeit (Exaktheit) von 0,04 ppm (0,09 ppm) für CO_2 und 0,3 ppb (1,5 ppb) für CH_4 fügt sich den WMO-Vorgaben. Die bislang gesammelten Daten (bis Juni 2011) zeigen einen jährlichen Anstieg von 2,62 ppm und eine Amplitude im Jahresgang von 28,3 ppm für CO_2 auf 301 m Höhe. Puffervolumen in jeder Ansaugleitung ermöglichen kontinuierliche, nahezu gleichzeitige Messungen von allen Turmhöhen mit nur einem Messgerät. Die Gradienten zwischen den Turmhöhen wurden gemeinsam mit meteorologischen Messungen ausgewertet, um den Tagesgang von lokalen CO_2- und CH_4-Flüssen für einzelne Sommermonate abzuschätzen, welche im Einklang mit früheren Studien sind. Schließlich wurden die CO_2- und CH_4-Beobachtungen in ein inverses atmosphärisches Transportmodell eingebunden um Flüsse für die boreale Zone Zentralsibiriens von 0,04 ± 0,11 PgC durch CO_2 und 8,4 ± 1,1 TgC durch CH_4 im Jahr 2009 zu errechnen.

Acknowledgements

Contents

List of figures

List of figures

List of figures

5

List of tables

Abbreviations and formula symbols

a.g.l.	above ground level	*NEE*	Net ecosystem exchange
a.s.l.	above sea level	NIES	National Institute for Environmental Studies, Japan
BIOME-BGC	Biome-BioGeochemical Cycles (an ecosystem process model)	NOAA	National Oceanic and Atmospheric Administration, USA
CO_2	Carbon dioxide	*NPP*	Net primary productivity
CH_4	Methane	PgC	Petagrams of Carbon (= 10^{15}g)
ECMWF	European Centre for Medium-Range Weather Forecasts	ppb	(molar) parts per billion
EDGAR	Emission Database for Global Atmospheric Research	ppm	(molar) parts per million
		sccm	standard cubic centimeter per minute
GEP	Gross ecosystem productivity		
GFED	Global Fire Emissions Database	slm	standard liter per minute
H_2O	Water vapor	STILT	Stochastic Time-Inverted Lagrangian Transport model
ICOS	Integrated Carbon Observation System	TgC	Teragrams of Carbon (= 10^{12}g)
KRAT	Krasnoyarsk time zone (winter time)	UTC	Coordinated Universal Time
LOC	Local solar time	WMO	World Meteorological Organization
LSCE	Laboratoire des Sciences du Climat et l'Environnement, Gif-sur-Yvette, France	WRF-VPRM	Weather Research and Forecasting model coupled to the Vegetation Photosynthesis and Respiration Model
MPI-BGC	Max Planck Institute for Biogeochemistry, Jena, Germany	ZOTTO	ZOtino Tall Tower Observatory

7

$\mathbf{A}$	transport matrix	f	flow rate [m³/s] / flux [mol/(m²s)]
a_0	offset of harmonic fit [ppm]	$\mathbf{F}$	flux matrix (in space and time)
a_1	linear trend of harmonic fit [ppm/yr]	f_{coarse}	flux estimate on coarse, global grid
a,b	parameter of water correction function	F_{Eddy}	eddy covariance flux [mol/(m²s)]
		f_{fine}	flux estimate on fine, regional grid
b	vector of inversion model, see equation (24)	f_{fix}	fixed a-priori flux component
b_i	fitting parameter of harmonic fit	F_{hAdv}	horizontal advection flux [mol/(m²s)]
$c(t)$	concentration	f_{shape}	weighting function of flux in space and time
$\bar{c}$	low-frequency component (30 min average) of concentration time series (Raynolds averaging)	F_{Stor}	storage flux [mol/(m²s)]
		F_{vAdv}	vertical advection flux [mol/(m²s)]
c'	high-frequency component (deviation from 30 min average) of concentration time series (Raynolds averaging)	$g(t)$	response function of measurement system
		$g_i^{time}(t)\,g_i^{space}$	temporal and spatial decomposition functions of the flux field
$\langle c \rangle$	average concentration in control volume, see equation (17)	H	heat flux [W/m²]
c_0	starting concentration	H_2O	water vapor mixing ratio [%]
c_1	arbitrary concentration	H_2O_{CRDS}	water vapor mixing ratio; raw signal from analyzer [%]
c_{coarse}	global model concentration output	J	cost function
c_{fine}	regional model concentration output	K_C	eddy diffusivity for trace constituent [m²/s]
CH_{4wet}	mixing ratio of wet CH_4 [ppb]		
CH_{4dry}	mixing ratio of dry CH_4 [ppb]	K_T	eddy diffusivity for heat [m²/s]
c_i	fitting parameter of harmonic fit	m	concentration mismatch between observation and model
c_{ini}	initial concentration		
c_{meas}	measured concentration	$\mathbf{M}$	matrix of inversion model, see equation (24)
c_{mod}	concentration given by model calculation	M_{Air}	molar weight of air (28.9644 g/mol)
CO_{2wet}	mixing ratio of wet CO_2 [ppm]	p	parameter vector (in space and time) of the flux field
CO_{2dry}	mixing ratio of dry CO_2 [ppm]	$\text{Prob}(...)$	probability
c_{obs}	observed concentration	q_0	offset
C_P	molar heat capacity (isobar) of air	q_1	amplitude
c_r	concentration at height z_r	q_2	phase shift
D	diffusion coefficient	$\mathbf{Q}_f$	covariance matrix of flux field

Abbreviations and formula symbols

$\mathbf{Q_m}$ — covariance matrix of concentration

$s(t)$ — high-frequency in-situ concentration (not buffered)

S — source strength [ppm/s]

t, t' — time [s]

T — temperature [°C]

T_{pot} — potential temperature [K]

$\bar{u}$ — wind component in x direction (see also $\bar{c}$)

u+, v+ — horizontal wind components measured in coordinates of anemometer [m/s]

$\bar{v}$ — wind component in y direction (see also $\bar{c}$)

V — volume [m³]

V_m — molare volume of air (22.4 l/mol at standard conditions)

$\bar{v}_{u+v}$ · — horizontal wind speed

$\bar{w}$ — true vertical wind component (see $\bar{c}$)

w' — high-frequency vertical wind component (see c')

$\bar{w}_{meas}$ — measured vertical wind component (see $\bar{c}$)

$\bar{w}_r$ — vertical wind component at height z_r

X_{wet} — wet mixing ratio: either CO_2 [ppm] or CH_4 [ppb]

X_{dry} — dry mixing ratio: either CO_2 [ppm] or CH_4 [ppb]

x — coordinate in horizontal direction (longitudinal) [m]

x_i — any of the three dimensional coordinates

y — coordinate in horizontal direction (latitudinal) [m]

z — coordinate in vertical direction (height, elevation) [m]

z_r — height of control volume, e.g. 301 m

ϑ — sensor tilt

μ — scaling factor in the Jena inversion system

π — Archimedes' constant pi = 3.1415…

ρ_{Air} — density of air (1293 g/m³ at standard conditions)

σ — standard deviation

τ — time constant of the ZOTTO measurement system

τ_0 — time constant of flask measurement

φ — wind direction [deg]

$\varphi+$ — wind direction in coordinate system of anemometer [deg]

Abbreviations and formula symbols

A Introduction

"Realists do not fear the results of their study."
Fyodor Dostoevsky (1821-1881)

The global climate has been changing throughout the last century [IPCC: Solomon et al., 2007]. One of the main drivers of this process is attributed to changes in atmospheric concentrations of greenhouse gases that are related to each other through the earth's multiple biogeochemical cycles. The three greenhouse gases water vapor (H_2O), carbon dioxide (CO_2), and methane (CH_4) have the most significant influence on the global climate balance [Kiehl et al., 1997]. Whereas human activities have only a small direct influence on the amount of atmospheric water vapor, CO_2 and CH_4 are altered strongly by humans and are the most important anthropogenic drivers of current climate change. Since preindustrial times until 2005, the global mean mixing ratio of CO_2 was raised from 280 µmol/mol (molar parts per million, ppm) to 379 ppm and CH_4 increased from about 700 nmol/mol (molar parts per billion, ppb) up to 1774 ppb. These gases are important components of the earth's carbon cycle, which is tightly coupled to the global climate change [IPCC: Solomon et al., 2007].

For a better understanding of the earth's global carbon cycle, long-term monitoring of sources and sinks of CO_2 and CH_4 is necessary. Such observations allow studying inter-seasonal variations of the earth's carbon cycle, which helps to constrain existing carbon coupled climate models and, therefore, to reduce the spread in future climate projections [Huntingford et al., 2009]. Therefore, model accuracy would benefit from more CO_2 and CH_4 observations.

The presented work is focused on the expansion of the existing monitoring network with a new high-precision CO_2 and CH_4 measurement system at a tall tower observatory. The site is located in the boreal forest area of Central Siberia, which is of particular interest for the carbon cycle, but where few measurements are available. The 304 m tall tower was built in an area largely covered by natural forests and is located far away from large anthropogenic carbon sources. To equip this remote site with a reliable measurement system, calibration efforts had to be minimized, and a new unique system with minimal maintenance requirements (e.g. without drying of air) was developed. The instrumentation of the ZOtino Tall Tower Observatory (ZOTTO) is described in detail in Chapter B.

High precision measurements of CO_2 and CH_4 mixing ratios from six tower levels were recorded and analyzed. The analysis of the trends, the mean annual cycles and specific events are presented in Chapter C.

The multiple observation levels on the tower allow for the observation of CO_2 and CH_4 vertical gradients and their diurnal cycles; at night, when the atmosphere is stable, emitted gases nearby the station remain close to the ground, and during day they are distributed upwards by turbulent mixing. The systematic investigation of the developing concentration gradients is presented in Chapter D. The analysis shows that the combination of the mixing ratio measurements and the meteorological data from all six tower levels allows estimating the diurnal cycle of local fluxes, which is of great importance for calculating local carbon budgets.

On regional to global scales, carbon budgets can be calculated with the help of atmospheric transport models, because the development of observed mixing ratios over time is driven by the strength of the sources and sinks that the air parcels passed by on their travel to the measurement site. This integrating character of the atmosphere can be used for estimating the surface carbon fluxes, by using the transport model inversely in time to trace back the origin of the air. The setup of such an atmospheric transport inversion system is described in the Chapter E. It combines a-priori knowledge about meteorological and flux fields with the CO_2 and CH_4 mixing ratio measurements from several Siberian stations. The new measurement time series from ZOTTO provides important constraints on the carbon flux estimates in Central Siberia.

Parts of the description of the ZOTTO measurement system (Chapter B and C) have been published in "Atmospheric Measurement Techniques" [Winderlich et al., 2010]. The results of the local carbon flux estimates for Central Siberia (Chapter D) have been submitted to "Environmental Research Letters" [Winderlich et al., 2011]. In the present work, the results were updated by using the most recent available data.

B CO$_2$/CH$_4$/H$_2$O measurement at Zotino Tall Tower Observatory (ZOTTO)

"The cleverest of all, in my opinion, is the man who calls himself a fool at least once a month."
Fyodor Dostoevsky (1821-1881)

B1 Introduction

Sites for measuring atmospheric background signals of CO$_2$ and CH$_4$ are mainly situated on remote coastal or mountain stations to suppress local disturbances for inverse model estimates of carbon sources and sinks. Terrestrial sites are difficult to incorporate into global models [Rödenbeck et al., 2003], in particular because of the heterogeneous sources and sinks and the complex meteorological conditions close to the surface [Gerbig et al., 2003a; Gerbig et al., 2009]. However, recent development in forward and inverse high resolution models show promising results of using these sites in atmospheric inversions [Peylin et al., 2005; Sarrat et al., 2007; Lauvaux et al., 2008; Trusilova et al., 2010].

Measurements from tall towers (> 200 m) provide access, at least during daytime, to the relatively well mixed planetary boundary layer [Stull, 1988] that is better represented in current global models and represents regions on larger scale than measurements closer to the ground [Gloor et al., 2001]. During nighttime, in addition to sampling the stable boundary layer profile, tall towers often allow sampling of the residual layer air, whose gas concentrations correspond to those of the previous day.

Greenhouse gas measurements at tall towers have been pioneered in the 1990s in the United States [Bakwin et al., 1998] and in Hungary [Haszpra et al., 2001], and the network has been extended during the last decade over Europe (CHIOTTO project [Vermeulen, 2007]). The Max Planck Institute for Biogeochemistry (MPI-BGC) has equipped tall towers with CO$_2$, CH$_4$, CO, N$_2$O, and O$_2$/N$_2$ (and partly SF$_6$) measurements in Bialystok in Poland [Popa et al., 2010], near Zotino in Russia [Kozlova et al., 2008], and on top of the Ochsenkopf mountain in Germany [Thompson et al., 2009].

In this chapter a new measurement system for CO$_2$ and CH$_4$ atmospheric concentrations at a tall tower site in Central Siberia is presented. Particular attention is given to the innovations of this system.

B1.1 Site description

The Zotino Tall Tower Observatory (ZOTTO) is located in Central Siberia at 60° 48' N, 89° 21' E, approximately 20 km west of the village Zotino at the Yenisei River (114 m a.s.l.). The ecosystem in the light taiga around the station comprises Pinus sylvestris forest stands (about 20 m height) on lichen covered sandy soils [Schulze et al., 2002]. The closest large city Krasnoyarsk (950,000 inhabitants) is situated about 600 km south of the station. Transport of equipment to this remote location, requiring two days, is only possible in winter, implying an inherent need to reduce maintenance efforts and the amount of consumables.

Siberian ecosystems are of major importance for future climate developments. They especially are projected to face increases in winter temperature and precipitation that feed back to the ecosystem [Bedritsky et al., 2008]. Nevertheless, they are poorly covered with atmospheric measurement stations (e.g. the Global Atmosphere Watch network, GAW). This lack will be reduced by long-term observations at the ZOTTO station. Additional stations are built up that mainly focus on South West Siberia, such as the so-called 9-tower network [Arshinov et al., 2009a]. Moreover, aircraft measurements have been performed in Central Siberia [Lloyd et al., 2002a; Styles et al., 2002; Arshinov et al., 2009b; Paris et al., 2010a].

In the past, the ecosystems especially around ZOTTO were monitored for several years by aircraft [Lloyd et al., 2001; Lloyd et al., 2002a; Styles et al., 2002] and eddy covariance measurement systems [Valentini et al., 2000; Röser et al., 2002; Shibistova et al., 2002]. The construction of a new 304 m tall tower finished in September 2006 [Schulze et al., 2011]. Aerosol and carbon monoxide measurements are done at 301 m and 52 m tower heights [Heintzenberg et al., 2008; Mayer et al., 2009; Heintzenberg et al., 2011; Vasileva et al., 2011]; ozone and NOx are analyzed from 30 m level [Vivchar et al., 2009]. Until June 2007, a complex gas measurement system for CO_2, O_2, CH_4, CO, and N_2O based on gas chromatography, paramagnetic sensors, and near-infrared spectroscopy was operated and provided trace gas information for five tower levels [Kozlova et al., 2009]. The new equipment of the site replaces this complex system with a new low maintenance high precision CO_2/CH_4 measurement system that started operating in April 2009. In the subsequent sections the detailed overall setup is described, how the data is validated, and the first data series are presented.

B2   Experimental setup

B2.1   Air flow diagram

Figure 1 *Flow diagram of the ZOTTO CO_2/CH_4 measurement system (further details in Table 1)*

The setup that allows selecting the air stream from one of the six tower levels (301 m, 227 m, 158 m, 92 m, 52 m, and 4 m a.g.l.) and transferring it to the gas analyzer is described in Figure 1. A detailed list of components is given in Table 1. The main part of the setup is placed in an air conditioned laboratory container inside a bunker at the base of the tower.

B CO_2/CH_4/H_2O measurement at Zotino Tall Tower Observatory (ZOTTO)

Table 1 *List of components in the ZOTTO setup*

Element	Company	Type	Symbol Figure 1
inlets	Solberg Filter, Continental Industrie GmbH, Germany	F-15-100	I1-6
filters 40 μm	Swagelok, BEST Fluidsysteme GmbH, Germany	SS-12TF-MM-LE and SS-8F-K4-40	F1-6
filters 2 μm	Swagelok, BEST Fluidsysteme GmbH, Germany	SS-4FW-2	F7-13
flushing pumps	Gardner Denver Thomas GmbH, Germany	617CD32	CF1-6
purge pump	KNF Neuberger GmbH, Germany	N86KNE	CP1
3-way solenoid valves	Gems Sensors GmbH, Germany	G3415-LC-24VDC-VAC	V1-8
12 position multiport valve	Valco Instruments Company Inc. from Machery-Nagel GmbH & Co. KG, Germany	EMTMA-CE	VA1
needle valves	Hy-Lok D Vertriebs GmbH, Germany	NV3H-12M-R	NV1-6
needle valves	Swagelok, BEST Fluidsysteme GmbH, Germany	SS-4MG SS-SS4	NV7-8 NV9-11
needle valves	Swagelok, BEST Fluidsysteme GmbH, Germany	SS-2MG	NV12-18
flow meters 0-20 l/min	Sensortechnics GmbH, Germany	FTAL020NU	FM1-6
flow meter 0-500 ml/min	MKS Instruments Deutschland GmbH, Germany	179B52CS3BM	FM7
flow meter 0-1000 sccm	Sensortechnics GmbH, Germany	FBAL001DU	FM8-14
pressure sensor 0-1 bara	Sensortechnics GmbH, Germany	CTE8001AK0	P1-7
pressure sensor 0-210 bar	Synotech Sensor und Meßtechnik GmbH, Germany	GCT-2251210BGC42C06	P8-11
pressure regulator	Tescom Europe GmbH & CO. KG, Germany	64-3441KA412-S	RE1-4
laboratory temperature and converter	Electrotherm GmbH, Germany LKM electronic GmbH, Germany	K6S-E-4LS-200C-G1/4A-120 and LKM-214	not shown

On the tower, the mushroom-shaped inlets (I1-I6) are equipped with polyester filters of 5 μm pore size. The relatively large surface of the ring-shaped vent minimizes the possibilities of blocking the line, e.g. due to freezing in winter. All inlets are connected to 12 mm tubing (EATON Synflex 1300, Sertoflex), through which air is drawn to the measurement bunker at a high flow rate of 15 l/min by piston pumps (CF1-CF6) to limit the residence time of air in the lines. A short contact to the surface of the airlines minimizes wall effects [Winderlich, 2007], such as the adsorption of CO_2 [Langenfelds et al., 2005] and the interaction of CO_2 with water with its induced time lags [Höfer, 2009].

In the measurement bunker the inlet lines are electronically isolated from the outside through Nylon fittings to avoid damages on the system by lightning strokes. A tee junction splits up the gas flow; a small amount of 150 sccm (standard cubic centimeters per minute) of air is extracted by the gas analyzer's internal pump from one tower level at a time. The air from all the lines not being analyzed is continuously purged at a flow rate of 150 sccm through a common line by a single purge pump (CP1) and controlled by a combination of needle valves (NV12-NV17) and flow meters (FM8-FM13) in order to assure similar conditioning of all lines.

B CO_2/CH_4/H_2O measurement at Zotino Tall Tower Observatory (ZOTTO)

The type of the needle valves (NV7-NV11) differs for different lines, according to its flow characteristics. On the 301 m level line, no needle valve is used to minimize the pressure drop; however, to avoid pressure fluctuations in the analyzer due to the motion of the pump piston, an additional air buffer volume is located upstream the flushing pump (CF1). The needle valves in all other lines are chosen to match the pressure conditions in the 301 m line (~ 680 to 700 mbar).

Downstream, custom-made 8 l stainless steel spheres act as air buffer volumes on each sample line. They allow a continuous, near-concurrent measurement of six heights with only one single analyzer. While one line is analyzed, the others are continuously flushed with the same flow. Laboratory experiments have demonstrated the ideal mixing characteristic of the buffers. Consequently they integrate the air signal from every inlet with an e-folding time of approximately 37 min (8 l / 150 sccm at 700 mbar, see also section B2.5), bridging the time span between two consecutive measurements for each line. In other words, each line buffers the atmospheric signal while it is not attached to the analyzer; and it releases a smoothed, 37 min representing signal while it is analyzed.

To allow selective measurements of individual tower levels, 3-way solenoid valves V1-V6 are installed further downstream that switch the airflow between the purge pump and the analyzer. Those valves are characterized by easy to seal NPT threads, a big orifice for minimal pressure drop, and small leak rates (< 1 µl/s guaranteed). If the power supply of the valves and sensors fails, the measurement from 301 m is done on default.

To select between measuring ambient air and calibration gases, the ambient air from the tall tower passes another two simultaneously switched 3-way solenoid valves V7-V8. For monitoring the analyzer's incoming air flow, a high quality, metal sealed, and well calibrated flow meter FM7 is installed. All flow meters in the setup are free of moving parts, thus requiring almost no maintenance and are, with the exception of flow meter FM7, not in contact with the analyzed air. The only active flow control of the whole system is performed by the analyzer itself.

In contrast to all tall tower instrumentation known to the author, the pump of the analyzer is located downstream of the measurement cell. This avoids an additional pump with its risk for leaks in the sampling line. The temperature corrected pressure record after an extensive 25 hour leak test showed leak rates below 0.4 µl/s in all lines. Taking a maximal observed CO_2 gradient of 1000 ppm in the laboratory container at 1 bar versus 300 ppm sample air at 0.7 bar, at the above leak rate the influence on the CO_2 concentration would be less than 0.02 ppm per line.

As there is no air drying system, adsorption on additional large surfaces and potential leaks are excluded. The remaining maintenance efforts include regular annual pump maintenance, adjustments of needle valves to keep the pressure in all

lines constant within a 650-700 mbar range, and biannual filter cleanings (primarily F1-F6).

B2.2 The CO_2/CH_4/H_2O analyzer

The CO_2, CH_4, and H_2O measurement is performed by an EnviroSense 3000i analyzer (Picarro Inc., USA, CFADS-17) based on the cavity ring-down spectroscopy technique (CRDS) [Crosson, 2008]. The decay time of laser light inside a cavity, which is equipped with highly reflective mirrors, is measured for several wavelengths around 1.651 µm for CO_2 and H_2O (data output after ~ 4 s) and 1.603 µm for CH_4 (data output after ~ 1 s). The volume mixing ratios of the main isotopologues $^{12}C^{16}O_2$, $^{12}C^1H_4$, and $^1H_2^{16}O$ are obtained by mathematical analysis of the spectral line shape. An outlet proportional valve controls the pressure and the temperature of the cavity to constant conditions of 187 mbar (140.0 ± 0.04 Torr) and 40.000 ± 0.004 °C. The mass flow of sample air through the cavity is linearly correlated with the inlet pressure (~ 150 sccm at 700 mbar).

Laboratory analyzer tests with humidified tank air (at 1.2 % H_2O level) show a typical standard deviation of the raw data (0.2 Hz) below 0.06 ppm for CO_2, 0.5 ppb for CH_4, and 0.001 % (10 ppm) for H_2O. To assess the long-term stability of the analyzer, 200 h continuous measurement of air from a high-pressure tank was analyzed by the Allan variance technique [Allan, 1987], using "Alamath AlaVar 5.2" software. The continuous decrease of the Allan variance suggests that the chosen calibration interval of 100 hours is sufficient.

Raw data from repeated measurements of calibration gas tanks reveal a long-term drift of the analyzer of less than 0.25 ppm and 3.2 ppb per year for CO_2 and CH_4, respectively (similar to Crosson [2008]).

The CRDS analyzer response is linear to the gas concentration. The standard deviations of the residuals from the measurement data to the linear fit are 0.05 ppm and 0.05 ppb for a concentration range of 354 – 453 ppm CO_2, and 1804 – 2296 ppb CH_4.

The characteristic of the CRDS technology does not easily allow calibrations with air of non-natural composition. Experiments with synthetic air revealed residuals in the CO_2 calibration up to 1 ppm related to pressure broadening effects due to varying N_2, O_2 and Ar content in the calibration gases and the isotopic composition of CO_2 [Tohjima et al., 2009; Chen et al., 2010]. To avoid problems, all calibration tanks were filled with air of ambient isotopic composition. Even though the CRDS analyzer still detects only the main isotopologues such as $^{12}C^{16}O_2$, there is no further isotope correction needed to also consider the other components such as $^{13}C^{16}O_2$, $^{12}C^{16}O^{18}O$ in the final value: the error that appears during the calibration emerges with the opposite sign during the measurement and thus cancels out. Measurement inaccuracies due to variations in the isotopic composition of ambient air ($\delta^{13}C_{VPDB}$ =

7.5-9.0 ‰, $\delta^{18}O_{VPDB}$ = 0.5-2.5 ‰) are too low to influence the measurement (< 0.01 ppm at 400 ppm level) [Allison et al., 2007; Chen et al., 2010].

The H_2O measurement was calibrated using a dew point mirror (Dewmet, Michell instruments Ltd., UK) in the 0.7 to 3.0 % H_2O range for another CRDS analyzer of the same type (model G1301-m, CFADS-30). Thus the actual values H_2O are calculated from the reported values H_2O_{CRDS} by the following formula (units in %):

$$H_2O = 0.0292 + 0.7719 \cdot H_2O_{CRDS} + 0.0197 \cdot H_2O_{CRDS}^2 \qquad \textbf{(1)}$$

The nonlinear component is due to the self pressure-broadening effect of water vapor. Note that H_2O measurements from all CRDS analyzers have been calibrated to the same scale after production, so this formula also applies to the ZOTTO instrument.

B2.3 Calibration system

To guarantee the required stability of the measurement, an automated calibration sequence is initialized every 100 hours. The notional life time of the 200 bar high pressure tanks exceeds 60 years, but every 10 years a successive recalibration of the tanks is advisable to exclude drifts in the mixing ratios and to adapt to the concentration range of the changing ambient air conditions. "Cucumber" intercomparison experiments between different stations and laboratories are intended to ensure the link to the scale of the World Meteorological Organization (WMO) during this time (cucumbers.uea.ac.uk). WMO recommends an inter-laboratory comparability of 0.1 ppm for CO_2, 2 ppb for CH_4 [*GAW Report No.186*, 2007]).

The long usage time challenges the long-term stability of the calibration gases. Therefore high pressure aluminum tanks are preferred to steel ones [Kitzis et al., 1999]. However, the calibration gas composition can be changed through diffusive and surface processes [Langenfelds et al., 2005]. High pressure tank regulators corrupt the gas concentration due to the long lasting storage, too [Da Costa et al., 1999]. Life times of at least 12 years can be guaranteed by careful gas handling like calibrations only after filling the tanks, usage exclusively above 30 bar and pre-use regulator flushing procedures [Kitzis et al., 1999; Daube Jr. et al., 2002; Keeling et al., 2007].

To further reduce effects from the pressure regulators, polychlorotrifluoroethylene (PCTFE) is preferentially used as sealant to reduce gas permeation [Sturm et al., 2004]. Laboratory experiments confirm the advantages of a PCTFE-equipped pressure regulator to suppress CO_2 corruption in the withdrawn air after storage [Winderlich, 2007]. Additionally, the stability of the CO_2 concentration in tanks was observed to be better when they are stored in horizontal position [Keeling et al., 2007].

Hence, the ZOTTO calibration system consists of four horizontally stored aluminum tanks (50 l, Luxfer, C/O Matar, Italy) equipped with Ceodeux PCTFE cylinder valves (D 200 series, D20030163, Rotarex Deutschland GmbH, Germany), PCTFE sealed pressure regulators (RE1-RE4 in Figure 1), and metal sealed high pressure transmitters (P8-P11).

As the analyzer has a linear response to the gas mixing ratio (section B2.2), the three tanks of the setup are sufficient for the calibration. The fourth tank is used as target gas for quality control and further experiments. The CO_2 and CH_4 concentrations in the gas tanks that are currently used at ZOTTO (Table 2) were determined in the GASLAB of the MPI-BGC Jena and are traceable to scales of the WMO maintained in the Earth System Research Laboratory of the National Oceanic and Atmospheric Administration (NOAA/ESRL; WMO-X2007 scale for CO_2 [Zhao et al., 2006], NOAA-2004 scale for CH_4 [Dlugokencky et al., 2005]).

Table 2 *CO_2 and CH_4 concentrations of calibration and target gases*

Tank name	ID number	CO_2 [ppm]	CH_4 [ppb]
Calibration Tank 1	D478665	354.71 ± 0.08	1804.73 ± 1.60
Calibration Tank 2	D436606	394.60 ± 0.06	1899.26 ± 1.49
Calibration Tank 3	D436607	453.12 ± 0.08	2296.69 ± 2.05
Target Tank	D478666	404.40 ± 0.08	1947.43 ± 1.37

B2.4 Water correction

Water influences the measurement of CO_2 and CH_4 by dilution and pressure-broadening. At constant pressure in the optical cavity, dilution decreases the trace gas concentration linearly with increasing water vapor pressure, whereas pressure broadening is a nonlinear effect [Chen et al., 2010]. For comparisons between different stations and for the use in atmospheric models, the dry mixing ratio CO_{2dry} is important, since wet mixing ratio CO_{2wet} shows alterations just by changing water concentrations.

The analyzer already includes a first order water correction function:

$$\frac{CO_{2wet}}{CO_{2dry}} = 1 - 0.01244 \cdot H_2O_{CRDS} \cdot \qquad \textbf{(2)}$$

Experiments with a Licor LI-610 Humidifier revealed the necessity for a second order water correction function [Chen et al., 2010]. The associated tests were performed for the CFADS-17 instrument in January 2009. A simpler setup had to be developed for ZOTTO, because the time-consuming laboratory experiments required a large amount of space, extensive flow regulations, and drift corrections due to temperature-dependent CO_2 dissolution in the water reservoir of the humidifier.

To humidify air, it suffices to pass it over a water droplet in a vessel [Frank Meinhardt and Rainer Schmitt, personal communication, 2008]. The modified setup

for the experiments in September 2009 and June 2010 is based on a stainless steel water trap with a volume of 19 cm³ and an inner surface area of less than 140 cm^2 to reduce surface effects (Figure 2a, adapted from Popa [2007]). The air from a high pressure tank flows through a dip-tube that almost touches a water droplet (< 1 ml) on the bottom of the trap. The humidified air leaves the trap through an outlet at its top towards the analyzer with the same pressure as it left the pressure regulator at the high pressure tank. Because temperature changes of the trap to achieve different dew points resulted in unstable conditions, the trap was held at constant temperature within a bath of iced water, whereas the pressure of the flushing gas was changed: with decreasing absolute pressure, the relative amount of water vapor increases, even though the partial water vapor pressure stays the same at constant temperature. For this freely controllable water vapor time series, the analyzer's readings give CO_2 and CH_4 wet mixing ratios X_{wet} for a H_2O_{CRDS} range from 0 % to almost 4 % (Figure 2b).
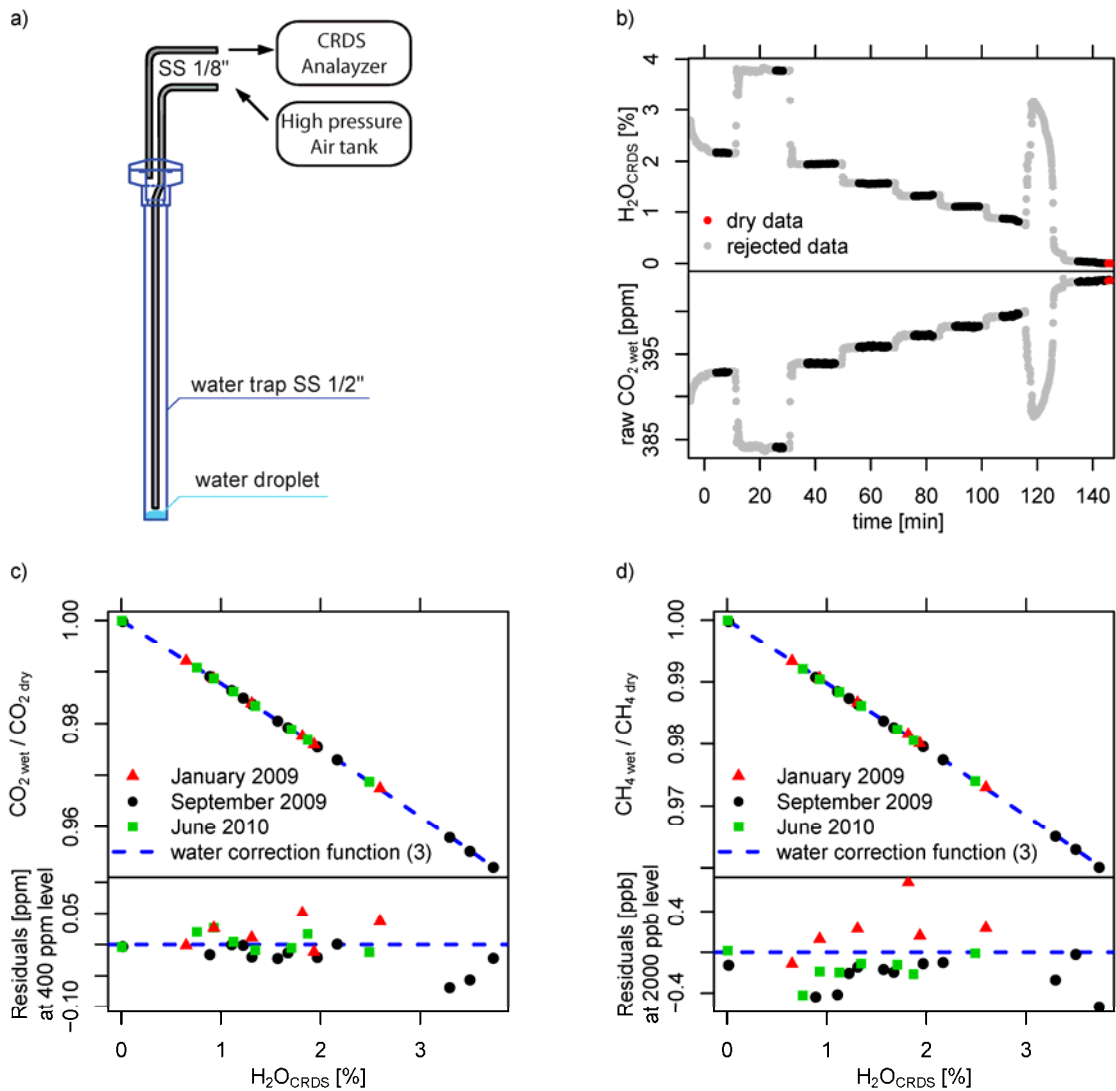
Figure 2 *Experiments at various water vapor levels:* **a)** *setup;* **b)** *H_2O and CO_2 time series of an experiment in Sept. 2009; correction function derived from all experiments for* **c)** *CO_2 and* **d)** *CH_4*

B $CO_2/CH_4/H_2O$ measurement at Zotino Tall Tower Observatory (ZOTTO)

The pressure variations trigger changes in the air adsorption processes at the metal surfaces of the trap. To ensure equilibration, data points 1.5 min before and 3 min after pressure changes are rejected (grey dots in Figure 2b). Additionally, the required pressure stability of the CO_2/CH_4 measurement was confirmed experimentally since changing inlet pressure did not influence the instrumental reading of the mixing ratios above the internal sample cell pressure (187 mbar).

When the water droplet is completely evaporated, the analyzer detects the dry mixing ratio X_{dry} for CO_2 and CH_4 (red dots in Figure 2b), and the water correction function can be directly inferred (Figure 2c, d). The relation between H_2O content and the X_{wet}/X_{dry} ratio for CO_2 and CH_4 are fitted with a second order H_2O correction function:

$$\frac{X_{wet}}{X_{dry}} = 1 - a \cdot H_2O_{CRDS} - b \cdot H_2O_{CRDS}{}^2 . \tag{3}$$

The experiments conducted in January and September 2009 are in good agreement, indicating temporal stability of the water correction function. The average fit parameters for both experiments are $a = (1.205 \pm 0.002) \cdot 10^{-2}$ / % and $b = (2.03 \pm 0.08) \cdot 10^{-4}$ / %^{2} for CO_2 and $a = (1.007 \pm 0.005) \cdot 10^{-2}$ / % and $b = (1.45 \pm 0.18) \cdot 10^{-4}$ / %^{2} for CH_4, while H_2O is given in percent. A repeated experiment in June 2010 confirms these parameter values. All raw data points (Figure 2b) were grouped according to the set H_2O levels; thus only the binned and averaged CO_2 and CH_4 ratios are shown in Figure 2c and d for better visibility.

The upper panels in Figure 2c and d visualize the functional relationship, whereas the lower panel shows the residuals from the quadratic fit. The standard deviation of these residuals of the individual fits indicates a repeatability of the water-corrected measurement within 0.03 ppm and 0.3 ppb for CO_2 and CH_4, respectively.

In summary, the CO_2 accuracy better than 0.1 ppm relies on the water vapor measurement having the precision better than 200 ppm H_2O at a 400 ppm CO_2 level, which is easily achieved with the CRDS technique.

B2.5 Influence of long inlet tubes

Although the analyzing system guarantees high quality data for moist ambient air samples, it has to be ensured that the air sample remains unaltered along the route from the different tower inlets to the analyzer. The most important source of disturbances is assumed to be caused by water vapor. Such concerns prompted the deployment of air drying systems directly at the inlet of some towers [Vermeulen, 2007].

Here the disturbances are evaluated that are caused by water vapor in the inlet system. Due to the 300 mbar pressure drop in the 300 m inlet tube, the dew point is suppressed by 1 to 2 K per 100 m (dew point calculation based on H_2O saturation

pressure from Goff equation [Murphy et al., 2005]). Thus, condensation of water is highly unlikely which permits neglecting liquid water in the first order estimates.

Two CRDS analyzers (CFCDS-3 and CFADS-14) were set up to measure ambient air simultaneously through a 2 m and a 200 m tube (1/2" Dekabon) at LSCE in Gif-sur-Yvette. The 200 m tube was stored outside (winter days, temperature -1 to 5 °C, relative humidity 79 to 98 %). The inlets of both lines were closely attached to each other. The data was recorded in 60 sec averages, corrected for dilution and pressure broadening by water (see section B2.3), and calibrated.

In the experiment, both instruments ran in parallel for three days. Accounting for the time delay, the linearly interpolated 200 m data was time shifted by 1683 s. Thereafter it differed from the 2 m line by -(0.03 ± 0.24) ppm CO_2, -(0.27 ± 0.59) ppb CH_4 (compare Figure 3) during the entire test period.
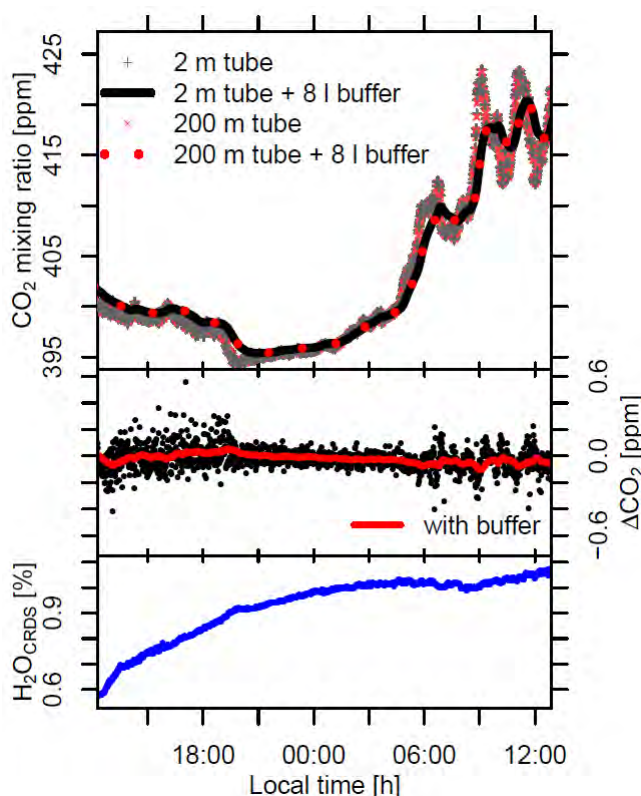
Figure 3 *Comparison of CO_2 measurements through 200 m and 2 m wet tubes (only a subset of the data is shown)*

To simulate the deployment of the 8 l buffer volumes, the time series were convolved with an exponential function. Any condensation at the walls of the stainless steel buffers can be excluded due to the reduced dew point associated with the low pressure (≤ 700 mbar). Because a well-mixed volume V with the concentration c_0 will respond to an incoming flow f and the arbitrary concentration c_1 with a time-dependent function $c(t)$

B $CO_2/CH_4/H_2O$ measurement at Zotino Tall Tower Observatory (ZOTTO)

$$c(t) = c_1 + (c_0 - c_1)\mathrm{e}^{-t/\tau} \text{ with time constant } \tau = \frac{V}{f}, \tag{4}$$

this function can be applied also to the buffer volumes (τ = 37 min, see section B2.1). The differences become less noisy: -(0.03 ± 0.04) ppm CO_2, -(0.28 ± 0.21) ppb CH_4.

This test accounts only for small flow rates of the analyzers (240 and 270 sccm). In ZOTTO the flushing of the tubes at a 60 times larger rate (15 l/min) will outweigh additional influences of the longer tube (300 m) and higher H_2O concentrations in summer. Hence, the influence of long tubing on the gas concentration measurement can be neglected.

B2.6 Data acquisition

A custom-made LabVIEW™ program (National Instruments Germany GmbH) installed on a central measurement PC controls all valve switching processes, calibration cycles, and signal processing. A data acquisition card (PCI-6225) acts as central hardware interface, to read sensor voltages (together with SCB-68 I/O card), and to control the solenoid valves with a relay board (ER-16 SPDT; all by National Instruments Germany GmbH). The central measurement PC is connected to the CRDS analyzer via serial RS232 cable.

For time synchronization of the different data sets collected on the site (meteorology, aerosols, CO), the measurement PC was equipped with a high quality time card (ClockCard PCI Pro, Beagle Software, USA) and was set as a central time server for other instruments via internal Ethernet network.

Data points are recorded every 30 seconds, including the average from the raw data of the analyzer and the current reading of all sensors. Additionally, all one second raw data from the CO_2/CH_4 analyzer are archived. Each tower level is sampled for 3 min. For data analysis, first three data points (1.5 min) are rejected in order to allow a sufficient flushing of the common sample line after each shift. All six tower levels, starting at the top, are consecutively measured within 18 min.

The post-processing code is written with the R software (http://www.r-project.org/) and removes a few outliers that originate from sporadic malfunction of valve V5 (replaced in Sept. 2009), maintenance interruptions, etc. Afterward, all data points are corrected for dilution and pressure broadening from water by applying a second order function of 30 s averaged H_2O raw data to CO_2 and CH_4 data (see section B2.3).

For CO_2 and CH_4 calibration, every 100 h each of the three calibration tanks is measured for 8 min. This time span generously allows the calibration gases to flush the pressure regulators and remove the wet ambient air from the part of the tubing used conjointly. The mean of the last four minutes gives the analysis values for the

B   CO$_2$/CH$_4$/H$_2$O measurement at Zotino Tall Tower Observatory (ZOTTO)

linear calibration curve (see sections B2.2 and B2.3). Between two calibrations, the fit parameters are linearly interpolated to account for the drift of the analyzer.

All processed data is finally flagged by an automatic data selection scheme. First, the data is rejected during known maintenance cycles, sometimes even only one line, e.g. for a flushing period of at least 2 hours after opening a buffer or during maintenance on the 301 m platform. Moreover, the flow entering the Picarro instruments needs to exceed 130 sccm. Time periods, when data transmission failed due to LabVIEW hardware problems, are deselected by choosing only data with > 200 ppm CO_2 and > 0 ppb CH_4. When the Picarro fine laser current drifted out of scale in first half of August 2010, the frequency of the data recording decreased. If there is no new data set within the measurement cycle of 30 sec (resulting in a zero standard deviation) the data is skipped. During this time the records are generally still reliable, if the full spectra could have been scanned. Nevertheless, some data points are completely off scale and show up in the 30 sec data with large standard deviations (> 0.5 ppm CO_2, > 2 ppb CH_4) and are omitted. This procedure does not influence usual atmospheric data: even the fastest atmospheric fluctuations are dampened anyway by the buffer volumes.

B2.7 Flask sampling system

To provide information on a larger number of species (CO_2, CH_4, CO, N_2O, isotopes, etc.), to validate continuous measurements and to bridge potential breakdowns of the continuous analyzer, air samples are collected from the 301 m level in 1 l glass flasks twice a week; however the series has several interruptions lasting for several weeks to months due to logistic problems.

To remove water vapor, the sampled air passes through a glass trap within a refrigerator at 2 to 5 °C and through two stainless steel traps cooled to -90 °C (Figure 1). Prior to filling the flasks, the tower tubing is flushed at a flow rate of 2 l/min for 40 min to prevent adsorption from affecting gas concentrations. During filling, air is pumped at a flow of 2 l/min through three flasks for 15 min by an upstream compressor pump (KNF Neuberger GmbH, Germany, Type: PM22619-814). When a pressure of 13 psig (~ 900 mbar above ambient) is reached in the flasks, flushing of the flasks continues, while the excess flow is released via an excess flow valve.

B2.8 Meteorological measurements

Various meteorological instruments were installed at the ZOTTO site in the year 2007 (Table 3). They record meteorological variables in a vertical profile on the tower as well as a number of soil parameters in vertical and horizontal profiles at two locations about 100 m southeast from the tower. One soil parameter measurement site is located within a densely wooded area (forest site), the other within a sparsely vegetated area (bare land site). At both places, the sandy soil is covered by lichens.

Table 3 *Meteorological instrumentation and their locations at ZOTTO*

Instrument	Tower	Bare land	Forest
Wind: 3D ultrasonic-anemometer	4, 52, 92, 158, 227, 301 m a.g.l.	-	-
Air temperature and rel. humidity sensor	4, 52, 92, 158, 227, 301 m a.g.l.	-	-
Air pressure transmitter	4, 92, 301 m a.g.l.	-	-
Radiation fluxes net radiometer	301 m a.g.l.	-	-
2x Photosynthetically active radiation sensors	301 m a.g.l.	-	-
3x Soil heat flux plates	-	Both sites at −0.03 m	
Soil temperature sensor	-	Both sites at: −0.02, −0.04, −0.08, −0.16, −0.32, −0.64, −1.28 m	
Soil moisture probe	-	Both sites at: −0.08, −0.16, −0.32, −0.64, −1.28 m	
Photosynthetically active radiation sunshine sensor	-	2 m	-
Precipitation: tipping bucket rain gauge	-	2 m (heated)	-

A scheme of the meteorological measurement setup, as well as the data handling and data distribution is shown in Figure 4 [O. Kolle, personal communication, 2010]. All data is transferred to the meteorology laptop, which collects all the data with customized software, stores it, and transfers it to the central measurement PC.
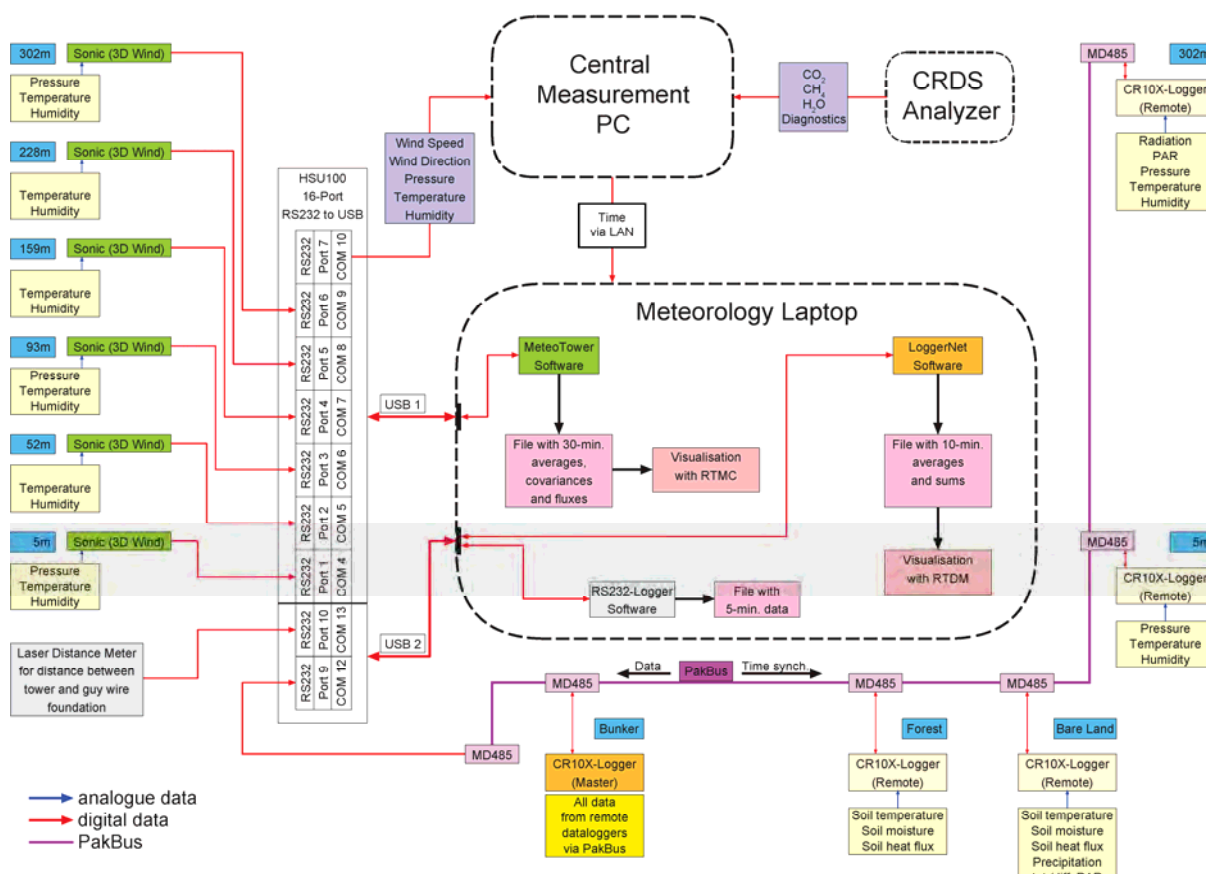
Figure 4 *Scheme of the meteorological measurement setup, the data handling and data distribution*

For the use of the recorded wind measurements it is crucial to understand the installation and coordinate system of the 3D wind anemometer (Gill Instruments Ltd., UK, type: R3). For convenience the sensors are aligned exactly in parallel to the arm

B CO_2/CH_4/H_2O measurement at Zotino Tall Tower Observatory (ZOTTO)

on which is it mounted. In the overall coordinate system (North = 0°) the arm is pointing towards 73.5° (Figure 5). The internal measurement of *u+* and *v+* is rotated by another 30°. Figure 5 implies the absolute wind direction φ (blue) by adding 46.5° to the internal wind direction measurement φ+ (orange).

The wind is measured in the horizontal directions u and v and the vertical component w. Each component is measured with 10 Hz frequency. Every 30 min, two elements of each wind component are recorded: the mean $\bar{u}$ and the fluctuating part u' around that mean (Reynolds averaging).
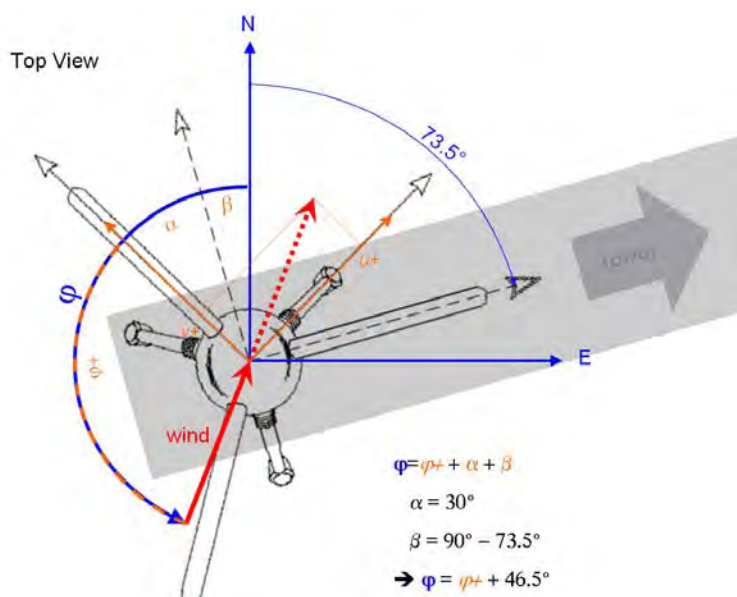
Figure 5 *Calculation of the wind direction from the rotated coordinate system of a sonic anemometer*

Through inevitable inaccuracies in the vertical alignment of the wind sensor, parts of the horizontal wind components $\bar{u}$ and $\bar{v}$ are reallocated in the naturally small parts of the vertical component $\bar{w}$, thus, induces large relative errors. To correct the vertical wind measurement $\bar{w}_{meas}$, Feigenwinter et al. [2004] and Paw U et al. [2000] suggested the following calculation:

$$\bar{w} = \bar{w}_{meas} - \overline{V}_{u+v} \cdot \tan(\vartheta) \qquad (5)$$
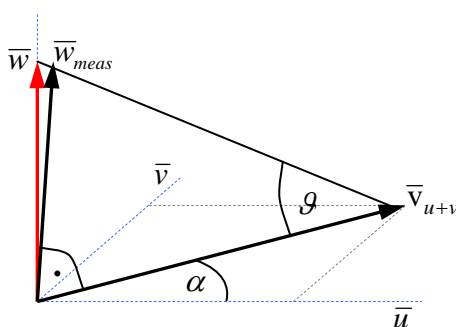
Figure 6 *Correction of the vertical wind measurement*

B   CO₂/CH₄/H₂O measurement at Zotino Tall Tower Observatory (ZOTTO)

The adjustment (Figure 6) depends on the horizontal wind speed $\overline{v}_{u+v}$ and the sensor tilt ϑ. The tilt is determined with a sinusoidal fit of $\overline{w}_{meas}/\overline{v}_{u+v}$ vs. horizontal wind direction φ in the parameters for offset q_0, amplitude q_1, and phase shift q_2:

$$\vartheta(\varphi) = \arctan\frac{\overline{w}_{meas}(\varphi)}{\overline{v}_{u+v}} = q_0 + q_1 \cdot \sin(\varphi + q_2) \qquad \textbf{(6)}$$
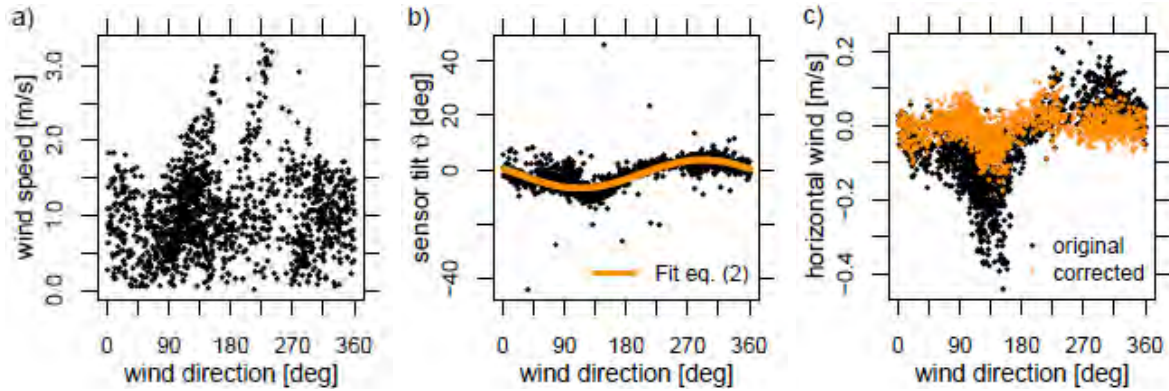
Figure 7 *Wind on 4 m level in July 2009:* **a)** *wind speed,* **b)** *sensor tilt and sinusoidal fit,* **c)** *uncorrected and corrected vertical wind velocity*

The sinusoidal function is particularly appropriate over level terrain and in the absence of mesoscale circulations: the resultant winds and deduced fluxes are orthogonal to the mean streamlines [Baldocchi et al., 2000]. Under natural conditions, the vertical wind component may be non-zero due to convection, synoptic scale subsidence, and local circulations [Lee, 1998]. To avoid the short term influences, the fit is done on monthly basis (Figure 7). Because of icing of the sensors in winter, the parameters are then averaged only for the summer months June-July-August 2009 and 2010 and repeated for all sensors on the six tower levels:

Table 4 *Fit results for vertical wind correction in the summer months June to August from Equation (6)*

Level [m]	q_0 [°]	q_1 [°]	q_2 [°]	Mean w [m/s] (uncorrected)	Mean w [m/s] (corrected)
301	1.83 ± 0.26	1.37 ± 0.31	150.9 ± 12.1	0.221 ± 0.073	-0.006 ± 0.016
227	0.96 ± 0.28	1.31 ± 0.20	76.6 ± 10.6	0.096 ± 0.040	0.001 ± 0.027
158	0.82 ± 0.20	0.68 ± 0.25	24.7 ± 25.3	0.077 ± 0.008	-0.001 ± 0.010
92	0.19 ± 0.15	-0.22 ± 0.36	121.0 ± 56.0	0.022 ± 0.011	0.006 ± 0.009
52	0.00 ± 0.22	-0.92 ± 0.23	139.7 ± 11.3	-0.003 ± 0.015	0.001 ± 0.010
4	-1.47 ± 0.10	5.20 ± 0.31	158.2 ± 4.9	-0.004 ± 0.029	0.006 ± 0.012

The result implies that the sensor on 92 m level is adjusted best. The other sensors' tilts are in the order of 0 to 3 degrees. The 4 m level requires an even larger correction up to 7 degrees. The reason might be that the nearby building and a group of trees distort the plane of mean wind streamlines from the parallel to the ground.

B   CO₂/CH₄/H₂O measurement at Zotino Tall Tower Observatory (ZOTTO)

These results underline that the tilt correction is obligatory for the vertical wind component. Despite the tilt ϑ is small, the comparably large horizontal winds $\overline{v}_{u+v}$ result in a large correction term in equation (5).

The correction does not yet adjust the vertical heat fluxes $H \sim w'T'$. In contrast to the wind correction, only the high frequency deviations w' drive the signal. Because the magnitude of the horizontal components u' and v' are comparable to the vertical w', the correction term generally will be less than $\tan(\vartheta) \sim 5\%$ of the signal. For an adequate tilt correction (described exemplarily for CO_2 flux $w'c'$ in Baldocchi et al. [1988], equation 12), the availability of the high frequency horizontal components of the sensible heat flux measurement $u'T'$ would be crucial, but present national regulations do not allow the export of raw data out of Russia. Therefore, the magnitude of the flux correction was tested with high frequency data of another test anemometer, and reproduced the number of $\sim 3\%$ error per degree of tilt, given by Baldocchi et al. [1988].

Figure 7a indicates that the tower in NEE direction (74°) may have a minor influence on the wind measurement (can be seen on all levels).

B3 Data evaluation

The station was equipped with the new analyzing system in April 2009. The measurement system is authorized by Russian Federal Service for Technical and Export Control (FSTEC) to be operational since May 20, 2009. Up to the most recent data (June 30, 2011), the total time of missing data due to humidification experiments (section B2.4), maintenance or malfunctions is limited to 29 days (3.7 % of 771 days).

To monitor the accuracy of the instrument, one target tank is measured every 200 h for 8 min randomly distributed between two calibration cycles, and is treated like ambient air measurement data. After applying the calibration procedure (section B2.6), the measured CO_2 and CH_4 concentrations of the target tank are 404.35 ± 0.04 ppm and 1947.5 ± 0.3 ppb for the whole time period so far (Figure 8). A comparison with values from the Jena GASLAB in Table 2 (404.40 ± 0.08 ppm / 1947.4 ± 1.4 ppb) indicates an adequate accuracy of the system for dry air measurements. The CO_2 measurement is slightly biased, but the deviation is still within the error limit of the Jena GASLAB calibration laboratory, thus statistically insignificant. Earlier calibrations of the CRDS system are highly repeatable, which indicates that the accuracy is limited by the noise of the laboratory calibration.

In conclusion the accuracy of the instrument is 0.09 ppm for CO_2 and 1.5 ppb for CH_4, if statistical independence between target tank measurement of the CRDS analyzer, calibration laboratory (Table 2), and H_2O correction (section B2.4) is assumed.

B   CO$_2$/CH$_4$/H$_2$O measurement at Zotino Tall Tower Observatory (ZOTTO)
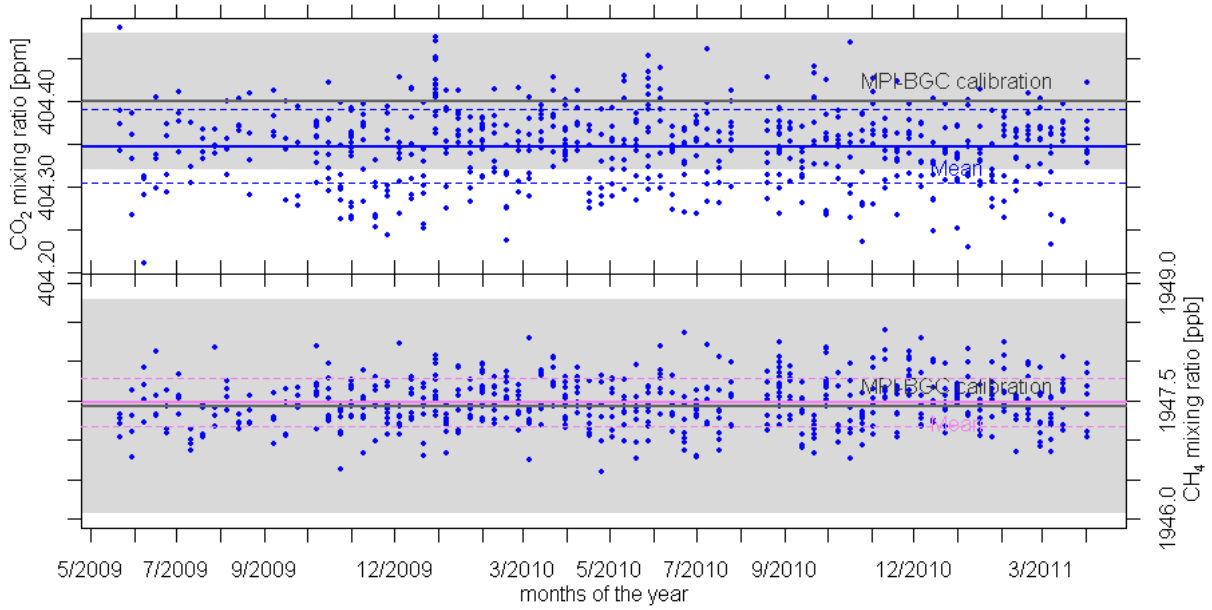
Figure 8 *Target tank time series (colored line represents the mean ± standard deviation, grey is laboratory standard ± error)*

Laboratory analysis results of the flask samples are compared to the CRDS data. Flask analysis has a measurement precision of 0.08 ppm CO_2 and 1.3 ppb CH_4. Influences on CO_2 and CH_4 concentrations through the long storage at ZOTTO (max. 363 days) can be excluded, as the storage in glass flasks using PCTFE seals was intensively investigated for periods up to 420 days [GAW Report No.161, 2003]. For the flask comparison, the integrating effect of the different air volumes has to be taken into account: τ = 37 min for the 8 l buffer and τ_0 = 0.5 min for 1 l flasks (at 2 slm flow, equation (4)). Generally, the measured concentration $c(t)$ through a well-mixed volume can be calculated by convolving the in-situ concentration $s(t)$ with the response function $g(t)$ of the volume:

$$c(t) = g(t) * s(t) = \int_0^t g(t-t')s(t')dt' \text{ with } g(t) = \frac{1}{\tau}e^{-t/\tau}, \tag{7}$$

The CRDS analyzer measures the integrated concentration $c(t)$. The derivative of Equation (7) gives an approximation for the highly variable in-situ data:

$$s(t) = c(t) + \tau \frac{dc(t)}{dt} \tag{8}$$

Figure 9 illustrates this deconvolution exemplarily for one flask measured in August 04, 2009. Three consecutive data points of the CRDS analyzer are combined to one (representing 1.5 min, grey dots) and give the basis for a smoothed spline (grey line, degrees of freedom is 2/3 of the length of the data series), representing $c(t)$. Equation (8) gives the approximate in-situ data (red line). To estimate the errors

(red dashed line), the standard deviation of the three combined CRDS data points (light grey bars) are scaled with the factor $\sqrt{\tau}/\sqrt{\tau_0}$ that accounts for the deconvolution uncertainty (τ_0 is time constant for the flask measurement).
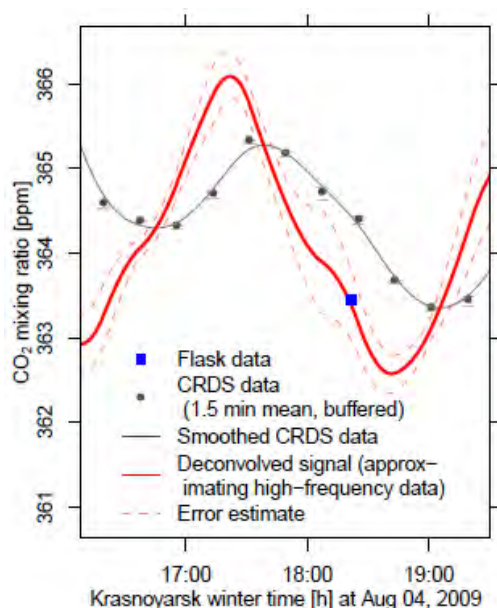
Figure 9 *Comparison of flask data with deconvolved CRDS data*
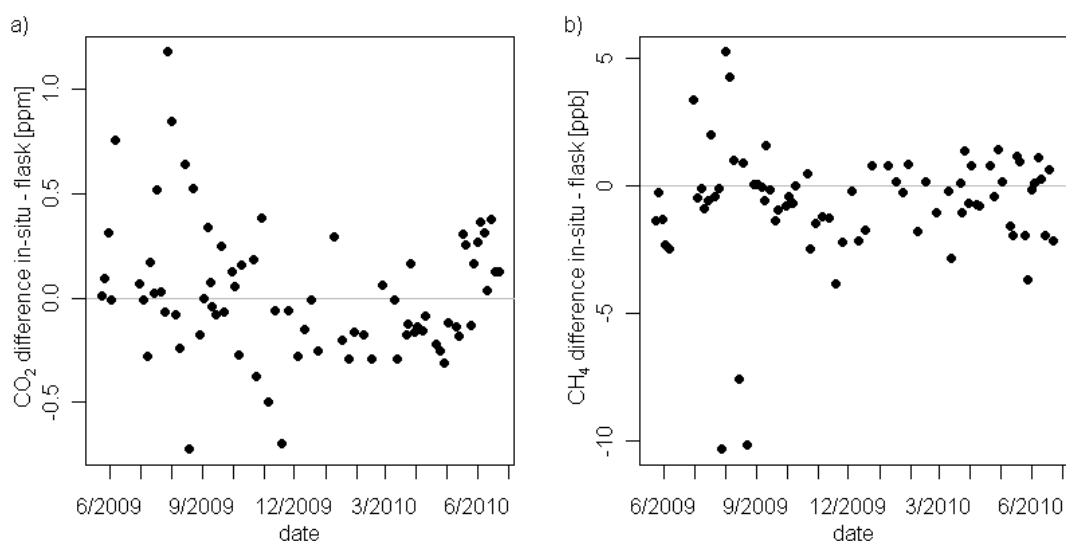
Figure 10 *Differences between deconvolved in-situ and flask data for* **a)** *CO_2 and* **b)** *CH_4*

For overall comparison of 156 flasks from 76 different points in time were used. The mean difference ± standard deviation between the in-situ approximation and all currently available flask data is +0.02 ± 0.32 ppm for CO_2 and -0.7 ± 2.3 ppb for CH_4 (Figure 10). The results are in line with other comparisons (e.g. Popa et al. [2010]), despite the fact the buffered signal $c(t)$ is available only without the high-frequency in-situ signal $s(t)$. Hence, larger deviations in Figure 10 are a sign of atmospheric

B CO_2/CH_4/H_2O measurement at Zotino Tall Tower Observatory (ZOTTO)

variability ($s(t)$) that was smoothed out by the 8 l buffer volumes in the CRDS data ($c(t)$).

The $CO_2/CH_4/H_2O$ measurement series from six tower levels covers almost 2 years, starting in May 2009 (Figure 11). A detailed analysis of the CO_2 and CH_4 series is given in Chapter C2.2.

The water vapor measurement was compared to the meteorological data series of air temperature and relative humidity. WMO recommends the Goff equation from 1957 to calculate the saturation water vapor pressure according to air temperature [Murphy et al., 2005]. The saturation water vapor pressure is multiplied with relative humidity and pressure from the tower top level to receive absolute H_2O concentration from meteorology (Figure 11c), which correlates well with the calibrated H_2O from the CRDS analyzer (equation (1)): the slope is 1.038 (still consistent with 1.3 % relative error in H_2O calibration and 2 % uncertainty in relative humidity measurement) and the correlation coefficient $R^2 = 0.995$. This procedure represents an independent check on the water calibration, and validates the transfer of laboratory tests with CFADS-30 (section B2.2) to the CFADS-17 instrument deployed in ZOTTO.
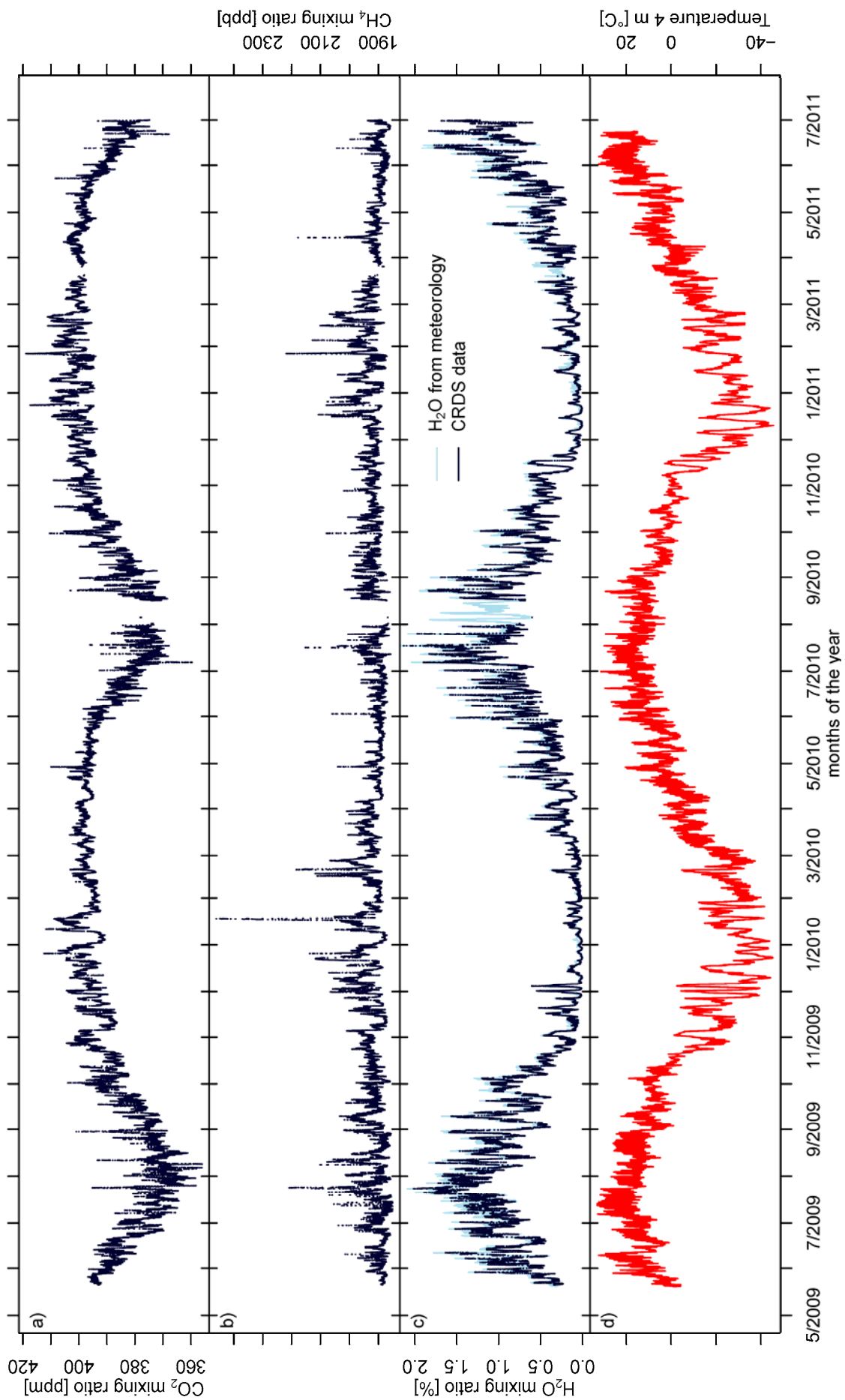
Figure 11 *ZOTTO time series for* **a)** *CO_2,* **b)** *CH_4, and* **c)** *H_2O for 301 m height level,* **d)** *4 m temperature from May 20, 2009 to June 30, 2011*

B CO_2/CH_4/H_2O measurement at Zotino Tall Tower Observatory (ZOTTO)

B4 Conclusions

Based on the extensive preparatory work in the laboratory of the MPI-BGC, it was possible to equip the Zotino Tall Tower station with a CRDS analyzer in April 2009 to measure CO_2, CH_4, and H_2O in non-dried sample air. The H_2O measurement and the associated correction is temporally stable enough to guarantee high quality for the CO_2 and CH_4 measurements and compares well to meteorological data. The water corrections on the CO_2 and CH_4 measurements were validated over a 17 month period with a simple experimental setup. The effect of molecular adsorption in the long air lines was investigated and shown to be negligible.

Regular target tank measurements reveal a precision of the instrument of 0.04 ppm for CO_2 and 0.3 ppb for CH_4. Adding measurement uncertainties of the calibration tanks and the water correction, the accuracy is 0.09 ppm CO_2 and 1.5 ppb CH_4. The difference between the continuous data and flask data is -0.02 ± 0.32 ppm for CO_2 and +0.7 ± 2.3 ppb for CH_4. This corroborates, in an independent way, the good quality of wet air measurements.

Without any air drying system the maintenance is considerably reduced in comparison to traditional setups. Furthermore, the system sensors for diagnostic values (e.g. flow, pressure, etc.) are free of moving parts, which minimizes the possibility of failures. Calibration tanks will have to be recalibrated on decadal timescale.

The data is temporally integrated by the use of buffer volumes in each air line, allowing a continuous, near-concurrent measurement from six tower height levels. The 37 min integration time of each line suffices to bridge the 18 min period during which the analyzer is measuring other lines. The results are six smooth data series, which are not influenced by high-frequency fluctuations associated with turbulent eddies. All data series can be analyzed in detail to investigate long-term trends and diurnal cycles (Chapter A). Moreover, they allow a temporally highly resolved observation of the nocturnal boundary layer developments, thus enabling to better estimate local nighttime respiration (Chapter D). Additionally, the data from the tower's uppermost level will provide a valuable basis for future inverse modeling approaches for the Central Siberian region (Chapter E).

C Analysis of CO₂, CH₄ concentration and meteorological time series

"Look deep into nature, and then you will understand everything better."

Albert Einstein (1879-1955)

C1 Introduction

Changes in atmospheric greenhouse gas concentrations alter the global climate [IPCC: Solomon et al., 2007]. Two greenhouse gases – CO_2 and CH_4 – are important participants in the earth's carbon cycle, which is tightly coupled to climate change through multiple feedbacks (e.g. the greenhouse effect).

CO_2 fluxes dominate the total carbon cycle. The biosphere absorbs and emits the largest amounts of carbon. The natural fluxes of uptake and emission are almost in balance. Anthropogenic emissions from fossil fuel burning and cement production add 7 % of the natural biospheric flux to the earth system [Denman et al., 2007; Friedlingstein et al., 2010].

Human induced emissions have increased the atmospheric CO_2 mixing ratio, which was first noticed and later quantitatively proved by Charles David Keeling [1960] at the remote location of Mauna Loa, Hawaii. This time series is shown in Figure 12a and reveals a growing and oscillating signal, which is caused by the seasonal cycle in the biospheric uptake – a fingerprint of the "breathing" of the earth.
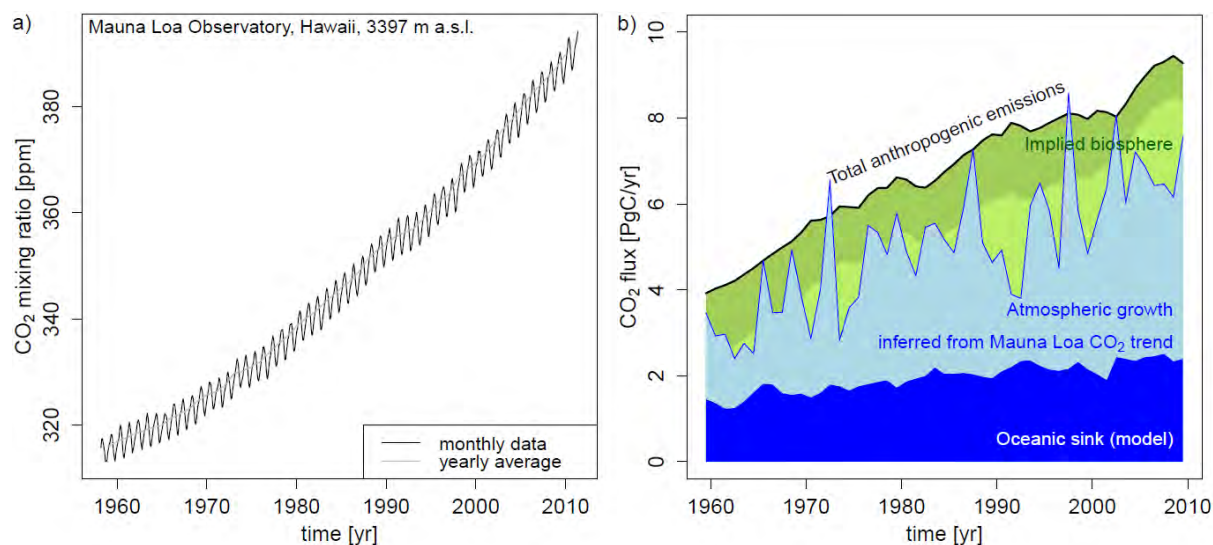
Figure 12 a) *Keeling curve by courtesy of Dr. Pieter Tans, NOAA/ESRL (www.esrl.noaa.gov/ gmd/ccgg/trends/) and Dr. Ralph Keeling, Scripps Institution of Oceanography (scrippsco2.ucsd.edu/);* **b)** *global CO₂ emissions [Le Quere et al., 2009] and atmospheric growth at Mauna Loa.*

The total amount of known CO_2 emissions can be compared to the atmospheric increase. The anthropogenic emissions are the best known part in the carbon cycle and have risen up to 9.3 PgC/yr until 2009, which include emissions from fossil fuel burning and cement production (light green part in Figure 12b), and land use change (dark green in Figure 12b) [Friedlingstein et al., 2010]. On the other side, the observed CO_2 concentrations at Mauna Loa can be used as an indicator for a global atmospheric mixing ratio, since the station is remotely located, far away from large CO_2 sources. The annual increase of that mixing ratio in Figure 12a can be related to the volume of the atmosphere to infer the global CO_2 fluxes into the atmosphere (light blue area in Figure 12b). Hence, only 39 to 45 % of the anthropogenic CO_2 emissions stay in the atmosphere. The remaining 55 % are taken up by the ocean (blue area in Figure 12b) and the biosphere (green area in Figure 12b) [Canadell et al., 2007; Le Quere et al., 2009].

The CO_2 fluxes in Figure 12b underlie large fluctuations. The emissions dropped in the beginning of the 1990s as a consequence of the economic break-down in the former communist states. The decline in 2009 represents the recent economic crisis. The partitioning of the fluxes between atmosphere and biosphere is determined by the strengths of the biospheric uptake, which is affected e.g. by the Pinatubo volcano eruption in 1991. Moreover, the peak in the emission pattern around 1972 can be explained by a strong "El Niño" event in the Southern Oscillation [Bacastow, 1976]. Generally, the trend of accelerated rising in the atmospheric CO_2 concentration during "El Niño" can be also witnessed in the following years [Heimann et al., 2008].

The global CH_4 mixing ratio has risen by about 1000 ppb in the last two centuries to 1774 ppb in 2005 according to the report of the Intergovernmental Panel on Climate Change [IPCC: Solomon et al., 2007]. Nowadays, it is likely that the atmosphere has reached equilibrium between CH_4 emissions and CH_4 removals. Therefore, the global CH_4 mean mixing ratio has leveled off since the 1990s. Most recent increases in the atmospheric CH_4 concentration in 2007-2008 are probably due to anomalous high arctic temperatures and above average tropical precipitation [Dlugokencky et al., 2009]. CH_4 concentrations cannot directly be attributed to one or several human activities, because they interact with several climate system feedbacks.

To understand the global carbon cycle, it is important to describe the boreal region with its large carbon stocks. Yet, only a few stations beside the Zotino Tall Tower Observatory (ZOTTO) monitor the carbon greenhouse gases of the Siberian region [Arshinov et al., 2009a; Winderlich et al., 2010].

C   Analysis of CO$_2$, CH$_4$ concentration and meteorological time series
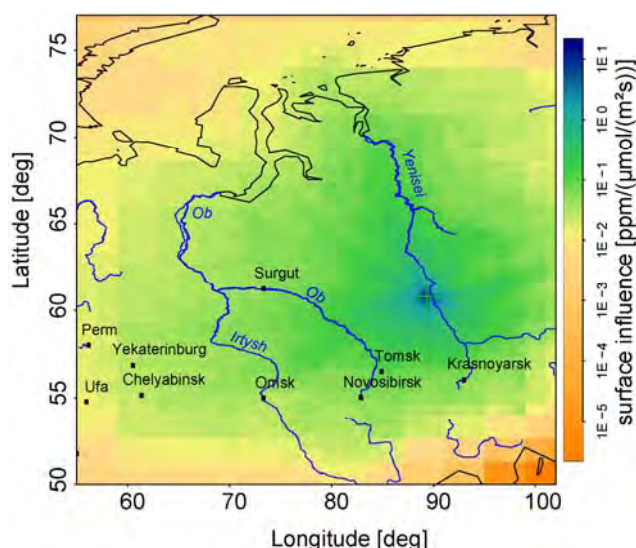
Figure 13 *Cumulated STILT footprints for ZOTTO 301 m level, made from 5 days back trajectories, for every hour from 1.5.-30.11.2009*

A further argument for long-term measurements at ZOTTO is supported by simulations of the station's footprint with the Lagrangian transport model STILT calculations [Lin et al., 2003; Gerbig et al., 2003b]. The integrated surface influence of 5 days back-trajectories based on forecast data from the European Centre for Medium-Range Weather Forecasts (ECMWF) for the 2009 vegetation period is plotted in Figure 13. It shows the near-field of the tower producing the main influence on the measured mixing ratios up to 10 ppm/(µmol/(m²s)). The area with a surface influence above 0.1 ppm/(µmol/(m²s)) covers about 1,000,000 km² of Central Siberia, slightly skewed into the west, where swamplands of the Ob River are located, and to the north along the Yenisei River. Thus, the ZOTTO footprint covers permafrost regions as well. Moreover, model simulations indicate a good signal to noise ratio especially in Central Siberia to detect changes in carbon fluxes in Eurasia with inverse methods [Karstens et al., 2006]. Altogether, it proves that ZOTTO is a good location for investigating the ecosystem functioning of the continental boreal region.

In this chapter the time series of CO_2 and CH_4 mixing ratios are analyzed for the period 2009 to 2011. The results have to be interpreted in the context of the continental location of ZOTTO. The boreal forest strongly alters CO_2 and CH_4 observations. Only in comparison with global background stations it is possible to conclude whether the data is representative globally or only on the local scale.

C Analysis of CO_2, CH_4 concentration and meteorological time series

C2 Data analysis

C2.1 Meteorological conditions

The climatic conditions of a mean annual temperature of 3.8 °C and a total precipitation of 536 mm taken from the weather station at Bor about 100 km away (61°36' N 90°01' E, 58 m a.s.l., [Schulze et al., 2002]) indicate a rather cold continental climate around ZOTTO. A temperature trend of +3 °C / 100 yr was observed there within the period of 1950-1999. This warming trend is representative for the larger Siberian region [Groisman et al., 2009].

Compared to the climatic average, the weather at ZOTTO was characterized by normal temperatures but low precipitation in 2009 and colder temperatures and normal precipitation in 2010 (see Table 5).

Table 5 *Weather conditions at ZOTTO in the year 2009 and 2010*

	Bor 1936-1999 [Schulze et al., 2002]	ZOTTO 2009	ZOTTO 2010
Mean T [°C]	-3.8	-3.6	-4.1
Min T [°C]	-56.0 (1987)	-45.7 (10.2.)	-45.4 (10.12.)
Max T [°C]	+36.1 (1999)	+33.3 (12.7.)	+31.6 (30.6.)
Precipitation [mm]	536	455	539

3D anemometers measured the wind speed at six tower height levels. Figure 14 reveals the diurnal cycle at the lowest 4 m level with maximum wind speed during the day. While the mean wind speed at 52 m has almost no diurnal variability, the upper levels have the highest wind speed during night. At night, the free troposphere is decoupled from the ground (due to the temperature inversion close to the ground) and allows air to travel with minimum friction.
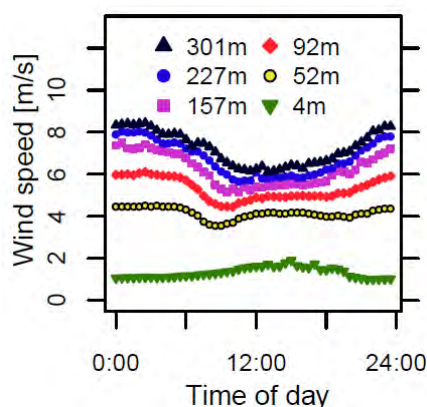
Figure 14 *Average diurnal cycle of wind speed at different tower levels for the summer months June-September in 2009 and 2010*

C Analysis of CO₂, CH₄ concentration and meteorological time series

C2.2 Long-term trend and annual cycle of CO_2

Since the installation of the system in 2009, ZOTTO monitors CO_2, CH_4 and H_2O mixing ratios in Central Siberia (Chapter A). These data series were already presented in Figure 11. Before analyzing details, this chapter looks for trends and annual cycles as well as the implications for the continental carbon cycle.

At first, attention is given to the CO_2 observation from the 301 m level at ZOTTO (dark blue in Figure 15). To understand the large scale carbon budgets, only afternoon data is used, because they are not influenced by local nighttime signals. These day-time values during well-mixed conditions in the planetary boundary layer (14:00 to 17:00 local time zone, orange dots in Figure 15) can be fitted by a 4th harmonic function (orange line in Figure 15)

$$c(t) = a_0 + a_1 \cdot t + \sum_{i=1}^{4} b_i \sin(2\pi \cdot i \cdot t / 365d) + c_i \cos(2\pi \cdot i \cdot t / 365d). \qquad (9)$$

This formula is applied to the in-situ data and gives the fitting parameters:

$c(t)$ / ppm = (259.2 ± 2.3) $+ (7.17 \pm 0.13) \cdot 10^{-3}/d \cdot t$
$+ (8.464 \pm 0.04) \cdot \sin(2\pi \cdot t/365d) + (8.754 \pm 0.04) \cdot \cos(2\pi \cdot t/365d)$
$+ (-5.19 \pm 0.04) \cdot \sin(2\pi \cdot 2t/365d) + (-0.41 \pm 0.04) \cdot \cos(2\pi \cdot 2t/365d)$
$+ (1.83 \pm 0.04) \cdot \sin(2\pi \cdot 3t/365d) + (-0.66 \pm 0.04) \cdot \cos(2\pi \cdot 3t/365d)$
$+ (-0.01 \pm 0.04) \cdot \sin(2\pi \cdot 4t/365d) + (0.38 \pm 0.04) \cdot \cos(2\pi \cdot 4t/365d)$
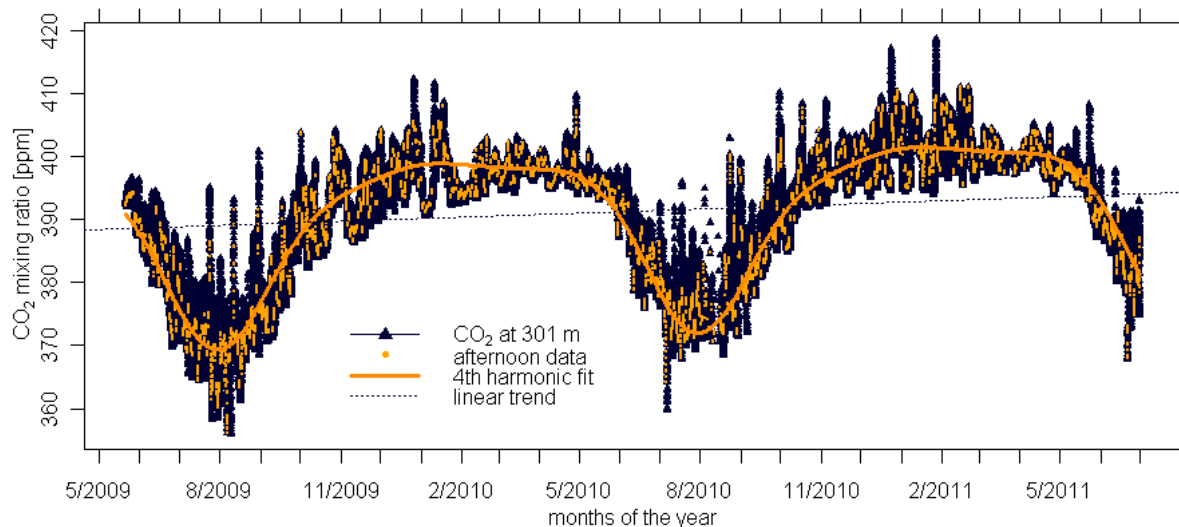
Figure 15 *CO_2 time series of afternoon data on 301 m level with 4th harmonic fitting*

The amplitude of the seasonal cycle is 28.3 ppm, after subtracting the linear part from the harmonic fitting. This number is comparable with previously reported values of 26.6 ppm at ZOTTO in the year 2007 [Kozlova et al., 2008]. The amplitude is more pronounced than at other tall tower sites with stronger marine influence, e.g. Bialystok, Poland with 23 ppm [Popa, 2007], or even Ochsenkopf, Germany with 15.5 ppm [Thompson et al., 2009] at the uppermost tower levels (300 and 163 m a.g.l., respectively).

C Analysis of CO_2, CH_4 concentration and meteorological time series

The linear trend of $(7.17 \pm 0.13) \cdot 10^{-3}$ ppm per day (dark blue dotted line in Figure 15) converts to (2.62 ± 0.05) ppm/yr, which is higher compared to the trend of 2.02 ppm/yr seen in 2006 [Kozlova et al., 2008].

Generally, the CO_2 trend varies over time and region. This can be visualized by deriving the CO_2 growth rate of the globally interpolated CO_2 data from the marine boundary layer [GLOBALVIEW-CO2, 2010]. The latitude of ZOTTO is marked in the according Figure 16 by a white dotted line and reveals enormous fluctuations from 0 to 4 ppm/yr over the past years.
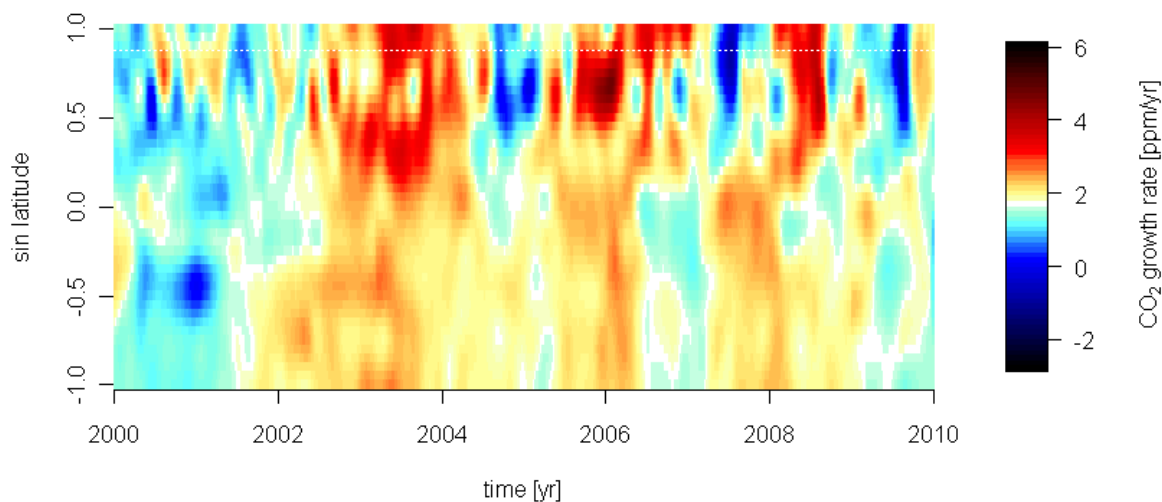
Figure 16 *Global annual latitudinal CO_2 growth rate in the reference marine boundary layer data [GLOBALVIEW-CO2, 2010]*

At ZOTTO the CO_2 trend has been anomalously high in the period from 2009-2011. Unfortunately, the GLOBALVIEW data set does not cover the whole time frame; nevertheless several independent indications give good reasons for that behavior. Below average CO_2 concentrations in 2009 might have been driven by an above average strong terrestrial uptake in 2008-2009 ([Le Quere et al., 2009], land sink ~ -4.6 PgC). Additionally, anthropogenic emissions had a small recession in 2009 due to the global economic crisis; thus, CO_2 mixing ratios have been presumably below the normal in 2009. On the contrary, the year 2010 was characterized by an extreme heat wave with extensive forest fires in the European part of Russia, where the temperature was up to 10.7 °C higher than climatic average 1970-1999 over a 31-day period [Barriopedro et al., 2011]. These conditions facilitate high CO_2 concentrations by fire emissions and reduced CO_2 uptake due to drought stress of the plants. In contrast to Europe, Siberia experienced lower temperatures during the summer of 2010 [ROSHYDROMET, 2011], which may reduce plant activities, and thus, reduce CO_2 uptake. This combination leads to the hypothesis of enriched CO_2 concentrations in Central Siberia in 2010. The observations at ZOTTO in Figure 17 support this theory: the CO_2 concentrations are clearly elevated in the summer months from mid of July to mid of September 2010 compared to the regular (or even intensified) minimum in 2009.

C   Analysis of CO_2, CH_4 concentration and meteorological time series
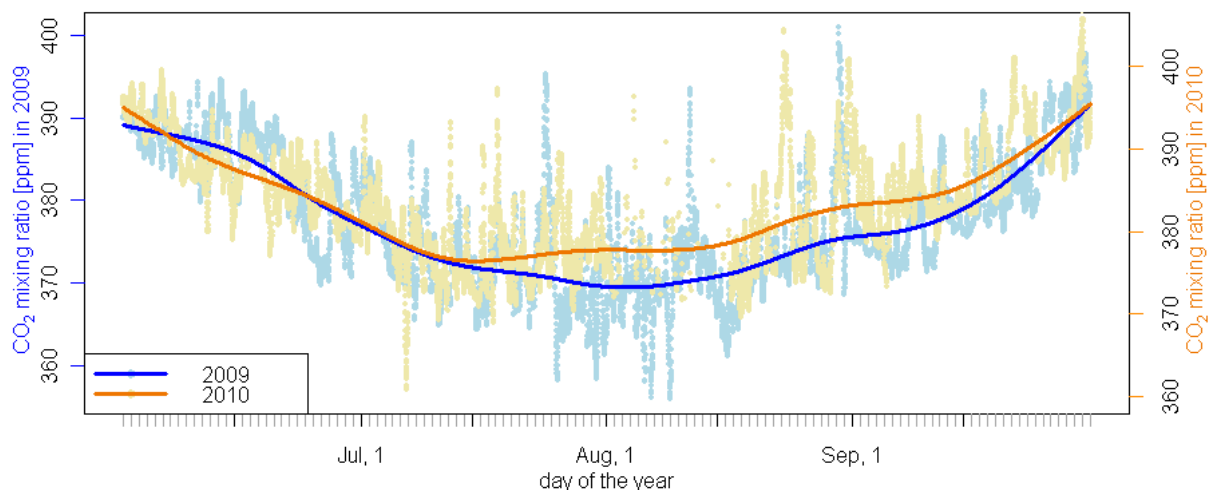
Figure 17 *Comparison of CO₂ seasonal cycle between 2009 and 2010; for better comparison the right CO₂ scale for 2010 is shifted by the annual growth rate of 2.62 ppm*

To get a better insight on perennial trends, the time series can be extended back in time by using the analysis results from the regular flask sampling. The flask time series has been started already in 2006, but had an interruption in 2007-2008 (Figure 18). The 4th harmonic analysis from equation (9) can also be applied to the flask data (orange in Figure 18) and reveals a detrended seasonal amplitude of 29.7 ppm, which is very close to the one of the continuous tall tower data. The growth rate in atmospheric CO_2 is 1.64 ppm/yr from October 22, 2006 to June 22, 2010. This almost ideally agrees with the globally representative Mauna Loa record, which had a 1.62 ppm growth rate in 2009 ([Canadell et al., 2007] and update from GlobalCarbonBudget 2009).
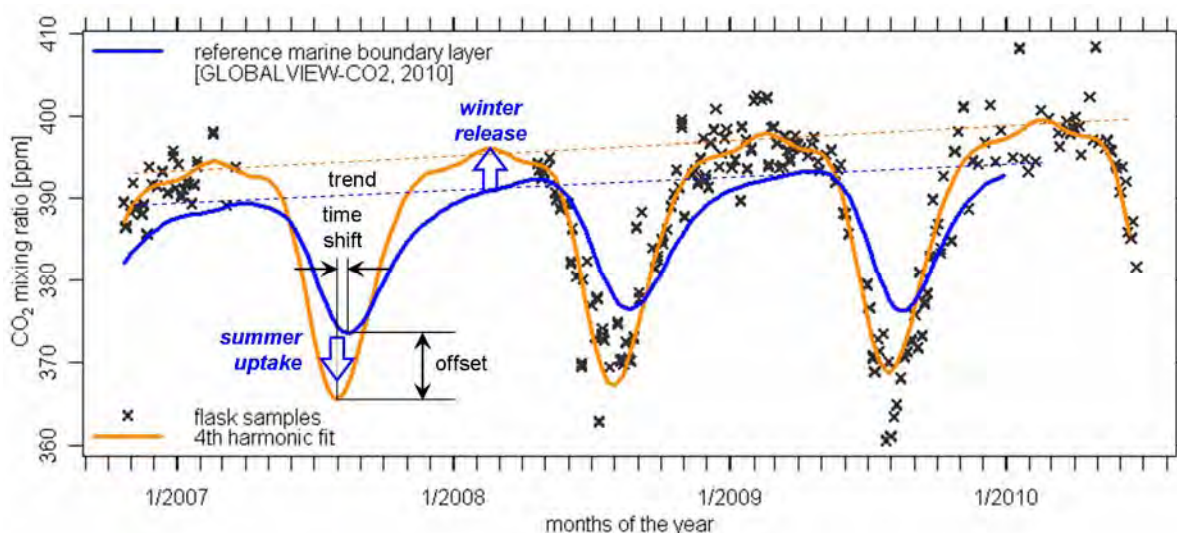
Figure 18 *Flask CO₂ time series of the continental ZOTTO station in comparison to the marine boundary layer [GLOBALVIEW-CO2, 2010]*

To study the influence of the continental location of the ZOTTO site on the observed data, the data can be compared to the reference marine boundary layer at

C Analysis of CO₂, CH₄ concentration and meteorological time series

the latitude of ZOTTO (blue in Figure 18, [GLOBALVIEW-CO2, 2010]). A clear pattern becomes evident: during winter, CO_2 is released over continents by biospheric respiration and anthropogenic emissions, while the ocean may even counteract the global CO_2 increase through increased CO_2 solubility in colder water. Apart from this winter CO_2 release by the continent, Figure 18 demonstrates the opposite behavior of CO_2 uptake during summer. The photosynthetic uptake from the biosphere over the continent amplifies the summer minimum in the CO_2 data and produces an offset to the marine reference data. Moreover, a time shift in the summer minima can be seen between ZOTTO and the maritime background. This time shift is induced by the transport of the CO_2 depleted air from the continents towards the ocean.

The overall trend of the flask data allows for a similar analysis as for the Mauna Loa data in the introduction C1. Assuming this average growth rate to be globally representative, the CO_2 input of 1.64 ppm/yr dispersed into the earth's atmosphere ($5.15 \cdot 10^{18}$ kg air, 28.9644 g/mol) would lead to a global net atmospheric source of 3.5 PgC/yr. The relation to the total anthropogenic emissions of 9.3 PgC/yr in 2006-2009 [Le Quere et al., 2009; Friedlingstein et al., 2010] gives an airborne fraction of ~ 38 % that is slightly smaller than reference values of 39 to 45 % [Canadell et al., 2007; Knorr, 2009; Le Quere et al., 2009]. One reason might be the intense land carbon sink in 2008 that has been induced by stable positive "La Niña" state in the Southern Oscillation [Le Quere et al., 2009] (also visible in Figure 12b).

C2.3 Long-term trend and annual cycle of CH_4

In contrast to CO_2, CH_4 concentrations have an almost flat baseline, which does not vary throughout the year (Figure 11b, Figure 19), but has characteristic spikes in the concentration time series. They are pronounced during midsummer, when most biotic activity in the surrounding bogs takes place and forest fires occur. The reason for enhanced CH_4 emissions during winter is assessed in the following Chapter C2.4.

The in-situ CH_4 data were analyzed with the 4th harmonic fit (orange line in Figure 19) and characterized by an annual growth rate of -1.0 ± 0.4 ppb for 2009 to 2011. The most recent flask data show a growth rate of 1.15 ppb/yr since 20. May 2009. The full data series of the flask samples covers the years 2006-2007 as well, and indicates an increase of 7.7 ppb/yr. In summary, the ZOTTO data reveals a decline in the CH_4 growth rate in most recent years. This is in agreement with the globally averaged methane observations: While they didn't rise from 1999 to 2006, they have risen by 7.9 ppb in 2007, 7.0 ppb in 2008, and finally by only 2.4 ppb in 2009 ([Dlugokencky et al., 2009] updated with http://www.esrl.noaa.gov/gmd/annualconference/previous/2010/slides.html). The reasons for the intermediate increase are enlarged boreal and tropic wetland emissions during "La Niña" in 2007-2008. Climate feedbacks from permafrost and marine CH_4 hydrates are unlikely to cause those sudden large changes [Dlugokencky et al., 2009].

C Analysis of CO_2, CH_4 concentration and meteorological time series
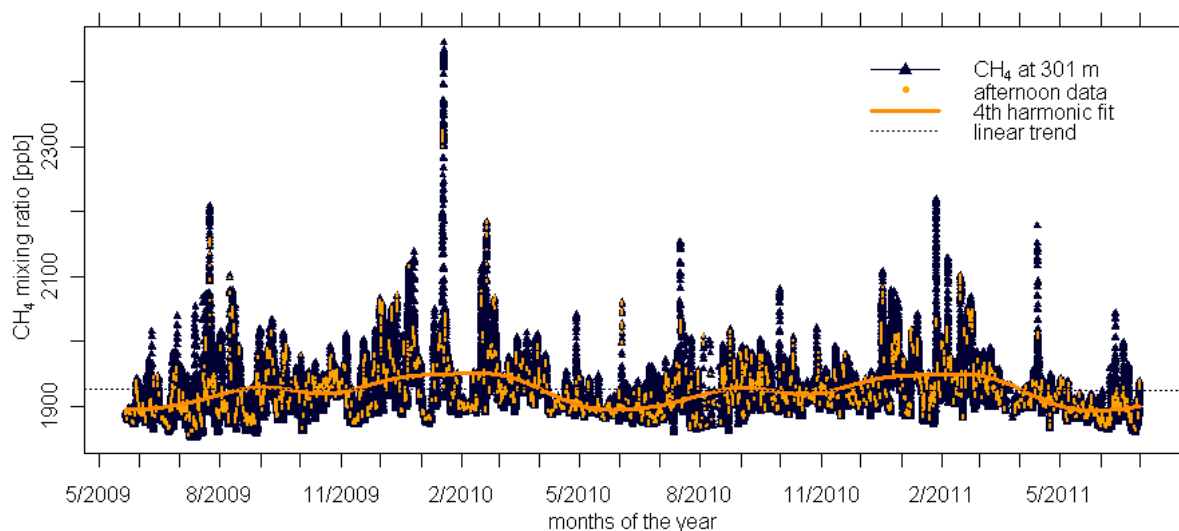
Figure 19 *CH₄ time series of afternoon data on 301 m level at ZOTTO with 4th harmonic fitting*

The harmonic analysis shows a small seasonal amplitude of 56 ppb. The maximum CH_4 concentrations are seen in winter, when the atmospheric OH concentrations that acts as a CH_4 sink are low (orange line in Figure 19). There is a small second peak in the late summer due to enlarged local wetland emissions that has been observed also at other stations in Western Siberia [Sasakawa et al., 2010].

Assuming the general growth rate to be globally representative, the amount of 7.7 ppb/yr CH_4 dispersed into the whole atmosphere ($5.15 \cdot 10^{18}$ kg air, 28.9644 g/mol) would lead to a global carbon source of 16.4 TgC, which is less than CO_2 by several orders of magnitude.

C2.4 Synoptic winter events

After analyzing the long-term, globally impacting trends, it is interesting to analyze individual synoptic events. While numerous spikes during summer indicate wetland emissions, the spikes in winter need detailed analysis.

In November 2006, under low temperature and high-pressure conditions a strong CO_2 increase has been observed at the ZOTTO site [Kozlova et al., 2008]. Even before, winter conditions with low wind speed and increased CO_2 concentrations have been studied at a nearby location by Eneroth et al. [2003]. This explains the CO_2 increase by low but steady biogenic activity and long interaction times of the air with the ground due to low wind speeds. In the recent ZOTTO data several of those events have been detected.

Figure 20 shows increased CO_2 concentrations in periods of high atmospheric pressure and very low temperatures. Not shown is the slow-down in wind speed and the distinct establishment of a temperature inversion during this time.

The ZOTTO data, one exemplary period is plotted in Figure 20, suggests pressure above 1010 mbar and ground temperature below -20 °C are a required but

C Analysis of CO₂, CH₄ concentration and meteorological time series

not sufficient condition for the development of decoupled mixing ratios at different tower heights.
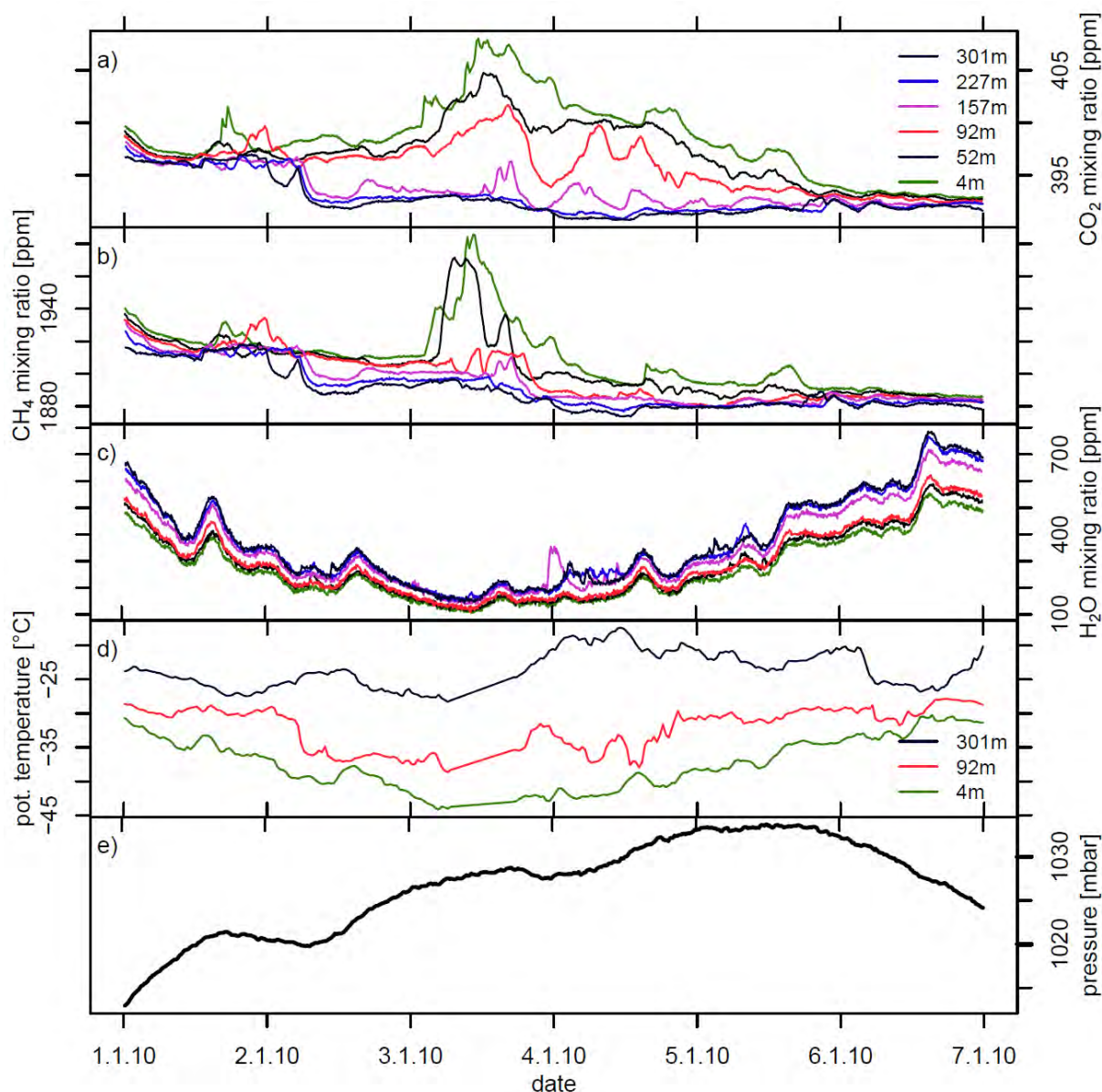
Figure 20 *Observations at ZOTTO during one synoptic winter event:* **a)** *CO_2,* **b)** *CH_4,* **c)** *H_2O,* **d)** *potential temperature, and* **e)** *4 m atmospheric pressure in the first week of January 2010*

Due to the very low temperatures, the water vapor concentration reaches even below the CO_2 concentrations (Figure 20c). The temperature profile from the ZOTTO tower in Figure 20d implies a very strong temperature inversion during this period. The temperatures are 20 °C higher 301 m above the ground. Since those strong temperature inversions are fairly persistent in the arctic regions throughout the winter [Serreze et al., 1992], radiosonde observations from the nearest weather station Bor (see Chapter C2.1) can enlighten the temperature profile above. The data from the sounding on 3.1.10 in Figure 21 shows an even further temperature increase up to 1.5 km height. At this altitude the wind speed reaches a local maximum. Below this

C Analysis of CO_2, CH_4 concentration and meteorological time series

height, the wind speed decreases strongly, and the change in the wind direction indicates a complete decoupling of the free tropospheric air from the ground.
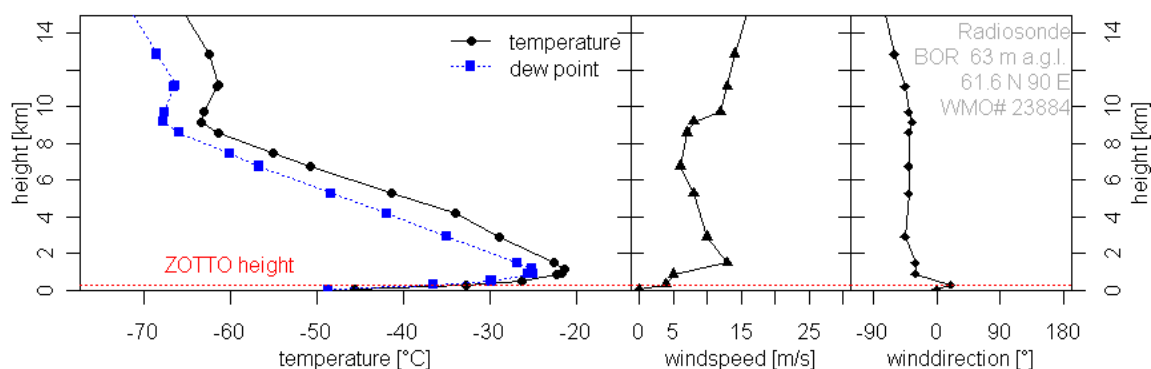
Figure 21 *Radiosonde data (temperature, wind speed, and wind direction) from neighbored station Bor on 3.1.2010 at 7:00am KRAT from NOAA/ESRL Radiosonde database www.esrl.noaa.gov/raobs/*

The most prominent peak in the CH_4 time series in Figure 19 occurs on January 18, 2010. The corresponding CO_2 and CH_4 observations and the pressure and temperature measurements are summarized in Figure 22. Interestingly the strongest decrease in the 301 m CO_2 observation coincides with abrupt increases in temperature at this level (Figure 22c). This indicates that overlaying warm air masses have been mixed into the lower layers. This upper air is depleted in CO_2, because it did not have contact to the sources on the ground for a long time.
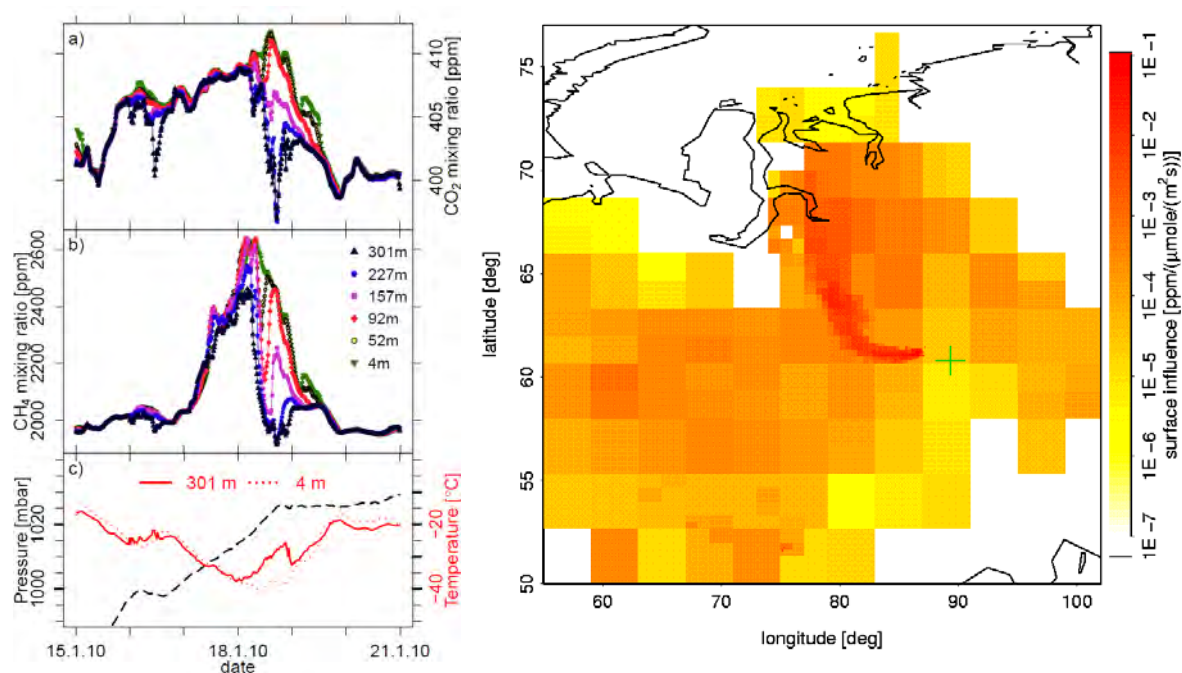
Figure 22 *Time series of various parameters during the CH_4 spiking event on January 18, 2010:* **a)** *CO_2 and* **b)** *CH_4 mixing ratio,* **c)** *temperature and pressure* **d)** *footprint at 301 m*

Fossil fuel burning or natural gas production sites are potential reasons for the distinct CH_4 spikes during winter (Figure 22b). This is emphasized by the surface influence function in Figure 22d, which was computed with the STILT transport

C Analysis of CO_2, CH_4 concentration and meteorological time series

model. It describes the origin of the air that has been sampled on January 18, 6 am at 301 m level and indicates westerly winds, where large Russian oil and natural gas production sites are located. Some skepticism arises, when the distance to these sources is taken into account. The oil and gas production are located more than 300 km away (satellite images). Former studies suggest that this might be too far to notably modify the air constitution at ZOTTO. Tohjima et al. [1996] discovered CH_4 mixing ratios of 2900 ppb in only 150 m altitude above an oil production site, while the signal has already been vented away in 250 m altitude. Moreover, natural gas emissions sum up to 1 to 10 % of the overall wetland emissions only, and emissions from leaking pipes in cities dominate over the one from pipelines from the production sites [Tarasova et al., 2009].

In conclusion, the CH_4 spikes in winter most likely originate not directly from fossil fuels, but the same process as the decoupled CO_2 mixing ratios from different tower heights that has been described before. The indicators are less clear and the CH_4 spikes do not always coincide perfectly in time with decoupled CO_2 mixing ratios at different tower levels. However, enriched CH_4 concentrations at 301 m level correlate to enhanced CO_2 mixing ratios at the top of the tower, and all CH_4 spikes occur at temperatures below ~ -20 °C. Hence, it is likely that the cold air forms a temperature inversion that keeps the local air close to the ground. Wind measurements are rarely available in the winter period due to icing of the instrumentation, but they indicate low wind speed and varying directions and therefore support the argumentation. This air layer accumulates CO_2 and CH_4.

This winter phenomenon has been witnessed on subcontinental scale in Western Siberia, when CH_4 enrichments above 2000 ppb occurred during high pressure situations in combination with temperature inversions with temperatures below -20°C [Sasakawa et al., 2010].

The origin of the gases remains uncertain. The biosphere is mostly inactive, although the heavy snow cover insolates the ground and cools the soil to a few degrees below zero only and freezes to less than 1.28 m depth. The biosphere releases only small amounts of the gases that would allow increases of up to ~2.6 ppm CO_2 per day [Eneroth et al., 2003]. Fossil fuel emissions are an unlikely cause as well; because horizontal transport from large polluters are suppressed during the temperature inversion conditions, and local sources are unlikely to correlate on distances of hundreds of kilometers. Moreover, no strong CO increase has been detected that would have indicated burning processes [Kozlova et al., 2008]. Another hypothesis would be a physical demixing of the gases towards the ground, as the increase on low tower levels often coincides with a decrease above. It is known that air is gravimetrically separated in its components in the upper atmosphere (thermosphere), but e.g. an increase of Argon has been observed also close to the ground driven by thermal and gravimetrical diffusion [Adachi et al., 2006]. However, diffusion would separate CO_2 and CH_4 conversely, as CO_2 is lighter and

CH_4 heavier than air. Hence, it is worth looking for common characteristics: both are greenhouse gases. With the low water vapor concentrations CO_2 and CH_4 become important for the radiation budget. CO_2 rich air layers experience a stronger radiative cooling [Panofsky, 1947]; thus, they may subside preferably and accumulate close to the ground. Despite all hypotheses, the true answer remains open, but the ZOTTO data may trigger further studies.

C2.5 Diurnal cycle throughout the year

After the analysis of the long-term trends, which describe continental to global features of the carbon cycle, and after the synoptic events in winter, which affects the air masses on subcontinental scale, the diurnal cycle should give information about local carbon exchanges. The ZOTTO setup has excellent qualifications for a detailed investigation.

The specifications of the measurement system with its implemented air buffer volumes and the fast line-to-line switching allow for a quasi-continuous measurement from all tower heights with only one instrument (see B2.1). Furthermore, they remove short term fluctuations from atmospheric turbulences. Such fluctuations have for example been observed in the Bialystok time series of CO_2 at the 300 m top level [Popa et al., 2010], with a standard deviation of 3 min integrated samples over 40 min (the buffer integration time) yields 1.1 ppm during July 2009. This facilitates interpretation when using atmospheric transport models, which do not represent turbulence. As a side effect, the buffered, less variable data takes full advantage of the low-noise analyzer signal.

The low-noise measurements provide six dense, clear structured time series from different tower height levels (Figure 23b). As the air buffer volumes make each data point representative for the time, when the other air lines are sampled, the consecutive measurements from the different heights can be interpreted as a snap-shot of the vertical profile along the tower.

Compared to other up-to-date tall tower data series, where a distinct diurnal cycle in CO_2 and CH_4 profiles usually becomes visible on monthly average only (e.g. July 2009, Figure 23a), it can be seen already on hourly timescales in the ZOTTO data, e.g. during the summer night from 22nd to 23rd of July 2009 shown in Figure 23b. Immediately after sunset, the ground cools faster than the overlaying air, because it has a broader long wave radiation spectrum. Thus, the air in the lower 300 to 500 m stratifies to a stable nocturnal boundary layer [Stull, 1988]. This inversion layer traps the emitted CO_2 and CH_4 at night. The closer to the ground the air parcel is located, the higher the concentration rises. As soon as the morning sunlight warms the surface again (starting shortly before 06:00, Figure 23), the air is vertically mixed from the ground and the carbon that was trapped in the surface layer is diluted with increasing air layer thickness. Thus, the concentration differences between adjacent tower heights fade away until they all reach the concentration of the well-mixed

boundary layer during the day. The concentration profiles generally behave similar throughout the summer season, but the concentrations of different heights split up at varying times. Occasionally, local convective transport merges the concentration time series of different levels and large-scale transport may alter the concentration at all levels.
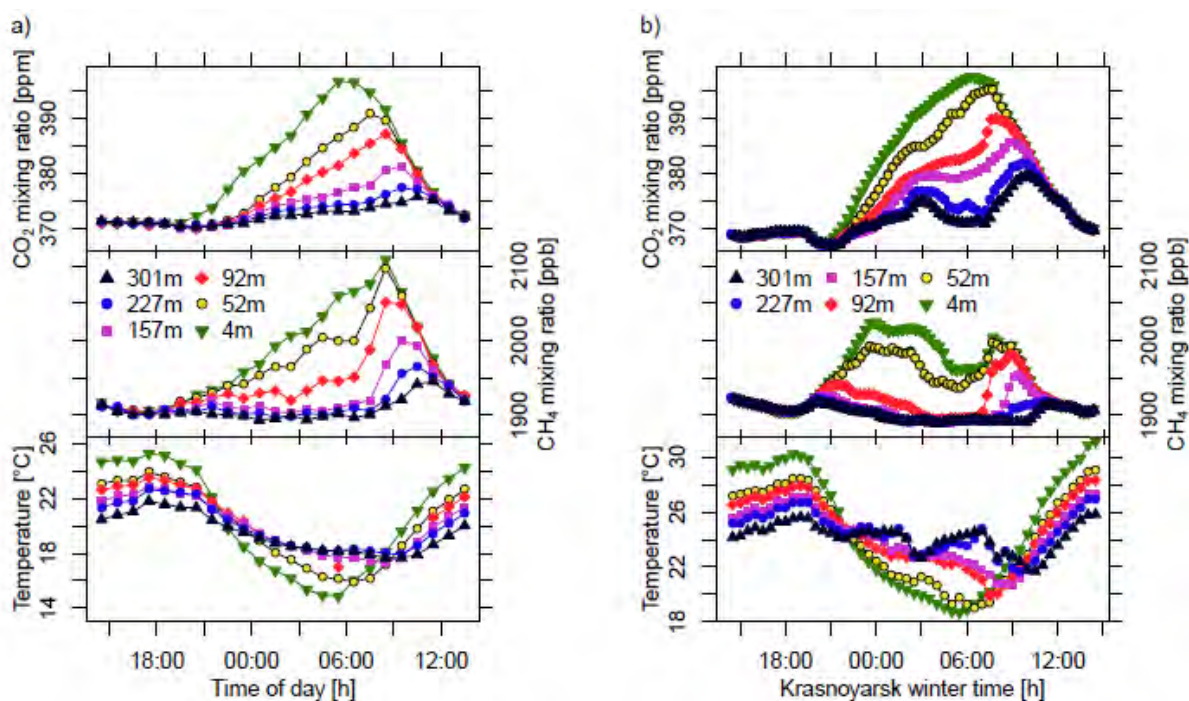
Figure 23 *ZOTTO time series from 6 tower heights for CO_2, CH_4, and temperature:* **a)** *average July 2009;* **b)** *in-situ data from July 22nd to 23rd, 2009*

Throughout the whole year, the CO_2 diurnal cycle is dominated by the diurnal cycle of the boundary layer. At night, all emitted gases are kept close to the ground through a temperature inversion. The intensity of the vertical mixing is tightly coupled to the solar radiation. Thus, in the morning hours, the heated and CO_2/CH_4 enriched air gets lifted up from the ground and passes by the 301 m level of ZOTTO (Figure 24). During this time, the measured concentrations are no more representing the overlying residual layer, whose air was representative for a large region from the previous day. In the course of the day, the boundary layer gets fully mixed again and represents a larger region again. This is especially important for model simulations on regional scale (Chapter E).

The observed CO_2 amplitude of 30 ppm at ZOTTO in Figure 24 is comparable to the one measured at other tall towers [Popa et al., 2010; Vermeulen et al., 2011]. The summer months June-September 2010 have been 2.2 °C colder compared to 2009, which may explain the weaker diurnal cycles in 2010 due to reduced respiration. During winter the absence of sunlight leads to a stratified atmosphere, where all tower height levels are decoupled from each other.
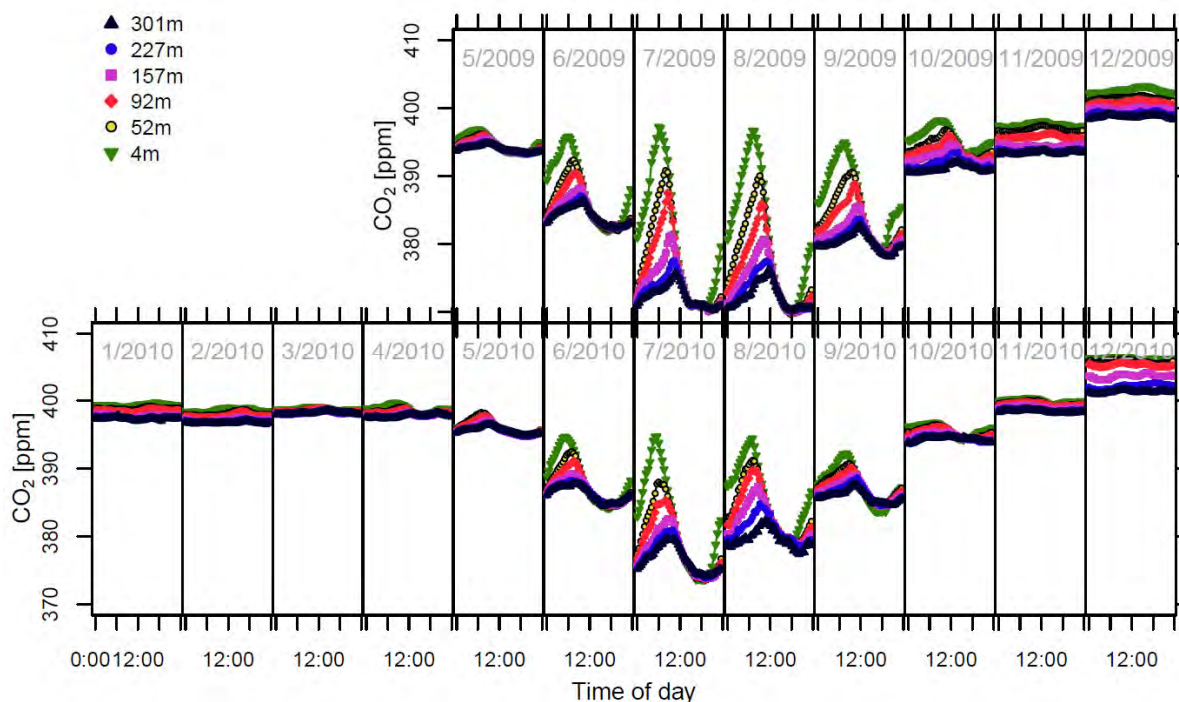
Figure 24 *Average CO₂ diurnal cycle for individual months*
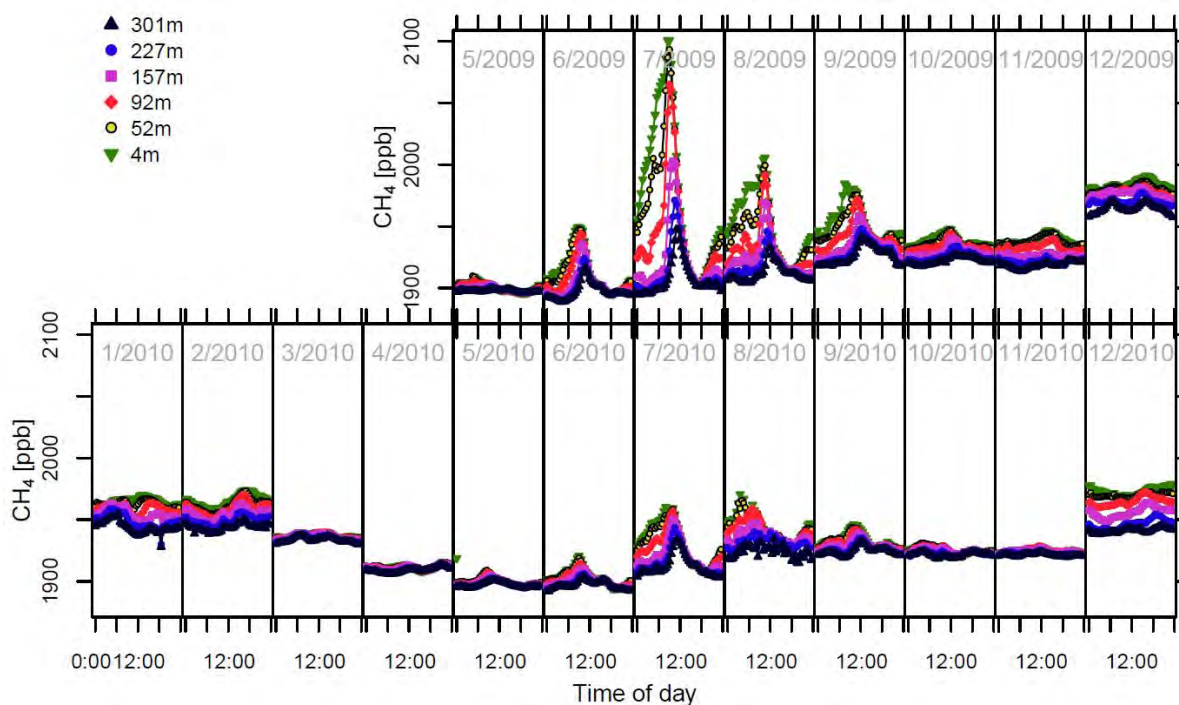
Figure 25 *Average CH₄ diurnal cycle for individual months*

For CH_4 the diurnal variations are shown in Figure 25. The amount of CH_4 emitted into the lower atmosphere during summer is much higher than in the other months. The maximum of ~200 ppb amplitude in July is induced by changes in the boundary layer mixing height. The largest contributions are expected from wetlands in summer, which is confirmed by the more intense diurnal cycle than compared to a European rural site with ~80 ppb for June-September 2006 [Popa et al., 2010].

C Analysis of CO₂, CH₄ concentration and meteorological time series

Emissions from fossil fuel (incl. production, transport and distribution of coal and natural gas) drive the general increase of CH_4 concentrations during winter [Sasakawa et al., 2010].

C3 Conclusions

Of particular interest is the measurement series from the highest 301 m level of the ZOTTO site. Although the actual value of the time series for climate research lies in its longevity, it already allows some basic conclusions. The observed CO_2 growth of 2.62 ppm/yr in the year 2009-2010 is higher than the global average. This result is the consequence of anomalous weather conditions in the summer 2010. The heat wave in the European part of Russia with extensive forest fires and the cool summer in western Siberia caused increased CO_2 mixing ratios at ZOTTO in 2010, thus, an above global average growth rate. The seasonal cycle of CO_2 is characteristically high with 28.3 ppm for a continental station. The CH_4 data series is basically flat with low seasonal signals.

On shorter time scales of days to months, large scale climate alterations become visible in the CO_2 and CH_4 signals. Especially in winter under high-pressure and low-temperature conditions, a strong temperature inversion has been observed. The different air layers that are captured by the 301 m tower height show decoupled gas mixing ratios over several days.

The fully time-resolved CO_2 and CH_4 measurements illustrate numerous individual events, whose interpretation leave challenges for transport models. The winter anomalies or the numerous local emission events from anthropogenic fossil burning, natural wetlands, or forest fires cannot always be attributed to the right emission source. However, atmospheric measurements make it possible to add these events to the overall carbon budget, because all these emissions end up in the atmosphere, even without necessarily knowing all underlying processes in detail.

The unique characteristics of the ZOTTO setup give temporally highly resolved information from all tower height levels. This continuous surveillance of concentration profiles along the tower allows for analyzing the data for individual days instead of long-term averages only. The average diurnal cycle of the CO_2 and CH_4 profiles reveals the importance of the boundary layer dynamics on the observed mixing ratios. The amount of carbon that is captured in the nocturnal boundary layer enables the quantification of carbon fluxes. These flux estimates are presented in the next Chapter D.

D Local flux estimates from tower profiles

"When we try to pick out anything by itself,
we find it hitched to everything else in the universe."
John Muir (1838-1914)

D1 Introduction

The ZOTTO setup provides gas concentration measurements of the atmosphere. The final scientific goal is the quantification of the carbon exchange between different ecosystem components and the atmosphere. Information about the spatial distribution of sources and sinks of greenhouse gases facilitates the interpretation of these concentration measurements.

The Siberian region is currently only sparsely covered by CO_2 flux measurements [www.fluxnet.ornl.gov], whereas several tens of stations are in service e.g. in the North American boreal zone. In the 1990s, in the Asian boreal forest region, CO_2 flux measurement sites were established in Yakutsk, Zotino [Heimann, 2005], and Tura [Nakai et al., 2008]. In the vicinity of ZOTTO, eddy measurements were operating from 1996 to 2004 [Schulze et al., 1999; Valentini et al., 2000].

The carbon cycle is determined not only by CO_2, but also CH_4; however, the annual magnitude of CH_4 flux is more than a factor of 20 smaller [Lloyd et al., 2002b; Rinne et al., 2007]. Usually, CH_4 fluxes are assessed by chamber measurements, which approximately represent the size of only one square meter. The first annual cycle of CH_4 fluxes measured by the eddy covariance technique was recorded only recently [Rinne et al., 2007].

The area represented by eddy covariance flux measurements is about 1 km² [Davis et al., 2003]; thus, the informative value is restricted to local signals. To further expand this area, mixing ratio measurements are performed on tall towers (> 200 m) [Bakwin et al., 1998; Haszpra et al., 2001; Vermeulen, 2007]. Transport inversion models make use of these concentration measurements on high altitudes to estimate surface-atmosphere fluxes on global scale [Rödenbeck et al., 2003; Bergamaschi et al., 2009].

The combination of profile information from a tall tower and eddy covariance data allows for flux estimates on intermediate scale (local to regional), as studies in northern Wisconsin, USA [Davis et al., 2003] and Hungary [Haszpra et al., 2005] exemplarily demonstrate.

Nevertheless, the CO_2 fluxes in the near-field (within about 100 km radius) dominate the measured signal even on tall tower sites. The near-field signal originates from the atmospheric boundary layer and superimposes the far-field contributions from the free troposphere [Gerbig et al., 2009]. Therefore, the knowledge of concentrations in the free troposphere allow for boundary layer budgeting methods, which represent the regional scale with one day footprint areas of 10^4 - 10^6 km² [Bakwin et al., 2004; Helliker et al., 2004]. Such a method applied to aircraft profile measurements over the ZOTTO site provided flux estimates of -3.3 to -9.6 µmol/m²/s for two summer days in 1996; but associated uncertainties ranged up to 11.8 µmol/m²/s due to unknown entrainment fluxes [Lloyd et al., 2001]. To further constrain the entrainment flux, profile data from a tall tower can additionally be used to estimate regional fluxes [Chen et al., 2007; Wang et al., 2007].

Various circumstances hinder the correct assignment of the measured fluxes to the original source area. Firstly, it is crucial to understand the transport of the analyzed air parcels, e.g. whether the pathways come from the polar region, from Europe or the nearby Central Siberian area [Eneroth et al., 2003; Paris et al., 2010b]. The local topography complicates the interpretation, because it induces mesoscale atmospheric circulations. These circulations drive a CO_2 accumulation in the Yenisei River basin in the transition from the west Siberian lowlands to the east Siberian plains [van der Molen et al., 2007]. On even smaller scale, Flessa et al. [2008] observed heterogeneities in CH_4 fluxes depending on landscape patterns such as forests, and bogs. On these small scales, investigations are limited by the coarse spatial resolution of the ecosystem classification in biosphere models.

Examining all the different techniques for flux estimates on different scales, many of them would not be applicable due to too few currently available data streams at the ZOTTO site. Therefore, it is made use of the CO_2 and CH_4 profile data in combination with the wind measurements from ZOTTO to estimate fluxes on intermediate scale in this Chapter D. At first, the flux estimation method is introduced. Then, the method is applied to the continuous CO_2/CH_4 concentration data. The last section summarizes the investigation.

D2 Methods

The measurement system at the ZOTTO site provides time series of CO_2, CH_4 and meteorological data, such as three dimensional wind from six tower levels (301 m, 228 m, 158 m, 92 m, 52 m, 4 m) from May 2009 to December 2010 [Winderlich et al., 2010]. Chapter D2.1 gives an overview, how the meteorological measurement allows assessing surface-atmosphere exchange fluxes for CO_2 and CH_4 at intermediate scales.

The different data streams are combined at a temporal resolution of 30 minutes. All times are given for the local Krasnoyarsk time zone (KRAT = UTC + 7 h), which is shifted by one hour compared to solar time (KRAT = LOC + 1 h).

The three spatial directions of the wind are measured with 3D wind anemometers (Gill Instruments Ltd., UK, type: R3) with 10 Hz frequency. Every 30 min, the mean $\bar{u}$ and the fluctuating part u' around that mean (Reynolds averaging) of each wind component are recorded. The vertical wind measurement is corrected for sensor tilt with a sinusoidal fit (see Chapter B2.8)

During winter, the wind sensors are very vulnerable to icing, thus, all winter data is not available for the flux analysis. Therefore, the data analysis focuses on the summer months, when the largest biotic activity signals can be measured.

D2.1 Micrometeorological flux estimates

The mass conservation inside a certain volume in the atmosphere determines the source strength S of a certain gas as a function of time t and place (x, y, z) [Businger, 1986; Baldocchi et al., 1988]:

$$S(t,x,y,z) = \frac{\partial c}{\partial t} + \frac{\partial uc}{\partial x} + \frac{\partial vc}{\partial y} + \frac{\partial wc}{\partial z} + D\frac{\partial^2 c}{\partial x_i^2}$$

(10)

where u, v, w are the wind components in x, y, z direction and c is the concentration of the observed gas. Hence, the net ecosystem exchange *NEE* can be calculated [Finnigan, 1999; Yi et al., 2000; Feigenwinter et al., 2004]:

$$NEE = \int_0^{z_r} \frac{1}{V_m} s(t,z)dz + \left(\frac{1}{V_m} \cdot \overline{w'c'} \right)_{z=0}$$

(11)

given the molar volume $V_m(z) = M_{Air} / \rho_{Air}(z)$ and the height of the control volume z_r. After combining equation (10) and (11), followed by Reynolds averaging ($u = \bar{u} + u'$, etc.), the *NEE* splits up into the following terms [Yi et al., 2000; Aubinet et al., 2005; Feigenwinter et al., 2008]:

$$NEE\cdot = \int_0^{z_r} \frac{1}{V_m} \cdot \frac{\partial \bar{c}}{\partial t} dz \qquad\qquad \text{Storage } F_{Stor}$$

$$+ \frac{1}{V_m} \cdot \overline{w'c'}(z_r) \qquad\qquad \text{Eddy turbulence } F_{Eddy}$$

(12)

$$+ \overline{w}(z_r)\left(\frac{1}{V_m} \cdot \bar{c}(z_r) - \frac{1}{z_r}\int_0^{z_r} \frac{1}{V_m} \cdot \bar{c}(z)dz \right) \qquad \text{Vertical advection } F_{vAdv}$$

$$+ \int_0^{z_r} \frac{1}{V_m} \cdot \left(\bar{u}(z)\frac{\partial \bar{c}(z)}{\partial x} + \bar{v}(z)\frac{\partial \bar{c}(z)}{\partial y} \right)dz \qquad \text{Horizontal advection } F_{hAdv}$$

D   Local flux estimates from tower profiles

The individual terms are discussed in detail in the subsequent sections. The sign convention used here gives positive *NEE* for ecosystem emissions, where a positive flux term (= source) corresponds to a transport out of the control volume [Feigenwinter et al., 2004].

Generally, the total flux is estimated on a monthly timescale. Thus, synoptic events such as front passages [Hurwitz et al., 2004] are averaged out.

D2.2 Storage flux

The storage term F_{Stor} in equation (12) describes the amount of carbon that is accumulated over time below the observation height z_r. For illustration, the diurnal development of the CO_2 profile along the tower is given in Figure 26. During night, the atmospheric conditions are calm and the gases that are emitted from the surface accumulate in the stratified nocturnal boundary layer. With sunrise two processes start: 1) photosynthesis assimilates the CO_2 close to the ground and 2) heat drives upward turbulent transport of CO_2 enriched air parcels. At noon, the atmosphere is well mixed, photosynthesis reduces CO_2 concentration at all heights.
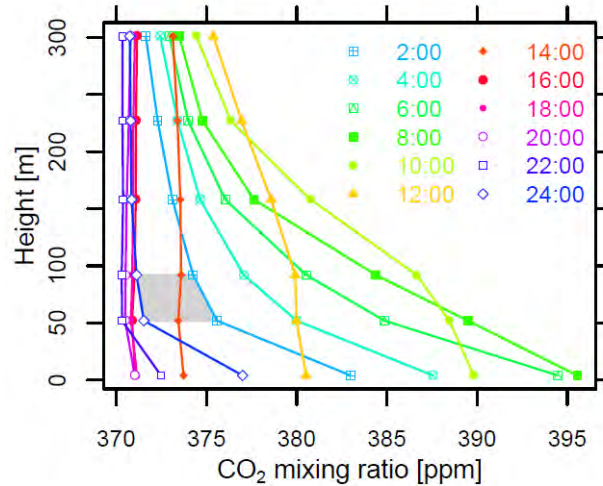
Figure 26 *Average diurnal development of the CO_2 profile along the tall tower during July 2009; grey shaded area illustrates storage flux component between 52 m and 92 m level*

According to equation (12), the storage flux can be visualized through trapezoidal areas between the half-hourly time steps and the different tower heights (grey shaded area in Figure 26), thus, it adds up to:

$$F_{Stor}\left(t_i,z_h\right) = \int_{z_{h+1}}^{z_h} \frac{1}{V_m} \cdot \frac{\partial \overline{c}(t_i)}{\partial t} dz = \int_{z_{h+1}}^{z_h} \frac{\rho_{Air}(z)}{M_{Air}} \cdot \frac{\partial \overline{c}(t_i)}{\partial t} dz$$

$$\cong \sum_{h=1}^{5} \frac{\frac{1}{2}\left(\rho_h + \rho_{h+1}\right)}{28.9644\,g/mol} \cdot \frac{\frac{1}{2}\left(\left(c_h(t_{i+1}) - c_h(t_i)\right) + \left(c_{h+1}(t_{i+1}) - c_{h+1}(t_i)\right)\right)}{t_{i+1} - t_i} \cdot \left(z_h - z_{h+1}\right)$$

(13)

with the air density ρ, mixing ratio c, and height z. The index $h = 1\ldots6$ describes the tower levels ($z_1 = 301$ m, …); index i marks the different time steps. To cover the full

tower height, the storage flux terms between all heights are summed up and the mixing ratio below 4 m is assumed to be constant.

During night from 23:00 to 4:00 am, before atmospheric mixing starts again, the storage flux F_{Stor} dominates the total flux in equation (12) (see Figure 26). If the trapped amount of carbon is interpreted as a result of a homogeneously distributed flux field, nighttime respiration fluxes can be estimated.

The varying concentration at the 301 m level indicates that some CO_2 escapes aloft. In the present approach, the flux beyond 301 m can only be captured by including other flux components, like the eddy flux.

D2.3 Eddy flux

The carbon flux of ecosystems is commonly detected by the eddy covariance method. The underlying essential condition is wind and gas concentration measurement at high frequency (~ 5-40 Hz). Restricted by the measurement frequency of the CO_2/CH_4 analyzer (0.2 Hz), the long tubing (up to 320 m), and the deployment of buffer volumes (mixing time ~ 40 min. ~ 0.0004 Hz) the ZOTTO data does not allow direct eddy flux measurements, F_{Eddy}.

Several alternative methods for flux detection are presented in the literature [Businger, 1986; Verma, 1990; Moncrieff et al., 1997]. Following these approaches, it can be assumed that turbulent eddies act similar to molecular diffusion and distribute proportional to the vertical concentration gradient. By introducing the eddy diffusivity K_C it can be written:

$$F_{Eddy} \cdot V_m = \overline{w'c'} = K_C \frac{dc}{dz} \tag{14}$$

The Bowen ratio method gains the information about K_C by presuming the same atmospheric transport for heat, water vapor, and other trace gases. Thus, the sensible heat flux measurements H can be used from all heights at ZOTTO. H can be calculated out of the potential temperature gradient dT_{pot}/dz:

$$H = \rho_{Air} C_P K_T \frac{dT_{pot}}{dz} \tag{15}$$

The same transport for gas and heat implies $K_C = K_T$. The combination of equation (14) and (15) and following the "modified Bowen ratio method" [Businger, 1986] obtains:

$$F_{Eddy} = \frac{H}{C_p \cdot M_{Air}} \frac{\partial c / \partial z}{\partial T_{pot} / \partial z} \tag{16}$$

The concentration and temperature gradients between two adjacent tower heights are used to compute the eddy fluxes at five intermediate levels (28 m, 72 m, 125 m, 193 m, 264 m).

D Local flux estimates from tower profiles

The ratio of two noisy signals results in unreasonably large numbers, e.g. when dividing by a potential temperature difference close to zero. Instead of excluding fluxes that exceed certain thresholds (as in Werner et al. [2003]), the errors of the measurement are propagated (ΔCO_2 = 0.05 ppm, ΔCH_4 = 2 ppb, ΔTemp = 0.3 K, $\Delta H/H$ = 10 %, Δz = 1 m) and all 30 min flux data for which the error exceeds the signal are omitted.

The question arises about the dependence of the eddy flux on measurement height. In a horizontally uniform area, without advection and sources/sinks in the atmosphere, the turbulent flux is uniform over different heights [Baldocchi et al., 1988]. But during night, the flow becomes less turbulent, especially at higher altitudes. Thus, eddy measurements are preferred at the lowest level (30 m), to avoid increasing influence of storage and advection. Moreover, flux estimates from height levels above are influenced by a larger footprint, which strongly depends on the turbulence regime [Davis et al., 2003].

D2.4 Vertical advection

The integral in the vertical advection term in equation (12) gives the average gas concentration $\langle c \rangle$ within the observed air volume. Hence, vertical advection is the concentration difference to the overlaying air c_r times the vertical velocity $\overline{w}_r$:

$$F_{vAdv} = \overline{w}(z_r)\left(\overline{c}(z_r) - \frac{1}{z_r}\int_0^{z_r}\overline{c}(z)dz \right) = \overline{w}_r\left(c_r - \langle c \rangle\right) \tag{17}$$

With the detection of a non-zero mean in vertical wind velocity, Lee [1998] recommends not to ignore the advection term, particularly during night and over tall vegetation. A systematic underestimation of *NEE* during periods of weak atmospheric mixing has been attributed to drainage flows of advection [Davis et al., 2003; Feigenwinter et al., 2004]. Particularly during the morning hours, comparisons of *NEE* measurements on different tall tower levels suggest that advection can temporary dominate the total flux [Yi et al., 2000]. The underestimation of *NEE* by advection may be as large as 5-40 % [Loescher et al., 2006]. At tall towers the impact of total advection is estimated to be about 10 % on the overall flux [Yi et al., 2000].

Vertical advection was often observed to direct towards the soil in stable conditions, because of entrainment by katabatic flow close to the ground at sloping sites or leaf cooling. Depending on the topographic characteristic of the site, the vertical advection varies between 0.1 – 10 µmol/m²/s [Aubinet et al., 2005].

Investigating the fluxes at three different eddy covariance sites, vertical advection occurs only during night and is strongly site dependent as it is strongly influenced by the local topography [Feigenwinter et al., 2008].

D2.5 Horizontal advection

Horizontal advection is driven by the lateral flow of air (equation (12)). As there is no information about the horizontal distribution of CO_2 and CH_4, it is intrinsically impossible to judge its contribution to the measurement signal.

Presently, the eddy covariance community dedicates much investigation to the advection topic [Aubinet et al., 2005; Feigenwinter et al., 2008]. Whereas vertical advection especially increases in the morning, horizontal advection balances the vertical components during the whole night and can remain during the day [Feigenwinter et al., 2004]. But in general, there has been no clear relationship observed between vertical and horizontal advection. Advection is site dependent and mainly influenced by topography or land cover heterogeneity induced breezes [Aubinet, 2008; Aubinet et al., 2010]. Including only one term in the total flux estimate make it even worse than using none [Finnigan, 1999]. In cases where the advection estimates showed unrealistic results, they have been disregarded completely [Haszpra et al., 2005]. On longer timescales, the advection parts are assumed to be negligible over many synoptic cycles [Davis et al., 2003].

The above findings imply the necessity of a careful handling of advection data. The ZOTTO site is located on top of a small hill in a generally flat terrain with gentle slopes between heights of 50 and 150 m. Due to its location on the hill top, cooling air masses are likely to flow down-slope away from the tower and will deplete the air during the night. From this point of view, a positive sign is expected for the vertical and horizontal advection term, although there has been little advection seen at another site on a mountain top (Wetzstein site) [Feigenwinter et al., 2008].

Compared to the eddy sites, ZOTTO is much taller and low level jets may alter the advection flux as well. Low level jets have been observed in the US great plains with above average wind speeds at ~200 m height [Bonner, 1968; Sisterson et al., 1978; Kraus et al., 1985; Kurbatskiy et al., 2010; Van de Wiel et al., 2010].

Mesoscale models simulated a nocturnal buildup of CO_2 in the Yenisei River basin about 30 km east of the station [van der Molen et al., 2007]. In combination with the drainage in the morning of the accumulated air, a mesoscale circulation may occur. Easterly winds may blow CO_2 enriched air towards the tower, corresponding to a negative horizontal advection component during day.

D2.6 Contamination by local sources

The diesel engines used for power generation at the ZOTTO station are located about 150 m south east of the tower, and may alter the CO_2 measurements. The station consumes approximately 80 l fuel per day. Twice a week, about 10 kg wood is used to fire the sauna. The typical emissions for diesel engines are approximately 2.65 kg CO_2 per liter fuel, and 0.7-1.6 kg CO_2 per kilogram wood (fresh to air dried). This corresponds to an average emission of 9 kg CO_2 per hour (205 mol/h). In the

evening hours, when the fire burns (10 kg wood in 1 h), and the load is doubled for the generator, the emissions may rise up to 34 kgCO_2/h (772 mol/h). If these emissions are allocated to a circular area with 100 m radius, the total flux would be 1.8 – 6.8 µmol/m²/s. This worst case scenario is only true at calm wind conditions; but then, the heavier emissions may even flow gravimetrically driven down the slope away from the tower. If wind is blowing, in particular in the direction from the exhaust towards the tower, it is not possible to detect this short term emission events, due to the deployment of air buffer volumes in the measurement line. The placement of the buildings amidst the wind path cause further mixing and dilution of air.

To detect whether the emissions affect the *NEE* flux estimates, the nighttime storage flux (section D2.2) is plotted in wind rose form in Figure 27. The result implies no significant effect, because the fluxes in the direction of the generators (marked by the light yellow arrow) are not particularly elevated either in summer or in winter.
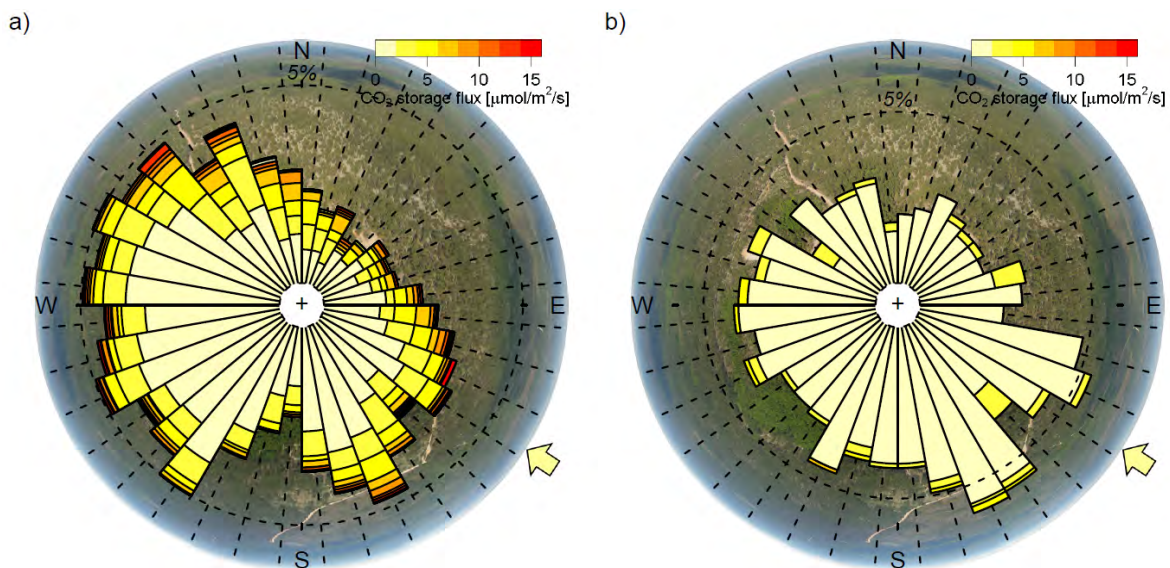
Figure 27 *Top view of ZOTTO centered on the tower with overlaid nighttime storage flux estimates (23:00 to 4:00) vs. wind direction.* **a)** *Summer months June-September,* **b)** *winter months November-February; overall length of the pedals give frequency how often flux from this direction is measured, arrow indicates direction of power generator*

D3   Results and discussion

D3.1 CO_2 storage fluxes

After analyzing all the diurnal time series, Figure 28 gives an overview of the full diurnal cycle of the CO_2 storage flux, F_{Stor}, in 2009 and 2010. May 2010 has been excluded because the lowest 4 m inlet line was blocked. The carbon amount that is stored during night in the nocturnal boundary layer gives a first idea of the respiration fluxes in the ZOTTO area. The average amount of 2.1 µmolC/m²/s flux from 16:00 to

4:00 am seems to be realistic as compared to ~2 µmolC/m²/s from a previous study [Schulze et al., 1999].
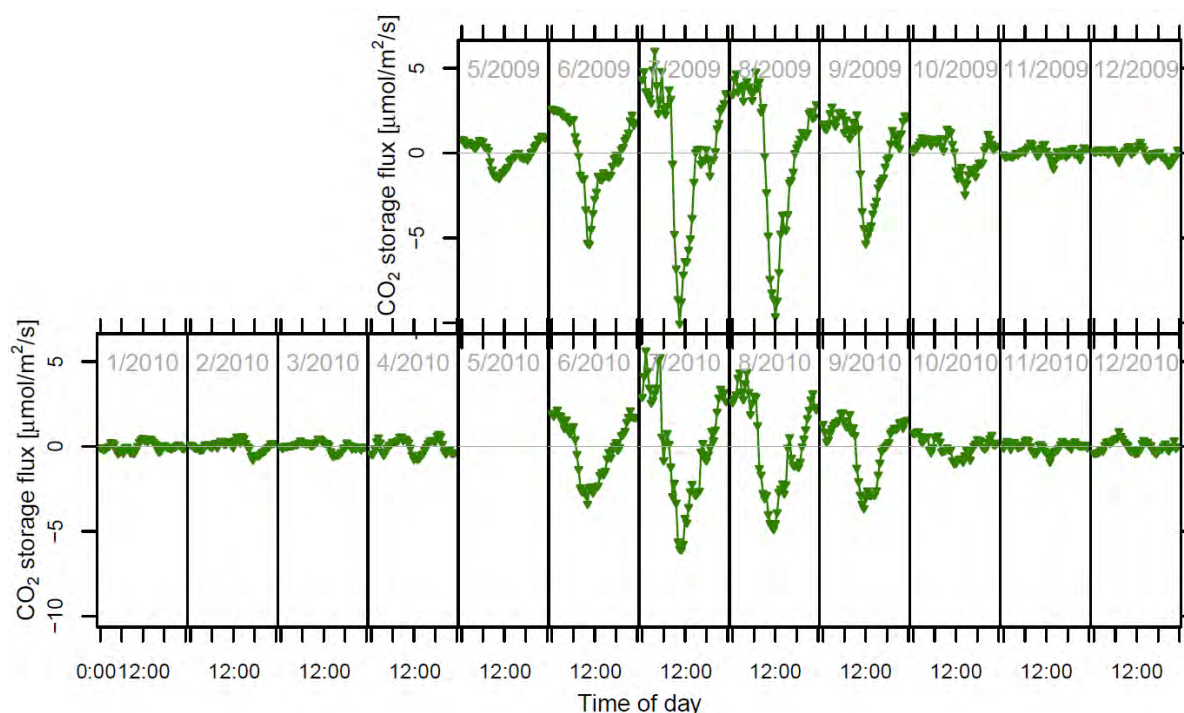
Figure 28 *Average diurnal cycle of the storage flux for individual months*

Figure 28 highlights a big advantage of a tall tower like ZOTTO over flux towers. Almost all CO_2 is captured, thus, the observed storage flux stays constant during the whole night. A decrease in the storage flux has been observed at different eddy covariance stations in Europe in the second part of the night [Aubinet et al., 2005], although there was no source decrease and no turbulence onset, but advection may explain the discrepancy. A small decline can also be seen in the nocturnal storage fluxes constrained by the tower levels below 52 m, but this is compensated, if the higher tower levels are included.

In the morning, the strong onset of mixing terminates the validity of the underlying assumptions, further flux components have to be taken into account to capture the full *NEE*.

D3.2 CO_2 eddy flux estimates

The Eddy flux estimates are based on the modified Bowen ratio method (Chapter D2.3). During day, the underlying heat flux measurements reach their maxima at 52 m level, where the turbulent fluxes are usually measured (Figure 29). The lowest level is below the canopy, causing it to miss the contributions from the canopy itself. On higher levels the flux transport is shifted from turbulent eddy transport towards larger scale advection. The same pattern appears in modeled eddy flux estimates [Sogachev et al., 2002].
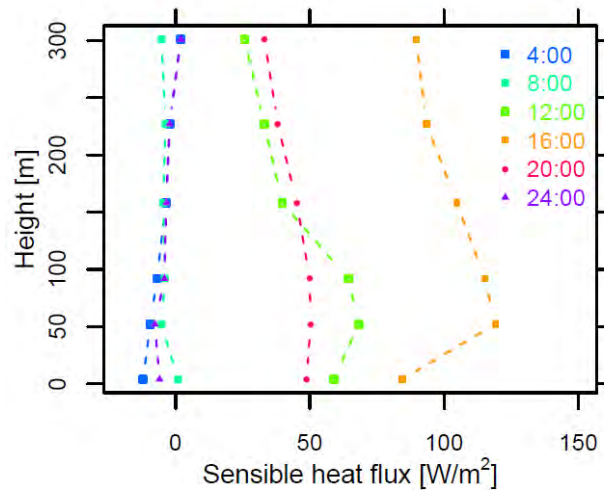
Figure 29 *Average diurnal cycle of the heat flux profile in July 2009*

The eddy flux estimates in Figure 30 do not allow such clear conclusions. The data is noisy and has gaps in the afternoon, when the errors became too large, mainly because the temperature differences between tower heights were too small.
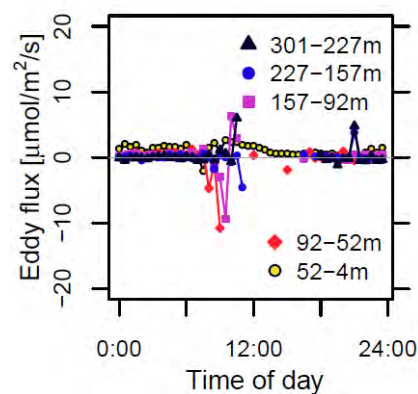
Figure 30 *Average diurnal cycle of the eddy flux for July 2009*

The basic assumption in equation (12) is a closed mass balance within the observed volume. Thus the usage of eddy flux data from one height demands the knowledge of storage fluxes from all heights below. If eddy covariance measurements are available, flux estimates are done for the heights with the larges signals; e.g. eddy flux at 30 m and gradient from 76-30m [Werner et al., 2003]. But at ZOTTO, the 301 m height of the tower allows for a much more accurate and, at least during night, an almost complete measurement of the storage flux; thus, storage flux is preferably used and the noisy eddy flux data give small corrections on the top tower level.

For a better understanding of the atmospheric stability, an overview of the 2009-2010 potential temperature distribution is give in Figure 31. In summer nights the stable layering becomes visible. During summer days, potential temperatures on all heights are the same as for the well-mixed boundary layer. This coincides with the maximum of the eddy fluxes. During winter, the air layers from the different heights

are decoupled especially during very cold periods below -20 °C, the turbulent transport is suppressed (Chapter C2.4).
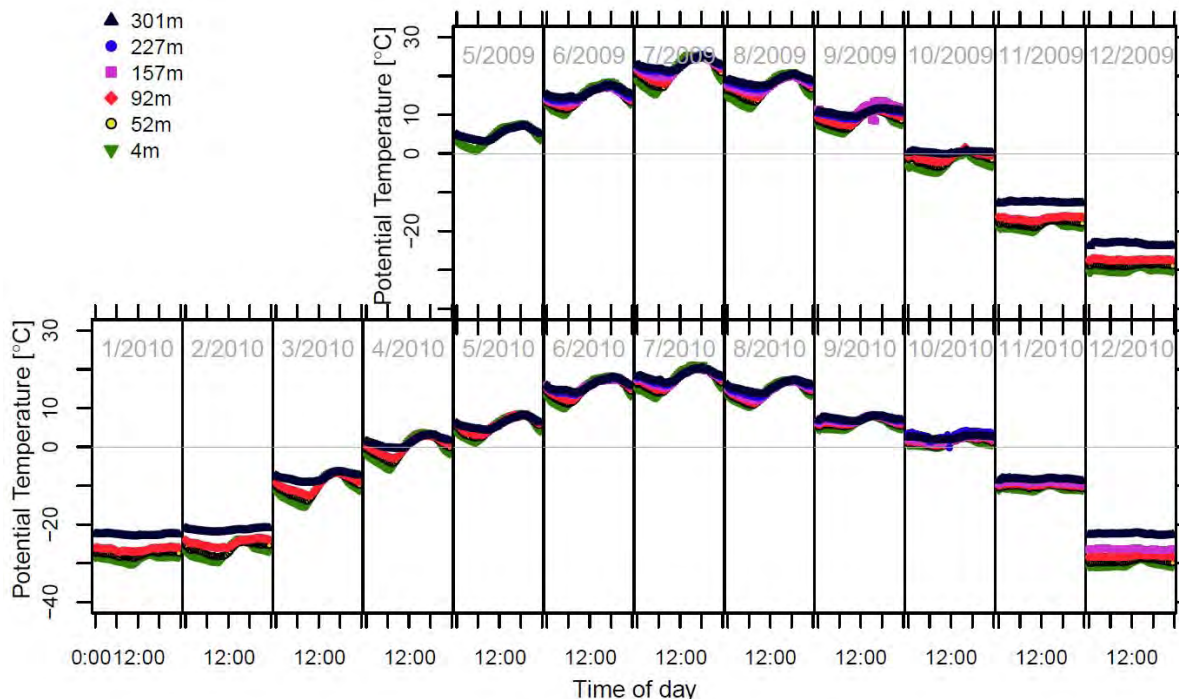
Figure 31 *Average diurnal cycle of the potential temperature for individual months*

D3.3 Advective CO$_2$ fluxes

Advection is a great unknown in flux calculations. Figure 32 gives an impression about the driving factors, the vertical wind speed and the concentration differences between the top of the control volume and the average concentration within the control volume ($c_r - \langle c \rangle$, equation (17)).
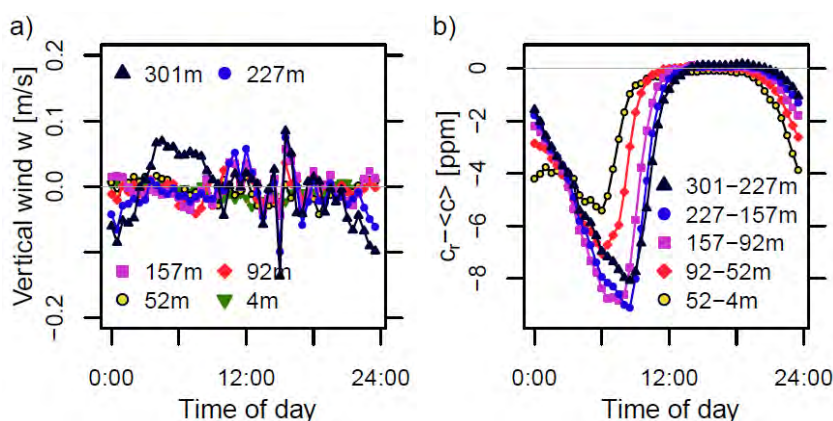
Figure 32 *Average diurnal cycle of components of the vertical advection:* **a)** *vertical wind speed and* **b)** *concentration difference in July 2009*

The time series of vertical wind at 52 m height during summer is comparable to the observations in Baldocchi et al. [2000] from 37 m height (most data points in between of -0.2 m/s and 0.2 m/s). On the 4 m level the wind speed decreases, with

D   Local flux estimates from tower profiles

higher altitudes the magnitude of *w* increases. The average speeds are close to zero, which implies the total advection flux to be close to zero as well. To allow advection flux estimates without knowing the exact vertical wind, Yi et al. [2000] and Feigenwinter et al. [2008] assumed a constant vertical wind speed at canopy height of -0.05 m/s or -0.01 m/s, respectively.

In contrast to Yi et al. [2000], the concentration difference $c_r - \langle c \rangle$, which correlates to the advection magnitude (Figure 32b), increases with tower height. Consequently, the calculated vertical advection has maximum values at the higher tower levels (Figure 33b).
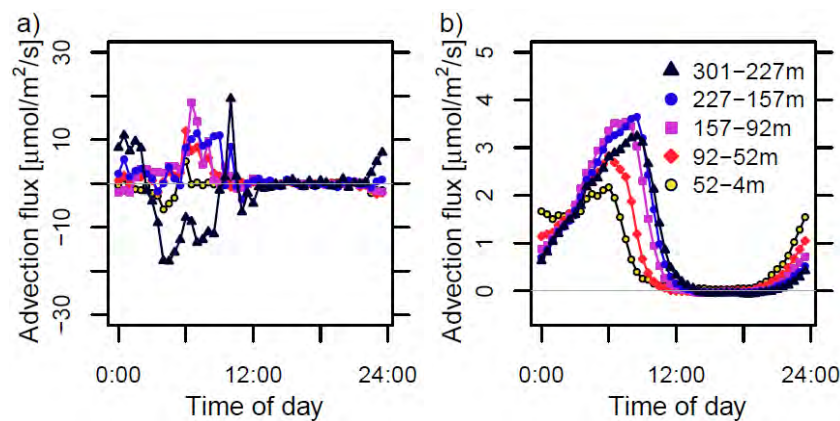
Figure 33 *Average diurnal CO_2 advection flux in July 2009 with **a)** measured vertical wind w **b)** with constant vertical wind w of -0.01 m/s*

The highest flux amplitudes up to 20 µmol/m²/s appear mainly during the morning hours, when the nocturnal boundary layer grows. As the magnitude of the vertical advection flux is dominating the total flux estimate, it is likely that it is partly compensated by horizontal advection. But without information about the horizontal CO_2 distribution, no horizontal fluxes can be estimated (see D2.5); accordingly contributions from advection are omitted in the combined flux estimate.

D3.4 Total CO_2 flux estimates

According to equation (12), the total flux includes storage, eddy, and advection components. Due to the large uncertainties in the advection fluxes, this part is excluded from the total sum. This was also done at other tall towers [Davis et al., 2003; Haszpra et al., 2005]. Including the vertical advection term would mainly increase nighttime and morning fluxes. They are likely to be compensated by the horizontal advection. This agrees with Chapter D2.5, where horizontal advection is assumed to lower *NEE* especially during the morning hours. But without knowing the horizontal advection term, the advective fluxes are ultimately ignored in the *NEE* estimates.

To solve equation (12), it has to be decided on the height level of the control volume. The comparison of calculations at different tower levels reveal that the

prominent negative photosynthesis peak in the morning transition occurs earlier when the eddy fluxes are used from lower tower levels (and, accordingly, the storage fluxes below this level). As it has been argued in D2.2, D2.3 and D3.1, the storage flux estimate is the most reliable flux component. In addition, the height of the tower is sufficient to capture most of the NEE as storage flux already, leaving the eddy flux as a day-time correction term.

In summary, the best and the most robust estimate appears to be the sum of the storage flux and the eddy flux at 301 m level.

All available eddy flux data can be summed up with the storage fluxes to achieve total *NEE* estimates (Figure 34). In the afternoon, due to the selection algorithm, only a few eddy flux estimates remain. For the monthly mean they have been omitted completely, if there were less than three data points left for a 30 min period. Those periods are marked in Figure 34 by grey dots. The error bars give the standard error of the mean of the monthly data.
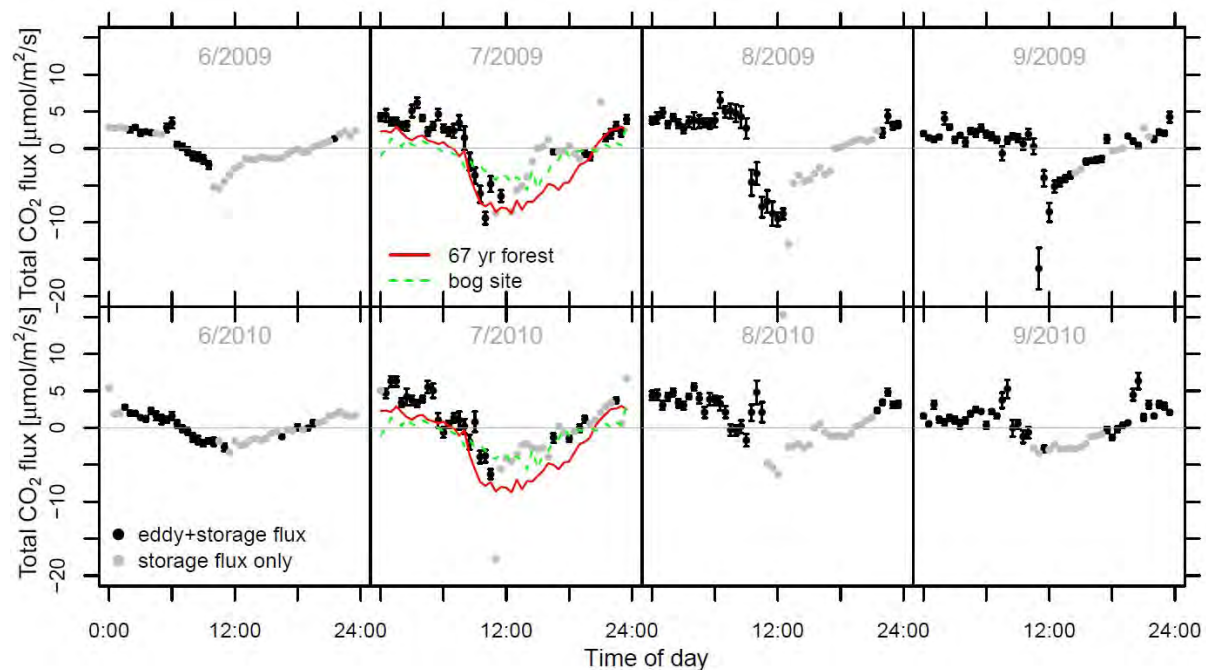
Figure 34 *Average diurnal cycle of the total CO_2 flux estimate with standard error of the mean for all summer months; colored lines in July are reference eddy covariance data from [Schulze et al., 1999]*

The *NEE* estimate in July 2009 compares well to estimates of previous investigations from July 1996 nearby Zotino [Schulze et al., 1999]. The use of this data set as a reference is backed by other data in the boreal zone [Davis et al., 2003; Wang et al., 2007]. Nevertheless, scientists have not corrected the eddy covariance flux measurements not for terms like storage fluxes or turbulence filtering in Schulze et al. [1999], which may cause a negative bias in the nighttime values [Aubinet, 2008]. Hence, the *NEE* estimate is – as expected – a little higher during night $(3.0 \pm 1.2 \ \mu molCO_2/m^2/s$ from 23:00 to 4:00) than the reference. In accordance with this finding, Acevedo et al. [2004] observed larger nocturnal fluxes through an

D   Local flux estimates from tower profiles

energy budget method than expected by the eddy covariance technique. Moreover, a flux decrease is not observed in the second part of the night [Aubinet et al., 2005], which was obvious in the 1996 reference data. The present study suggests that such behavior is a measurement artifact and could be avoided by using tall tower observations.

In the morning, the onset of photosynthesis dominates the flux. In July 2009, during the first half of day the photosynthetic uptake was well captured at about -8 µmol/m²/s. The other months show a slightly smaller carbon uptake, yet still in line with aircraft measurements over the site between -3.3 and -9.6 µmol/m²/s [Lloyd et al., 2001]. Some very negative outliers in September 2009 and July 2010 may be due to advection fluxes that have not been considered yet. This overestimation of the flux magnitude was already reported by Davis et al. [2003].

The shape of the diurnal cycle is not symmetrical to the noon time. A comparable pattern was observed at a tall tower in North America, where summer respiration rates are similar, but the photosynthetic uptake is more pronounced due to the more southern location at 46° N [Davis et al., 2003].

A shortcoming of the present method becomes visible in the well-mixed afternoon hours, when the mixing of air is not always captured (especially July 2009). Overall, the year 2010 showed less activity than 2009, this can be already seen in the mixing ratios, and was caused by the colder weather.

D3.5 Topographical effects

To study the influence of the topography on the observed CO_2 diurnal cycle, a run of the high-resolution "Weather Research and Forecasting Model" (WRF) was analyzed.

D Local flux estimates from tower profiles
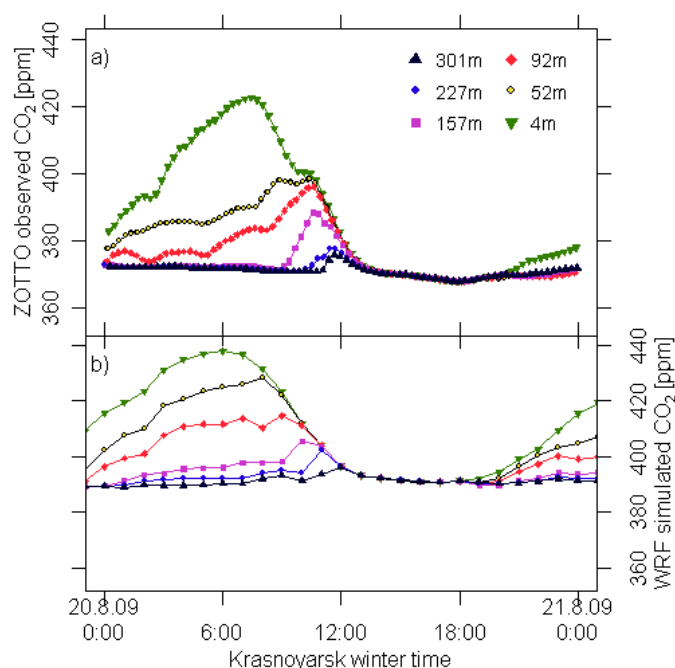
Figure 35 *CO_2 time series for 20 Aug. 2009:* **a)** *measurement at ZOTTO,* **b)** *simulation with WRF*

The comparison of the CO_2 model data with the measurements at the tower reveals a good expression of the general diurnal pattern, which indicates that regional circulations are captured. However, a slight time shift occurs and the absolute numbers have a substantial bias of ~ 19 ppm (Figure 35). The bias is mainly driven by global CO_2 background fields and inaccurate flux fields, which does not influence the interpretation of the air circulation.

Within the simulation period July to August 2009, a recurring CO_2 accumulation can be seen in the Yenisei River basin during the morning hours. This might be due to the absence of photosynthetic uptake as well as a reduced mixing of the respired CO_2 over the 2 km wide, cool water surface.

Figure 36 shows the east-west cross section through the region. The bold black line indicates the boundary layer height, with a height of 0 m above ground at the location of the Yenisei River. The model shows similar results to Van der Molen et al. [2007] as discussed in Chapter D2.5. In the morning, CO_2 enriched air is transported from the river towards the tower. But, a strong vertical mixing dominates and instead dilutes the CO_2 into the boundary layer, rather than transporting it horizontally.
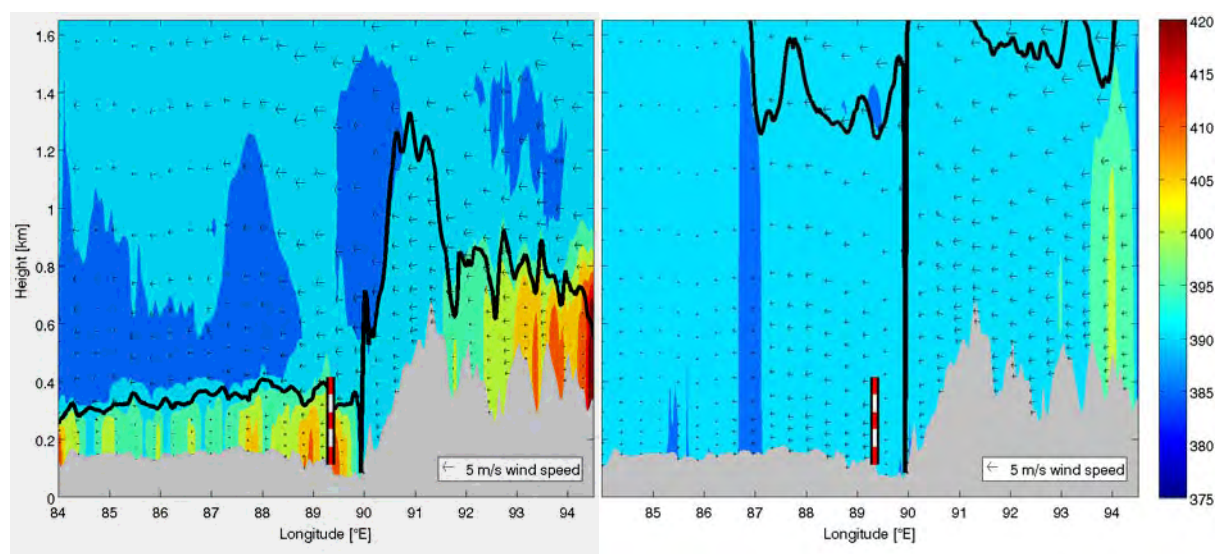
Figure 36 *Cross section of WRF simulated CO_2 mixing ratio at 10 am and 1 pm local time on 20 Aug 2009; thick black line represents boundary layer height; white/red symbol marks ZOTTO*

D3.6 CH_4 fluxes

In full analogues to the previous CO_2 flux analysis, the CH_4 total flux can be estimated as the sum of storage flux below 301 m level and the eddy flux at the highest level. Figure 37 shows the flux estimates in grey, when there are not enough eddy estimates available. Black dots sum eddy and storage fluxes and their error of the mean when summarizing each month.
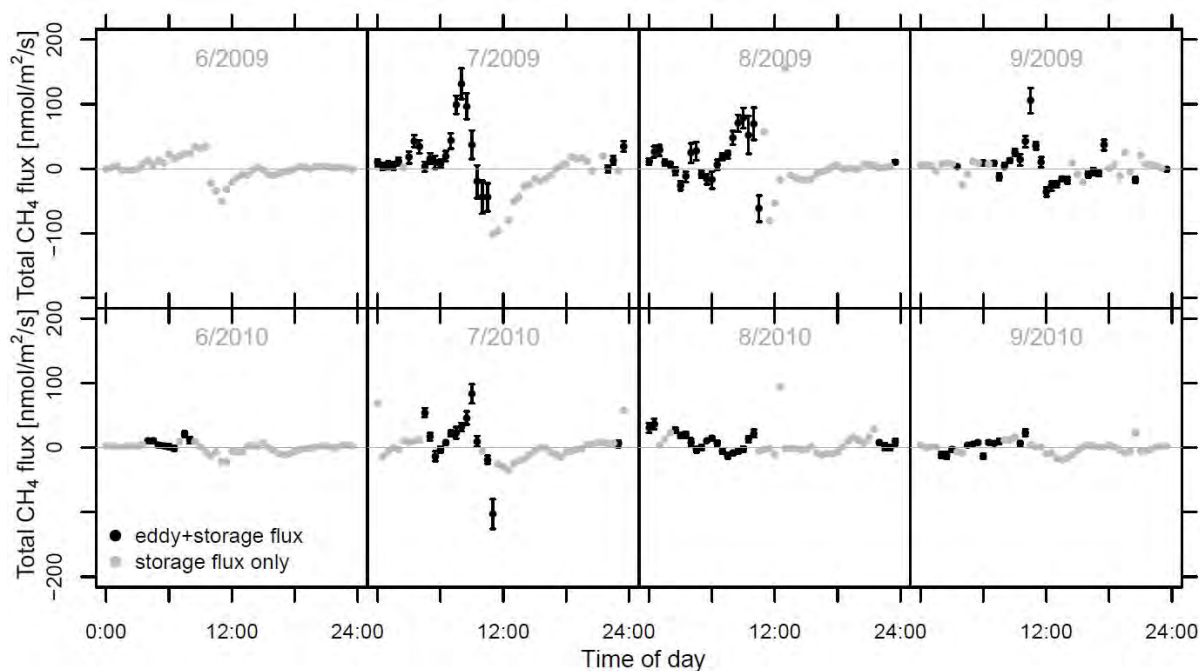
Figure 37 *Average diurnal cycle of the total CH₄ flux estimate with standard deviation of the mean for all summer months*

The pattern is dominated by the storage flux. The most remarkable feature occurs during the morning transition, when estimated CH_4 fluxes show values up to 130 nmol/m²/s. The most probable reason is the topography around the tower. The tower is located on top of a hill and is surrounded by bogs. During night, CH_4 is emitted and accumulates close to the ground. With the sun rises, the air layer mixes up to higher altitudes and passes the 301 m tower upwards. While rising from below to the height of the tower, a large positive flux signal occurs, whereas the venting aloft the control volume compensates the flux balance with negative fluxes thereafter. Thus, the morning signal mimics the real flux from a different time and place. A correct localization would require high resolution modeling.

The mean of the total nighttime flux (23:00 to 4:00) in all summer months is 9.9 ± 7.3 nmol/m²/s. To compare this number different units from other publications are converted to nmol/m²/s (10 nmol/m²/s = 0.86 mmol/m²/day = 0.054 mgCH₄/m²/d). Typical magnitudes of CH_4 fluxes vary widely and depend on measurement type, temperature, water level and topography: aircraft measurement in Siberia give 3 to 106 nmol/m²/s [Glagolev et al., 2008], chamber measurements in Canada result in fluxes at the edge of a fen of 12.5 nmol/m²/s [Rask et al., 2002], modified Bowen ratio method at a tall tower in boreal US give summer fluxes of 17.4±10.4 nmol/m²/s [Werner et al., 2003], and eddy measurements show typical summer emissions of 2.5 nmol/m²/s in a Finnish boreal fen [Rinne et al., 2007]. The ZOTTO data represents a typical example.

D4 Conclusions

Although neither aircraft nor eddy covariance data is available for the period 2009 to 2010, ecosystem fluxes are estimated just from the information given by the gradients between the six tower levels (301 m, 228 m, 158 m, 92 m, 52 m, 4 m).

Most information is gained during night, when the gases are captured in the nocturnal boundary layer and distinct differences between the measurement levels develop. This storage flux component is dominating nighttime fluxes completely. Additionally, measured heat fluxes help to estimate eddy covariance flux components by the modified Bowen ratio method. The nighttime fluxes (23:00 to 4:00) are 3.0 ± 1.2 µmolCO_2/m²/s and 9.9 ± 7.3 nmolCH_4/m²/s in the summer months June-September 2009 and 2010. The day time CO_2 fluxes (Figure 34) give a reasonable shape and magnitude compared to previous data. CH_4 fluxes are predominantly characterized by the morning transition, when emitted CH_4 from the surrounding bogs moves upwards, because the air gets warmed up by the sun, rises, and passes the tower (Figure 37).

Moreover, the potential contribution of advection fluxes is examined in relation to the total flux. Presumably, the vertical advection is compensated by the horizontal advective fluxes, which cannot be estimated due to missing horizontal gradient measurements.

In conclusion, the presented method to estimate carbon budgets is a good alternative for stations that have no direct eddy covariance data available. The method is also applicable to other gas species and also in winter periods, but the wind measurements needs improvement before (e.g. constant heating). In future, data series throughout the year may enable further improvements in the understanding of driving processes of the fluxes, e.g. observed differences in transport patterns in different seasons [Eneroth et al., 2003] can be explored. Moreover, the measurement of boundary layer heights would foster further investigations.

E   Regional flux estimation with the Jena inversion system for Central Siberia

"He who knows best knows how little he knows."
Thomas Jefferson (1743-1826)

E1   Introduction

On the global scale, the boreal regions – especially Siberia – contain the main part of the global terrestrial carbon storage [UNEP-WCMC, 2008]. In future, a warmer climate is becoming more likely; inducing the thawing of permafrost, increased microbial activity, and fire disturbances. This would increase the carbon transfer to the atmosphere on decadal time scales [Schuur et al., 2008]. Given the huge total estimate of 1672 Pg carbon stored in permafrost soils [Tarnocai et al., 2009; Grosse et al., 2011], even small changes in the carbon fluxes could have a large potential impact on the global carbon cycle [Schaefer et al., 2011]. In order to understand the long-term influence of climate change on these stocks, current flux patterns need to be mapped to allow pinpointing the most vulnerable areas.

The exchange of carbon between the different reservoirs of the global carbon cycle is dominated by atmospheric CO_2 fluxes: about 120 PgC are assimilated and respired by the vegetation each year [Denman et al., 2007]. Anthropogenic activities including fossil fuel burning, cement production, and land use change add another 9.3 PgC to the carbon cycle [Friedlingstein et al., 2010]. To illustrate this quantity of turned-over carbon, it is worth noting that 1 PgC is the same amount as contained in all above ground biomass in forest and wooded land of Germany (Russia: 26 PgC) [*FAO*, 2006].

All carbon inputs into the atmosphere either stay in the atmosphere, or are taken up by the ocean or the biosphere (see Chapter C1). Already in the 1990s observations of the latitudinal distribution of CO_2 indicated a "missing sink" of the carbon cycle in the terrestrial ecosystems of the northern hemisphere [Tans et al., 1990]. Generally, the amount and the spatial distribution of the carbon fluxes can be investigated by two fundamentally different methods:

1) Process oriented approaches such as flux measurements, remote sensing, and site inventory data allow quantifying the carbon exchange [Schulze et al., 1999; Myneni et al., 2001; Luyssaert et al., 2007]. In the so called "bottom-up" approach flux components are calculated for each process involved, e.g. the photosynthetic uptake [Beer et al., 2010] and ecosystem respiration [Mahecha et al., 2010]. A study

concentrating on the Russian territory states a net primary productivity (NPP) of -2.3 PgC/yr for all Russian forests [Shvidenko et al., 2008]. For the net balance of the ecosystem, litter and soil respiration need to be taken into account additionally [Schulze et al., 2000]. In total, the "bottom-up" approach estimates an overall sink of -1.3 ± 0.5 PgC/yr in primary forests in the boreal and temperate regions of the northern hemisphere [Luyssaert et al., 2008], and a sink of -0.9 PgC/yr on the Russian territory [Kurganova et al., 2010]. The uncertainties in the bottom-up estimates originate from upscaling the measurements from plot scale to larger areas.

2) The second approach makes use of the atmosphere as a natural integrator of the carbon fluxes. The knowledge of the atmospheric concentration and the atmospheric transport is used in the so-called "top-down" approach to constrain the carbon fluxes between the atmosphere and the surface. The flux pattern is estimated with atmospheric inversion models, which simulate the transport of the measured air parcels inversely in time back to their origin [Enting et al., 1989; Gurney et al., 2002; Rödenbeck et al., 2003; Peylin et al., 2005]. The "top-down" approach has a high potential for providing meaningful carbon budgets on regional to continental scales. The atmospheric signal has particular advantages compared to measurements on plot level (e.g. from eddy covariance or chamber measurements), because it integrates the heterogeneous carbon release due to natural (fire, pests, windstorms) and anthropogenic disturbances (forest management) [Körner, 2003]. These disturbances primarily influence the human footprint in the carbon cycle of temperate and boreal forests [Magnani et al., 2007]. Atmospheric inversion models suggest that a significant fraction of the northern hemisphere carbon sink is located in boreal forests [Schimel et al., 2001; Gurney et al., 2002; Rödenbeck et al., 2003]. The comprehensive Atmospheric Tracer Transport Model Intercomparison Project (TransCom) estimates the carbon budget for boreal Asia of roughly -0.5 ± 0.6 PgC; the large uncertainties are noteworthy [Gurney et al., 2002]. This estimate may even vary between roughly +0.5 to -0.4 PgC/yr with the selection of different sites or time frames [Rödenbeck et al., 2003]. The carbon sink of -1.5 ± 0.6 PgC/yr is identified in this region by analyzing the vertical distribution of CO_2 in the atmosphere [Stephens et al., 2007]. Recent publications quantify the net carbon uptake in temperate and boreal Eurasia to -1.0 ± 0.5 PgC/yr [Sarmiento et al., 2010].

The total carbon budgets of bottom-up and top-down approach agree remarkably well. Both approaches prove Russia to be the largest sink on the northern hemisphere [Ciais et al., 2010a].

The global atmospheric transport inversion models are driven to resolve a finer and finer grid to more exactly pinpoint the actual surface flux patterns. Some current up-to-date global models, which are available online, are:

E   Regional flux estimation with the Jena inversion system for Central Siberia

- CarbonTracker 1°x1° over North America [Peters et al., 2007] (reveals large uncertainties over Eurasia, see carbontracker.noaa.gov),

- CO_2 from Laboratoire des Sciences du Climat et l'Environnement (LSCE), CO_2 from MPI-BGC Jena, CO_2 from NOAA's CarbonTracker, and CH_4 from LSCE at the internet portal CarboScope www.carboscope.eu

- EU MACC project at www.gmes-atmosphere.eu

The global resolution of atmospheric inversions is limited by data availability and the high computing costs. However, high-resolution transport would be advantageous to reduce representation errors through a better representation of the measurement station in a finer resolved grid [Gerbig et al., 2003a]. Moreover, mesoscale models (e.g. WRF-VPRM) are able to better represent the meteorological conditions of continental stations [Ahmadov et al., 2009]. Mesoscale inversions for southwestern France demonstrated the large improvements on the regional flux estimates in tests with synthetic [Lauvaux et al., 2008] and real data [Lauvaux et al., 2009a]. Nevertheless, difficulties in the reproduction of local circulations [Sarrat et al., 2007] and nighttime observations [Lauvaux et al., 2009b] still restrict benefits from the fine-scale inversions.

Apart from the carbon that is bound in CO_2, the Siberian wetlands are an important source of methane [Friborg et al., 2003]. Similar to the bottom-up investigations on CO_2, several process-based studies exist for methane. Bohn et al. [2007] investigated CH_4 emissions from a 100x100 km area in wetlands of western Siberia. They estimated a CH_4 flux of 200 mg/m²/day for this area for July based on a multi-year average. Following the top-down approach, a global atmospheric inversion for CH_4 was set up by Bergamaschi et al. [2009] with regional zoom over tropical regions (see also www.gmes-atmosphere.eu).

In the present work the observations from the ZOTTO site are utilized in the "top-down" approach to retrieve CO_2 and CH_4 surface fluxes for the Central Siberian region. For this purpose the new 2-step atmospheric inversion scheme by Rödenbeck et al. [2009] from the MPI-BGC is used. The model framework has been already tested in Central Europe for both CO_2 within the CarboEurope project [Trusilova et al., 2010] and CH_4 within the NitroEurope project [U. Karstens, personal communication, 2011]. Now it is implemented and adapted to a less investigated region to operate a regional inversion model for Central Siberia for the first time.

A detailed description of the modeling framework is given in section E2. A set of tests of the inversions setup are described in Chapter E3. The optimized inversion system is used in combination with the atmospheric observations to estimate flux fields, which are presented and discussed. In the last Chapter E4, the perspective of the inversion applications is outlined for continuous tall tower observations.

E2 Model setup

E2.1 Global inversion model

This is a short overview of the construction of the global atmospheric inversion modeling system. A detailed description can be found in the MPI-BGC Technical Report no. 6 [Rödenbeck, 2005].

The modeled concentration c_{mod} is given by summing the flux field f transported by the atmospheric transport matrix $\mathbf{A}$ and the initial concentration value c_{ini}:

$$c_{mod} = \mathbf{A}f + c_{ini} \tag{18}$$

The transport is calculated with the Eulerian transport model TM3 [Heimann et al., 2003]. The driving meteorology is given by reanalysis fields of the National Centers of Environmental Prediction (NCEP).

The overall aim of the inversion is to find the specific flux field, which minimizes the mismatch m between observed c_{obs} and modeled concentration c_{mod}:

$$m = c_{obs} - c_{mod} \tag{19}$$

As the flux matrix $\mathbf{F}$ has much more degrees of freedom then the observations can constrain, a unitless parameter vector p is introduced

$$f = f_{fix} + \mathbf{F}p \text{ with} \left\langle p_{pri} \right\rangle = 0 \text{ and } \left\langle p_{pri} p_{pri}^T \right\rangle = \frac{1}{\mu}\mathbf{1} \tag{20}$$

where p_{pri} characterizes the prior state of the vector and f_{fix} is the expected value of the prior flux estimate $\left\langle f_{pri} \right\rangle$.

As the flux $\mathbf{F}$ is not explicitly known, the mathematical description depends on several assumptions. The following function is introduced and depends on various parameters. The dimension reduced parameter vector p is linked to all flux data points in space and time:

$$f(x,y,t) \sim \sum_i^{\substack{flux \\ components}} \left(f_{fix,i}(x,y,t) + f_{shape,i}(x,y,t) \sum_{time} \sum_{space} g_i^{time}(t) g_i^{space}(x,y) p_{time,space,i} \right) \tag{21}$$

The different flux components $f_{...,i}(x,y,t)$ represent numerous sources like biosphere, ocean or fossil fuel; but they can also describe several frequency components of the flux, e.g. the long-term component, seasonal variability or interannual changes. The shape function f_{shape} gives a weighting in space and time and is directly linked to the flux uncertainties. The functions $g_i^{time}(t)$, $g_i^{space}(x,y)$ determine the temporal and spatial decomposition into statistically independent

elements of the flux field. These functions define the spatial and temporal correlation lengths.

The Bayesian approach is used to find the optimal parameters, which minimizes the misfit m between the model output and the atmospheric data. It expresses the probability of a parameter vector under the condition of the observed misfit:

$$\text{Prob}(p|m) = \frac{\text{Prob}(m|p)\text{Prob}(p)}{\text{Prob}(m)} \tag{22}$$

Figure 38 illustrates this central formula (adapted from Tarantola [2005]). It is assumed that the initial a-priori flux has a known Gaussian distribution $\text{Prob}(p)$. This flux is linked to the measured atmospheric concentration $\text{Prob}(m)$ by the atmospheric transport model $\text{Prob}(m|p)$. The inversion combines all this information and gives a constrained estimate of the posterior flux distribution $\text{Prob}(p|m)$.
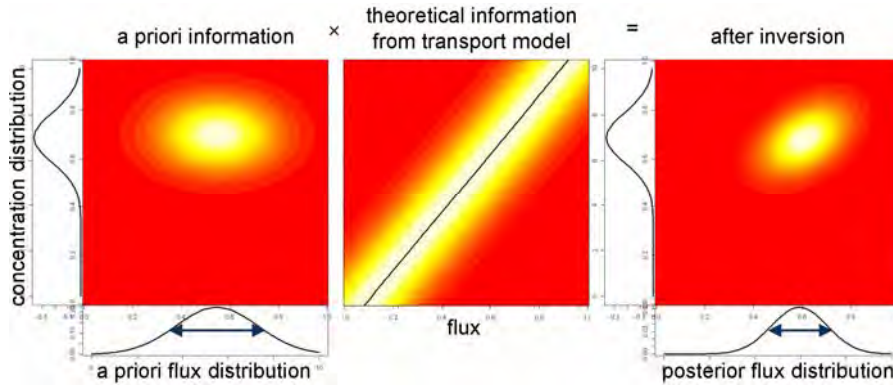
Figure 38 *Visualization of the conditional probabilities used in the Bayesian approach*

Mathematical theory allows the calculation of the probabilities to generate the cost function J in the following way:

$$J = -\ln(\text{Prob}(p|m)) \quad = -\ln(\text{Prob}(m|p)) - \ln(\text{Prob}(p)) + \ln(\text{Prob}(m))$$

In general:
$$J = \frac{1}{2}m^T\mathbf{Q_m^{-1}}m + \frac{1}{2}(f - f_{fix})^T\mathbf{Q}_f^{-1}(f - f_{fix}) + Const. \tag{23}$$

Implementation:
$$J = \frac{1}{2}m^T\mathbf{Q_m^{-1}}m + \frac{\mu}{2}p^T p + Const. \text{ [Rödenbeck, 2005]}$$

$\mathbf{Q_m}$ is the error covariance matrix of the concentration misfit. For simplification, it is reduced to a diagonal matrix, which gives the variances of the data points. $\mathbf{Q}_f$ is the error covariance matrix of the flux field, whose a-priori state is given by $\mu^{-1}\mathbf{FF}^T$. Thus, the first term in Equation (23) stands for the data constraints on the inversion, whereas the second term quantifies the a-priori flux information. The scaling factor μ allows different weighting of these terms. The standard $\mu = 1$ equally weighs the

observation misfit and a-priori fluxes; whereas $\mu = 0$ implies the full control through the atmospheric data; $\mu = \infty$ ties the posterior to the prior flux field.

The cost function reaches a minimum at the point of maximum conditional probability for the flux parameters, because it is linked to the probability by the negative logarithm (equation (23)). For the sake of completeness, the mathematical solution for the posterior flux parameter is given in equation (24):

$$\frac{\partial J}{\partial p^T} = \mathbf{M}p - b \quad \blacktriangleright \quad \underline{\underline{p_{post} = \mathbf{M}^{-1}b}}$$

(24)

With $\mathbf{M} = \mathbf{F}^T \mathbf{A}^T \mathbf{Q}_m^{-1} \mathbf{A} \mathbf{F}$ and $b = \mathbf{F}^T \mathbf{A}^T \mathbf{Q}_m^{-1} \left(c_{obs} - \left(\mathbf{A} f_{fix} + c_{ini} \right) \right)$

The matrix inversion in equation (24) is solved iteratively until a sufficient convergence level is reached (50 to 70 iterations).

E2.2 Regional inversion model

The global transport model has a spatial resolution of 4°x5° with 19 vertical levels. To resolve finer patterns on a regional scale, the coarse grid TM3 inversion system is linked to a finer resolved transport model STILT [Lin et al., 2003]. The setup of the 2-step TM3-STILT inversion system is reported in Rödenbeck et al. [2009] and Trusilova et al. [2010], and is also called Jena inversion system hereafter.

Table 6 and Figure 39 give an overview of the underlying principle. In the first step the global inversion is performed (c_{coarse}, blue in Figure 39). In an intermediate step, the global background contribution $c_{coarse,trans}$ to the observations from the area outside the regional domain is computed. This represents the global background concentration (green in Figure 39), which would be observed without any sources or sinks in the regional domain. The difference of the measurement (c_{meas}, black in Figure 39) to this global background is that part of the signal Δc_{remain} that exclusively originates from inside the regional domain. This signal is driving the second step of the regional inversion with the high-resolution transport model. The posterior result c_{fine} is shown in red in Figure 39.

Figure 39 gives additional information about the time frame, when the observational data is used. Whereas the continuous lines describe the full available hourly resolved data, the dots represent the results, if only afternoon data is used. This differentiation will become important, when the input data is prepared (Chapter E2.6). The figure shows that the global background $c_{coarse,trans}$ lies above the measured data, which suggests a CO_2 sink within the regional domain due to the photosynthetic activity of the boreal forests. As expected, the short time period shown in the chart indicates that the regional model simulates the mixing ratios closer to the observations than the global model.

Table 6 *Principle of the 2-step inversion, adapted from [Rödenbeck et al., 2009]*

Step 1		**Global inversion**
	coarse	$c_{meas} \rightarrow A_{coarse}^{global}$ as transport $\rightarrow f_{coarse}$ … global flux estimate

Intermediate step

Forward run globally

$$\Delta c_{coarse} = A_{coarse}^{global} \, f_{coarse}$$

$$\rightarrow c_{coarse} = A_{coarse}^{global} \, f_{coarse} + c_{ini} \quad \text{… should match measurements } c_{meas}$$

Forward run in the domain of interest

$$\Delta c_{coarse,cis} = A_{coarse}^{region} \, f_{coarse} \quad \text{…influence from inside the domain}$$

$$\rightarrow \Delta c_{coarse,trans} = \Delta c_{coarse} - \Delta c_{coarse,cis}$$

$$\rightarrow c_{coarse,trans} = \Delta c_{coarse,trans} + c_{ini} \quad \text{…influence from outside the domain}$$

$\rightarrow$ Remaining mixing ratio as input for the regional inversion:

$$\Delta c_{remain} = c_{meas} - c_{coarse,trans}$$

Step 2

Regional inversion

$$\Delta c_{remain} \rightarrow A_{fine}^{region} \text{ as transport} \rightarrow f_{fine} \quad \text{… regional flux estimate}$$

Forward run:

$$\rightarrow c_{fine} = A_{fine}^{region} f_{fine} + c_{coarse,trans} \quad \text{… should match measurements } c_{meas}$$

Legend

A_{coarse}^{global}	global, coarse transport matrix (TM3)	A_{fine}^{region}	regional, fine transport matrix (STILT)
A_{coarse}^{region}	global, coarse transport matrix (TM3), restricted to the domain of interest		
f_{coarse}	flux estimate on coarse, global grid	f_{fine}	flux estimate on fine, regional grid
c_{meas}	measured concentration $\Leftrightarrow c_{coarse} / c_{fine}$		global/regional model concentration output
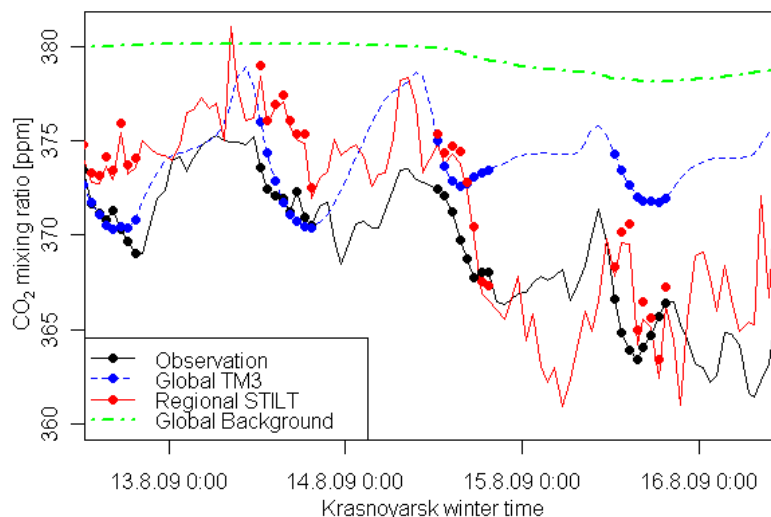
Figure 39 *CO_2 time series at ZOTTO from observation, global and regional inversion results (dots mark afternoon data)*

Technically, for the second step regional inversion the same model framework is used as in the first step (Chapter E2.1). The main difference is the use of the regional transport model STILT instead of TM3. Moreover, the prior fluxes need to be

E   Regional flux estimation with the Jena inversion system for Central Siberia

updated on a finer resolution (Chapters E2.4 and E2.5). For integrating those fluxes into the regional framework, all functions in equation (21) need to be reviewed. The total sum of the shape function needs to match the error estimates of the global inversion within the regional domain. The necessary normalization has been included in the current setup of the Jena inversion system (version 12.086) for CO_2. Implications on the correlation lengths in time and space are further investigated in Chapter E3.1.

A detailed view on the atmospheric transport with the STILT model is given in the following chapter.

E2.3 Footprint analysis

Footprints give a measure of the surface influence of the flux field on the concentration measurement. To calculate footprints, the Stochastic Time-Inverted Lagrangian Transport (STILT) model is used [Lin et al., 2003]. While the Eulerian model TM3 solves the transport equations for each grid cell, the Lagrangian approach solves them for the motion trajectories for individual particles. If the whole atmosphere is not of interest, but only a few stations, the Lagrangian approach has the advantage of reduced computing time, because it resolves only the space, where air parcels pass on their way to the receptor. By inverting the transport in time, each air parcel is followed back to the place, where it interacted with the ground. A stochastic process is involved in the simulation of the particle trajectories. Thus, the 100-fold repetition of the time inverted transport calculation gives a realistic representation of the footprint of one measurement in space and time.

The analysis of the footprints reveals that the near-field of the station has the main influence on the receptor (Fig. 1 in Gerbig et al. [2009]). The contribution dilutes with distance and time away from the observation point. This dilution is also subject to diurnal variations, because the weak turbulent mixing combined with slower advection near the ground during night restricts the footprint to a smaller area than during day [Gerbig et al., 2006].

The driving meteorological fields are prescribed into STILT by forecast values of the European Centre for Medium-Range Weather Forecasts (ECMWF http://www.ecmwf.int/). The forecast values of the atmospheric model (started 0:00 and 12:00 every day) from the operational archive have a spatial resolution of 0.25°x0.25° and a temporal resolution of three hours. The STILT-preprocessor uses the lowest 61 altitude levels (number 31 to 91) and ensures the mass conservation of the wind fields [F.-T. Koch, personal communication, 2011].

For the regional inversion in Siberia, it first has to be decided about the dimensions of the domain of interest. It should be almost centered on ZOTTO as the most important data distributor. The final choice for the ZOTTO domain is visualized in Figure 13 and Figure 41. It is shifted slightly westwards, because of the

predominantly westerly winds, and slightly towards the north to have a natural boundary by the Arctic Ocean. The longitude ranges from 55° to 102° east and the latitude from 50° to 77° north. The area is $6.94 \cdot 10^6$ km², which corresponds to a square of (2635 km)². The land fraction covers $6.1 \cdot 10^6$ km², about 4 % of the world's total land area.

The surface influence function (the footprint) is given by the sensitivity of the measurement in relation to the emitted surface flux. The footprint is defined for each pixel of the flux field as the change in mixing ratio at the point of interest induced by one standard unit of released surface flux.

At first, the extension of the surface influence function within the ZOTTO domain is studied for its dependency on the considered travel time of the air particles to the receptor point. Therefore, STILT is run 30 days back in time for 100 particles starting at 301 m a.g.l. every three hours for the period from January to April 2010. Table 7 presents an overview of the domain coverage varying with the length of the STILT simulations backwards in time. It can be assumed that the predominant part of the trajectories left the domain, when the particles have been followed 30 days back in time. Thus, Table 7 implies that only 32.3 % of the total footprint would be captured, if the trajectories reach only 24 h back in time. Similarly, 10 days (240 hours) back-trajectories cover 99 % of the overall footprint. Therefore, the implemented setting of 10 days is sufficiently long for a representative footprint.

Table 7 *Footprint analysis from the ZOTTO station in dependency of the back-trajectory length*

Time of back-trajectories in h

1	6	12	24	48	72	96	120	240	360	720

surface influence [ppm/(μmole/(m²s))]

0.9	7.7	16.5	32.3	56.6	70.5	80.8	87.3	99.0	99.97	100

Total surface footprint coverage in % (720 h back-trajectories = 100 %)
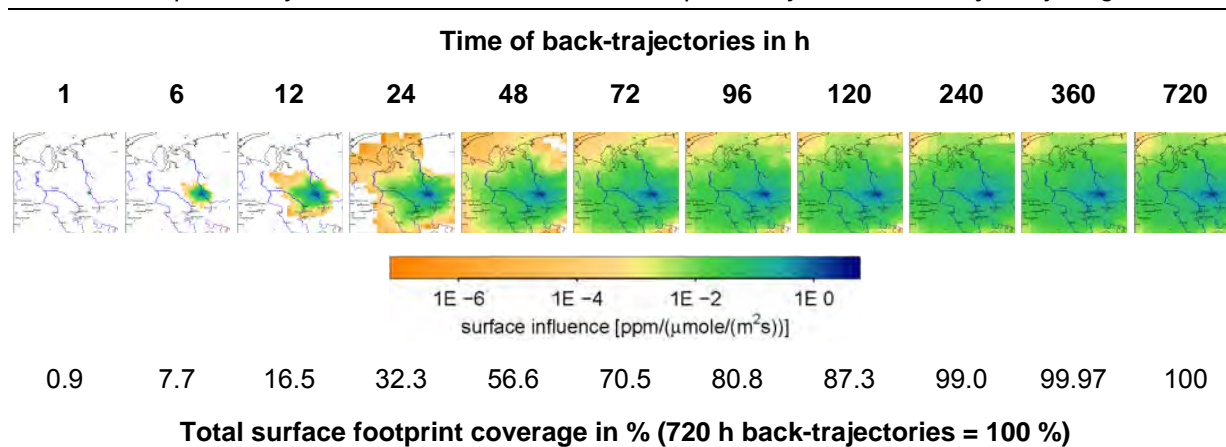
The footprint can also be analyzed by distance to the measurement station. Figure 40a shows the sum of the footprint influence function over distance: half of the influence of the domain is captured within 500 km distance from the ZOTTO site. This result is in good agreement with the finding in Gloor et al. [2001], who estimated a tower footprint of 10^6 km².

E   Regional flux estimation with the Jena inversion system for Central Siberia
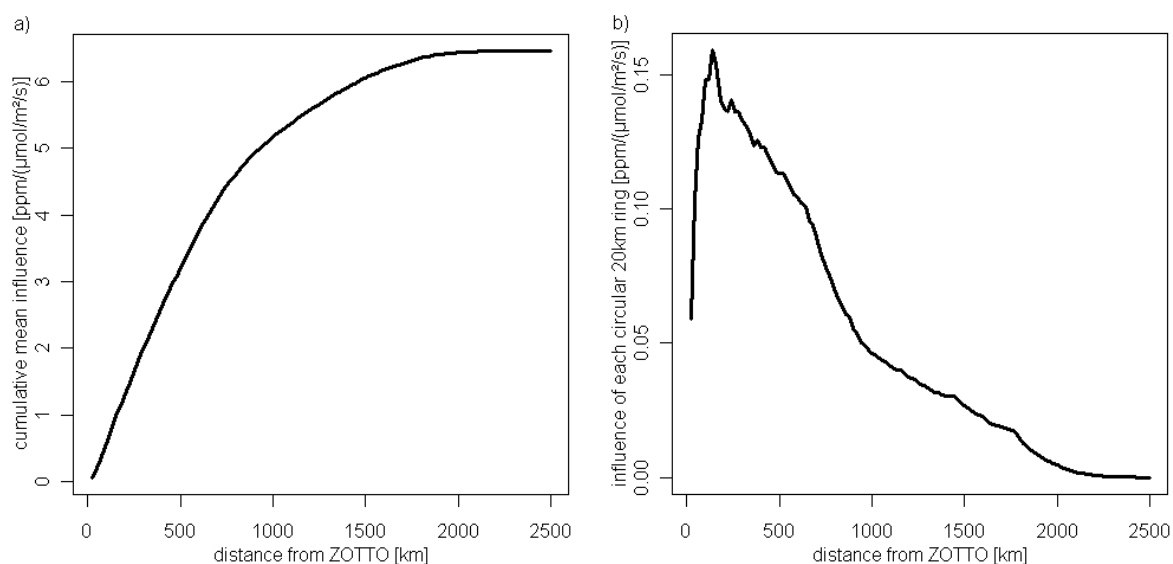
Figure 40 *Influence function for the 301 m level with 30 days back trajectories:* **a)** *cumulated over distance to ZOTTO;* **b)** *summed in 20 km equidistant rings around ZOTTO*

Figure 40b shows the fractional sum of the influence function within 20 km wide rings around the ZOTTO station. At the short distance below 200 km, the influence function does not yet reach its maximum. The reason is that nighttime signals are included: then, the air parcels at 301 m are above the nocturnal boundary layer and do not have contact with the ground until the next morning. In the far distance the influence function fades out, because the particles dilute over a larger area and into the upper free troposphere (Figure 40b).

The approximation of the footprint is only meaningful for tracers without a diurnal cycle in the fluxes such as CH_4. In contrast, the CO_2 flux is fluctuating from source to sink every day. Thus, positive and negative contributions cancel out and effectively lower the footprint to tens of kilometers [Gerbig et al., 2009].

The knowledge of the atmospheric transport is not sufficient to relate gas concentration measurements directly to gas fluxes. A large signal in the mixing ratio observations might either represent a small source nearby, or a spatially extensive or quantitatively large source in the distance.

The inversion has a data weighting algorithm, which increases the data uncertainty of individual mixing ratio data points with the square root of the number of measurements within one week (more exact: the average number of weekly data points within a 3 week period). The reason is to give flask data a similar weight as a continuous data set would have. Hence, intrinsically given by the system, the continuous data stream of the tower cannot provide a higher information gain than weekly flask measurements. However, the continuous data supplies a more reliable estimate of a weekly representative value. Hence, it may improve the temporal flux distribution (which in turn is limited by the temporal correlation length in the fluxes - equation (21)).

E   Regional flux estimation with the Jena inversion system for Central Siberia

In the Siberian domain, there is data available from six stations: ZOTTO (ZOT), Surgut (SUR), Novosibirsk (NOV), Demyanskoe (DEM), Igrim (IGR), and Karasevoe (KRS). More details are discussed later in Chapter E2.6 (esp. Table 10). For each available data point (up to hourly resolution), the footprint has been calculated with STILT. Afterwards all these instantaneous footprints have been summed up, weighted by the data density as described above. The results are presented in Figure 41 for the CO_2 measurement sites and Figure 42 for CH_4 measurement sites. Through the density weighting, the footprints only illustrates what the inversion system "sees" and cannot be used for any quantification. Nevertheless, it is a useful tool to compare the importance of the different sites in different seasons.
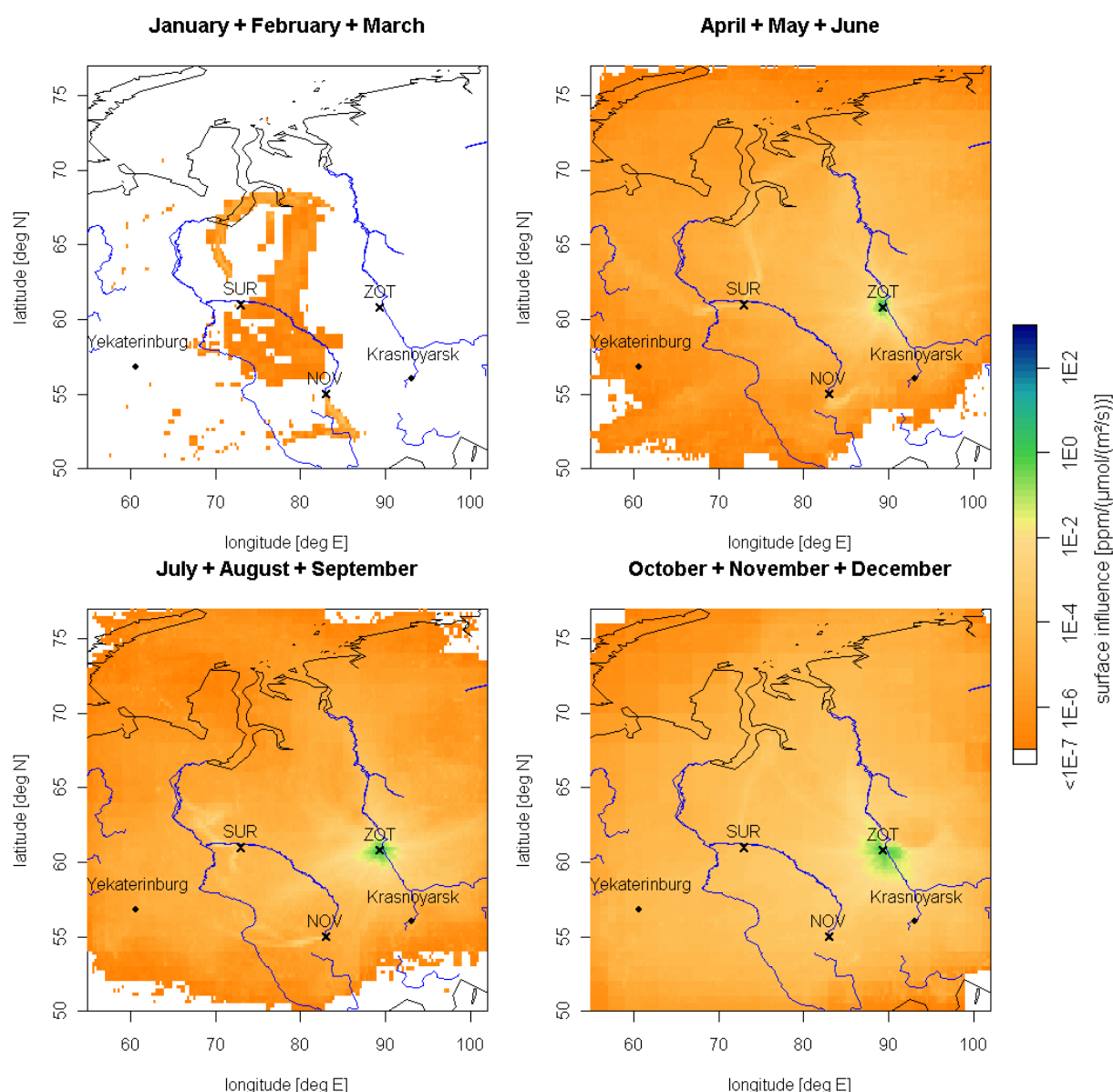
Figure 41 *Data density weighted footprints from all CO_2 measurement stations (Table 10) in 2009*

Figure 41 reveals that the CO_2 flux estimates are mainly driven by the ZOTTO site. The other two stations (NOV, SUR) are monthly aircraft based measurements and do not contribute as much as ZOTTO to the knowledge gain of the flux fields.

E   Regional flux estimation with the Jena inversion system for Central Siberia

The CH$_4$ measurements in Figure 42 are evenly distributed and the footprints show a good coverage of the boreal Siberian region. Throughout the year, the footprint of the station network slightly varies, driven by diverse weather conditions in different seasons and variable data availability.
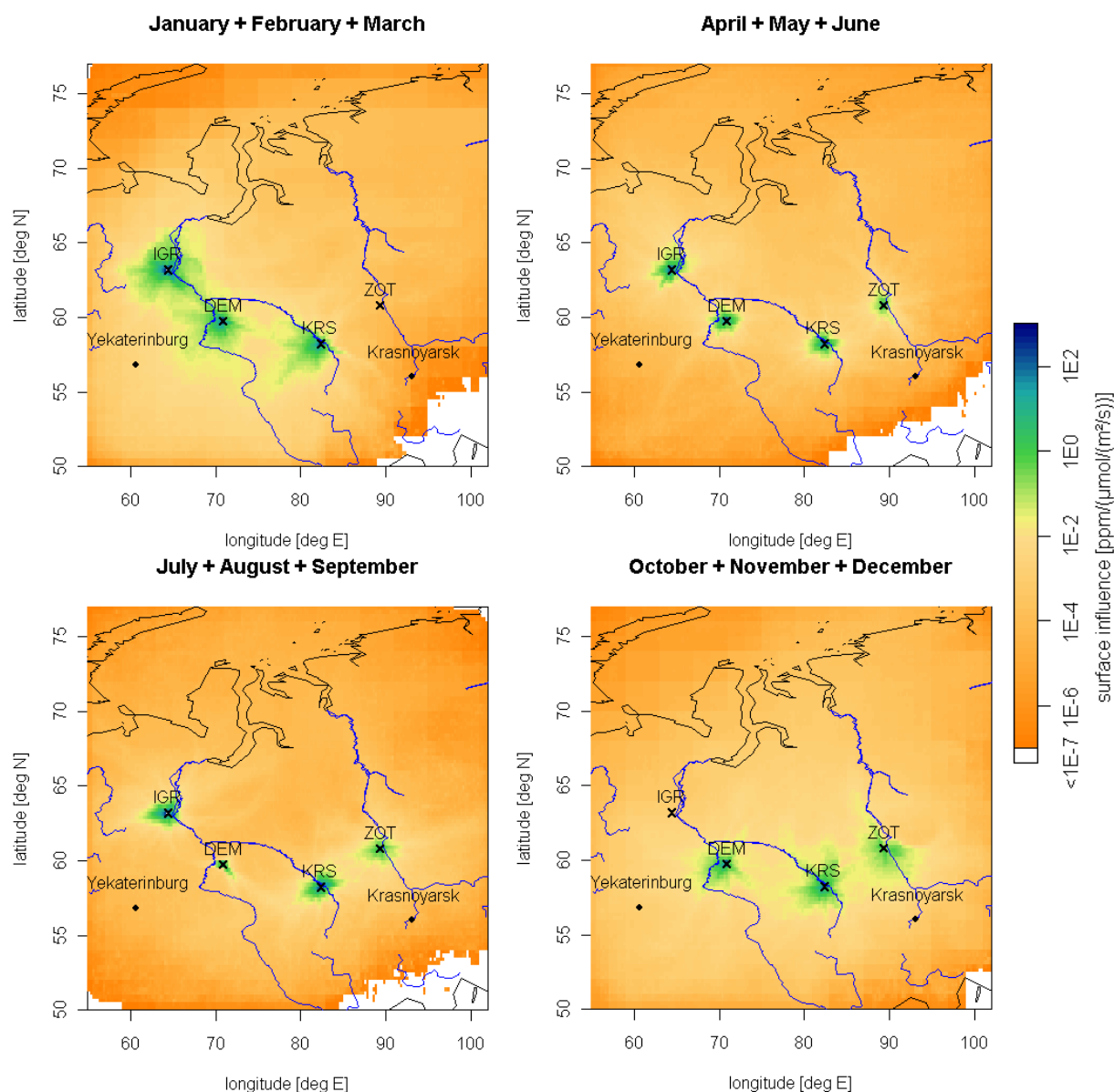
Figure 42 *Data density weighted footprints from all CH$_4$ measurement stations (Table 10) in 2009*

E2.4 CO$_2$ prior fluxes

To calculate the gas concentrations at the measurement stations, the atmospheric footprint has to be multiplied with a flux field. The considered fluxes for this a-priori information include biosphere, ocean, fossil fuel and biomass burning. As starting point, the global Jena inversion system has already successfully implemented various models to generate the flux patterns for the global fields. The output of these different models has been adapted to the finer resolution of the ZOTTO domain (Table 8):

E   Regional flux estimation with the Jena inversion system for Central Siberia

Table 8 *Characteristics of the a-priori fluxes in the standard setup of the Jena inversion system*

Flux component	Model / Data set	Spatial resolution	Time resolution	References
Biosphere NEE	BIOME-BGC	1°x1°	3 h	[Trusilova et al., 2008]
Ocean	See text	4°x5°	Monthly	[Mikaloff Fletcher et al., 2007]
Fossil fuel	EDGAR 4.0	1°x1°	Yearly	http://edgar.jrc.ec.europa.eu/
Biomass burning	GFED-3	0.5°x0.5°	3 h	[van der Werf et al., 2010] [Mu et al., 2011] http://www.globalfiredata.org/

The time resolution of the model output for the biosphere and biomass burning fluxes is one day on default. To achieve a three hourly resolution, each day is superimposed by an average diurnal cycle. The biospheric cycle is driven by the geometrically maximal available insolation. The diurnal cycle of the biomass burning is generated by using the mean diurnal cycle observed in the years 2007-2009 for each individual month, as described by Mu et al. [2011].

The net ocean-atmosphere carbon flux is the sum of the ocean uptake flux induced by the anthropogenic perturbation as compiled by Mikaloff Fletcher et al. [2006], the preindustrial air-sea fluxes from Mikaloff Fletcher et al. [2007], and the river fluxes of Jacobson et al. [2007]. The ocean flux is represented by a climatologic average and is not specifically adapted to the conditions in 2009, because it is characterized by small variations only.

The fossil fuel emissions from EDGAR inventory dataset are available until 2005. Therefore, these data have been extrapolated to 2009. For 2006-2008 the extrapolation was proportional to the total oil, coal and natural gas emissions reported by the oil company BP p. l. c. [www.bp.com, last access 7.6.2011], for 2009 a continued increase in global emissions of 2 % was assumed.

The sum of all prior flux information gives a total budget of 0.07 PgC for the whole ZOTTO domain in 2009 (Figure 43a). All negative fluxes (carbon sinks) add up to -2.4 PgC by the biosphere and -0.001 PgC by the ocean. Homogeneously distributed over the land, this biospheric uptake averages to -1 µmol/m²/s. Positive fluxes (sources) are in total 2.25 PgC from respiration during winter and nighttime, and 0.2 PgC by fossil fuel and biomass burning.

The regional inversion can cover the year 2009 only, because satellite data driving the vegetation models for flux estimates is not yet available for 2010 in processed form.

E Regional flux estimation with the Jena inversion system for Central Siberia
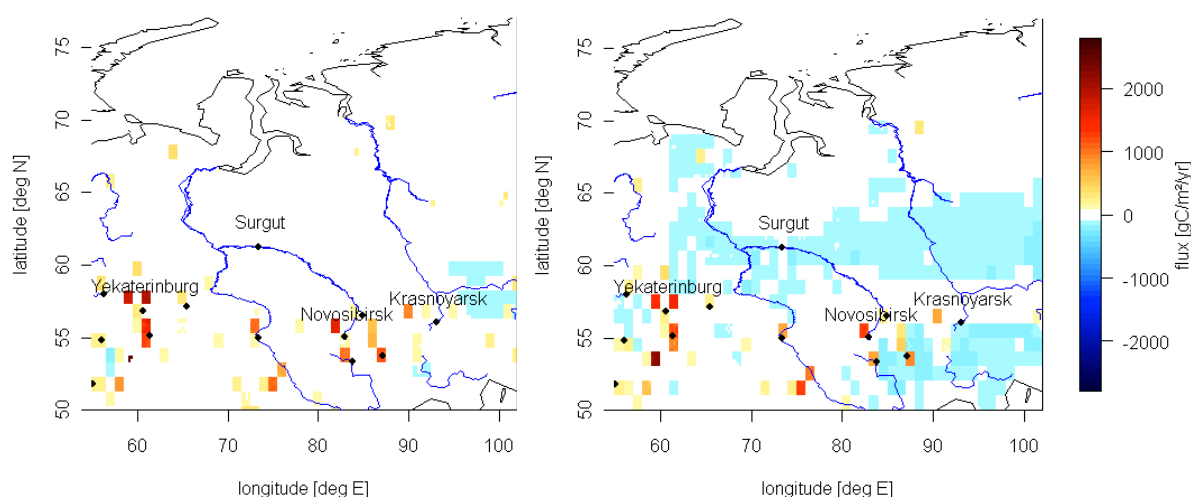
Figure 43 *Prior distribution of the annual CO_2 fluxes for 2009:* **a)** *standard inversion (Table 8),* **b)** *Carbon Tracker (Table 9)*

An alternative a-priori flux estimate (Figure 43b) is produced by the publicly available CarbonTracker model [Peters et al., 2007] and is listed in Table 9 :

Table 9 *Characteristics of the a-priori fluxes in the Jena inversion system given by Carbon Tracker*

Flux component	Model / Data set	Spatial resolution	Time resolution	Reference
Biosphere NEE and Ocean	CarbonTracker 2010	1°x1°	3 h	[Peters et al., 2007] http://carbontracker.noaa.gov/
Fossil fuel and biomass burning	CarbonTracker 2010	1°x1°	Monthly	

CarbonTracker is a product of a global inversion model. The flux estimates can be used as a-priori data for the ZOTTO regional inversion, because none of the atmospheric data form the ZOTTO region has been included in CarbonTracker. The overall budget of all fluxes in the ZOTTO domain is -0.2 PgC in 2009, net -0.4 PgC from the biosphere, a source of 0.2 PgC from fossil and biomass burning and a negligible source of $8 \cdot 10^{-5}$ PgC from the ocean.

The spatial resolution of the fluxes of 0.5° to 1° is generally not as fine as the resolution of the transport model with 0.25°, but yet a substantial improvement to the global model with 4°x5° resolution.

E2.5 CH₄ prior fluxes

More than half of global CH_4 emissions are induced by humans, in form of domestic ruminants, rice and landfill emissions and are deduced from comprehensive data inventories. One third of all emissions come from natural wetlands; this part dominates the natural CH_4 sources with 75 % [Denman et al., 2007] and can be incorporated in the total budget through several models for CH_4

wetland emissions [Cao et al., 1996; Walter et al., 2001; Kaplan, 2002; Kaplan et al., 2006; Bohn et al., 2007; Wania, 2007].

For simplicity, an already well composed flux dataset with a 1°x1° nominal spatial resolution is used. It was compiled by the NitroEurope community and is documented in the NitroEurope A6.2 Modeling Protocol [U. Karstens, personal communication, 2011]. An overview about the included CH$_4$ sources is given in Table 4 in Bergamaschi et al. [2009]. The wetland emissions represent a climatologic average given by the Kaplan model [Bergamaschi et al., 2007]. The anthropogenic emissions have been updated with the latest EDGAR v4.1 inventory [EDGAR, 2010], which does not yet include the newest gas production fields opened in 2008. Biomass burning is given by the GFED3 data base with 0.5 x 0.5 degree three-hourly resolution [van der Werf et al., 2010; Mu et al., 2011].

The tropospheric photochemistry driven by OH radicals is the most important sink in the global CH$_4$ cycle [Denman et al., 2007]. Uncertainties in the OH fields influence the global CH$_4$ distribution, but have only a minor effect on the regional CH$_4$ distribution [Bergamaschi et al., 2010]. The average lifetime of CH$_4$ is 10 years, thus, the tropospheric destruction process has to be included into global background fields and can be ignored in the fine-scale regional inversion step over the Siberian domain.

The sum of all CH$_4$ flux fields is shown in Figure 44 with some evident sources around the big cities and in the West Siberian plains around Surgut.
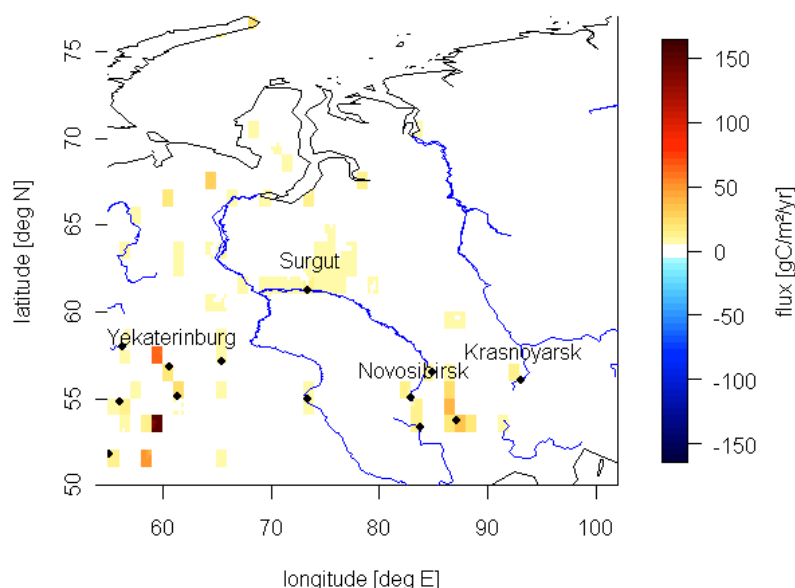
Figure 44 *Prior distribution of total CH$_4$ fluxes in 2009 (see text)*

E   Regional flux estimation with the Jena inversion system for Central Siberia

E2.6 Atmospheric data

The a-priori flux data can now be combined with the transport model to calculate mixing ratios at all stations of interest. A comparison to the true measured data is required to gain knowledge about the validity of the model output; therefore, the atmospheric mixing ratio observations are the key variables in the top-down inversion approach.

For the global CO_2 first-step inversion (Chapter E2.1), 56 stations around the world are used (dataset "S19c", station list "M99j", [Rödenbeck, 2005]). Within the ZOTTO domain, there is data available from three additional stations: ZOTTO itself, and two stations of aircraft measurements (data by T. Machida, personal communication, see Barkley et al. [2007], Table 10). They are primarily used for the second-step regional inversion (Chapter E2.2), but they can be included in the global run as well (see different inversion settings in Table 11).

The global CH_4 inversion is driven by 59 stations around the world (dataset "S01b", station list "NEUch4", NitroEurope A6.2 Modeling Protocol, [Bergamaschi et al., 2009]). Within the regional domain, CH_4 data is kindly provided by M. Sasakawa from NIES, Japan for three towers of the 9-tower-network until the end of 2009 (see Sasakawa et al. [2010], Table 10). To adapt the independent gravimetric scale of the Japanese National Institute for Environmental Studies (NIES) to the same one used in ZOTTO (NOAA-2004), the data of the 9-tower-network has to be multiplied with a factor of 0.997 before using it in the model framework [*GAW Report No.186*, 2007].

Most of the atmospheric data streams are subject to data post-processing procedures and are often available with a time delay of more than one year. Even the raw data from ZOTTO is available with a delay of up to several months. Thus, the availability of mixing ratio observations also restricts the investigation with the atmospheric inversion model to the year 2009.

Table 10 *Overview of gas observation sites, which were used in the regional inversion for 2009*

Site Name	Lat. °N	Lon. °E	m a.s.l.	Months available	CO_2	CH_4	Type	References
ZOT ZOTTO	60° 48'	89° 21'	114	05-12	X	X	Continuous 301 m tower	[Winderlich et al., 2010]
SUR Surgut	61°	73°	≤7000	01-12	X	-	Monthly flight	[Machida, personal communication, 2011] [Barkley et al., 2007]
NOV Novosibirsk	55°	83°	≤7000	01-12	X	-	Monthly flight	[Machida, personal communication, 2011] [Barkley et al., 2007]
DEM Demyanskoe	59° 47'	70° 52'	75	01-12	-	X	Continuous 63 m tower	[Sasakawa et al., 2010]
IGR Igrim	63° 11'	64° 25'	25	01-09	-	X	Continuous 47 m tower	[Sasakawa et al., 2010]
KRS Karasevoe	58° 14'	82° 22'	50	01-12	-	X	Continuous 67 m tower	[Sasakawa et al., 2010]

E Regional flux estimation with the Jena inversion system for Central Siberia

The time series of mixing ratios have to be carefully selected to suit the inversion setup in order to produce plausible results. Therefore, several features of the modeling system have to be taken into account:

1) It is desirable that models represent well the different sampling heights from the measurement tower (Figure 45a). For testing, forward transport model runs were performed to understand the representation of the six different tall tower levels. The coarse TM3 model covers the tower height with only two model levels. The diffusive processes during night are captured well, whereas it overestimates the concentration gradients during the well mixed situation in the afternoon (Figure 45b). The fine-scale STILT model is not able to capture all vertical transport processes (Figure 45c). Although the STILT model computationally captures the boundary layer height down to 58 m, the transport model cannot reproduce the characteristic mixing ratio increases of the ZOTTO observations at the lower levels during night with its low boundary layer heights. Those known deficiencies are targeted by current research [Stephens et al., 2007; Gerbig et al., 2008; McGrath-Spangler et al., 2010]. Thus, information from all six model heights does not yet give additional information for the Jena modeling framework and is ignored hereafter.
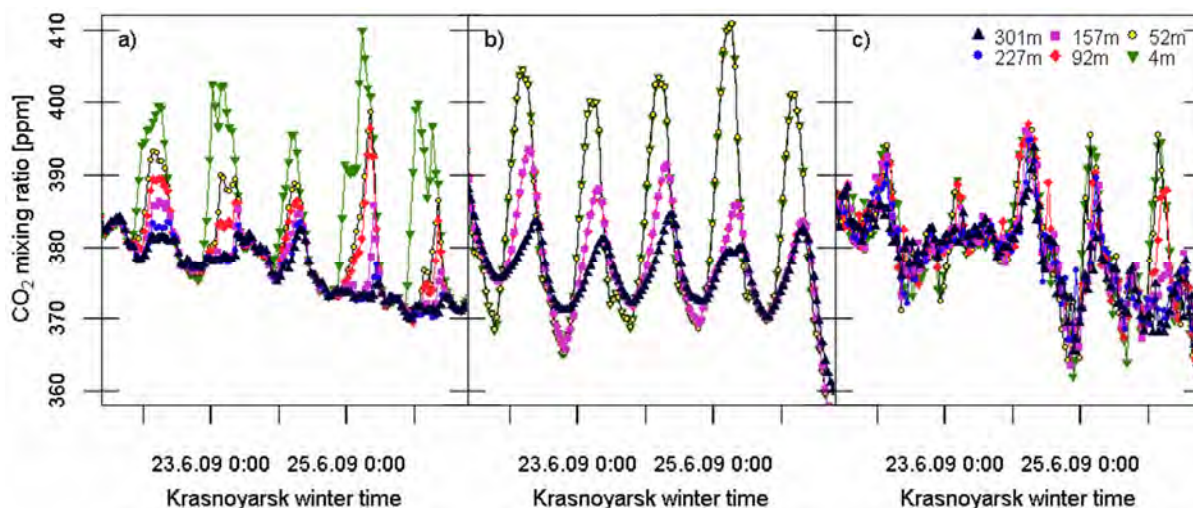
Figure 45 CO_2 *time series at the 6 ZOTTO levels:* **a)** *observation;* **b)** *TM3 model;* **c)** *STILT model*

2) Only those atmospheric data should be selected that can be represented correctly by the atmospheric transport models. The comparison of different transport inversion models revealed that models generally underestimate the daily variability of the trace gases [Geels et al., 2007]. For this reason daytime-selected data from high sampling heights (esp. towers) is preferred. Geels et al. [2007] have shown in detail that the use of data from the well-mixed atmosphere in the afternoon increases the comparability between different transport models. Therefore, global and regional modelers prefer data sets from the afternoon hours only [Butler et al., 2010; Göckede et al., 2010; Peters et al., 2010]. For extremely tall towers with heights above 400 m it has been suggested to use the full 24 h data set [Gourdji et al., 2010]. However, the diurnal cycle of the observed CO_2 data in Figure 24 demonstrates that

the 301 m measurement level gets enriched during night; thus, ZOTTO is not yet tall enough to continuously sample the well-mixed troposphere above the nocturnal boundary layer. The average diurnal cycle also suggests the use of data between 12 pm and 8 pm local time, when different tower levels lie in the same well-mixed air layer.

Temperature inversions may occur along the tower height levels especially during winter (Chapter C2.4). These atmospheric conditions are unlikely to be correctly represented in the atmospheric transport models, as the observed concentration is strongly height-dependent. To exclude this data, the ZOTTO day time data is chosen only when the CO_2 concentrations at 301 m and 227 m levels differ by less than 0.5 ppm. This selection algorithm excludes 72 % of all hourly data points. The average boundary layer height (as given by the STILT model) increases from 515 m for all data to 970 m height for the selected afternoon-data, which is a good indicator for a well-mixed atmosphere.

E2.7 Uncertainty assessment

Several approximations, assumptions and variables are incorporated into the inverse modeling system so far and all cause uncertainties in the result. These uncertainties originate from the transport model, the measurement and the flux model [Gerbig et al., 2009]. A reason for the errors in the transport models can be advective, convective or other mesoscale processes [Gerbig et al., 2009; Ciais et al., 2010b]. This includes especially the inaccuracy in the vertical mixing and according calculations of the boundary layer heights [Gerbig et al., 2003b; Gerbig et al., 2008]. The comparison of two different convection schemes has shown the impact especially in boreal forests on the modeled CO_2 distribution and its accompanying potential for a misinterpretation of sources and sinks [Bian et al., 2006].

The driver of the regional transport model STILT, the assimilated ECMWF data product (Chapter E2.3), has some errors in representing the true weather conditions at the ZOTTO station. A comparison of the data for the summer months June to August 2009 with the local wind measurement at the ZOTTO 301 m level (Figure 46) generally shows good agreement with a correlation coefficient $r^2 = 0.91$ for the wind speed (Figure 47a), and a linear 1:1 dependency between modeled and measured wind direction (Figure 47b, 0° and 360° are identical). However, the small remaining inaccuracies can still cause large errors in the flux allocation. A large signal emitted by a bog or a settlement may be incorrectly assigned to a forest, even if the wind direction differs only marginally from the reality but leads into a different air stream.
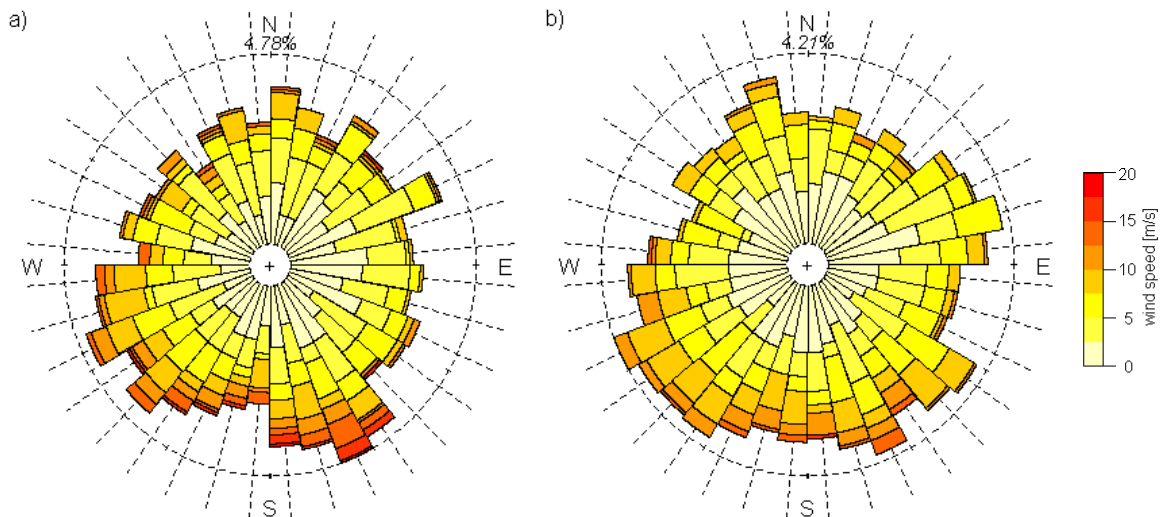
Figure 46 *Comparison of the wind roses for June-August 2009 at 301 m tower level between* **a)** *measurement and* **b)** *ECMWF data*
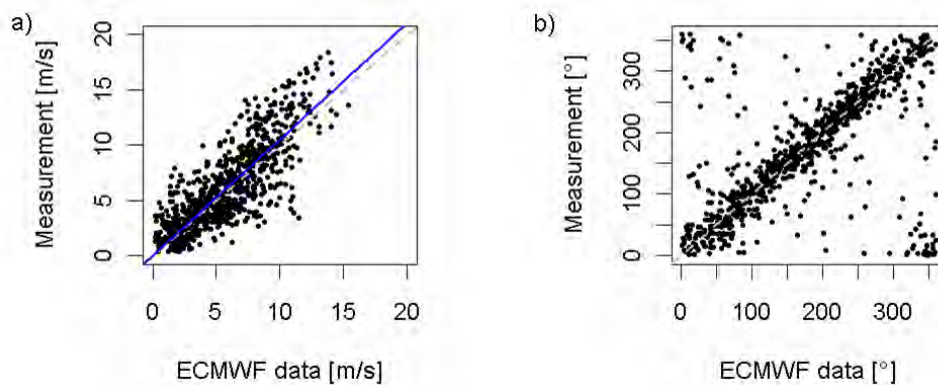
Figure 47 *Comparison of wind fields from ECMWF data and from measurement for June-August 2009 at 301 m tower level:* **a)** *wind speed with linear fit in blue (slope = 1.05 ± 0.01, r² = 0.91),* **b)** *wind direction*

Due to the discretization of time and space in the transport models, the location of the measurement site is subject to a representation error that varies with different grid sizes [Gerbig et al., 2003a]. An air parcel needs the time Δt to travel through a grid cell with the length Δx. Given a wind speed of v = 10 m/s from Figure 14, the time Δt ~ Δx/v will be in the order of 6 hours for the global model TM3 (Δx = 4° ~ 200 km at 60 °N), and for the regional transport model STILT (Δx = 0.25° ~ 15 km at 60 °N) approximately 24 minutes. Remarkably, this is in the same order of response time from the air buffer volumes installed at ZOTTO (37 min; Chapter B2.1). Signals with higher frequency can inherently not be represented well by the transport model, despite temporally higher resolved transport and flux fields.

Different ideas exist, how to limit the representation error. The use of tall towers instead of surface stations leads to a better representation of the data in inverse models [Geels et al., 2007]. Figure 11 in Van der Molen et al. [2007] suggests to use afternoon (1 pm) and evening (8 pm) data that reduce the representation error by a factor of 5 compared to morning data. A larger sampling height reduces the error

even in the morning. Obviously, a smaller grid size reduces the representation error. One reason is the better resolved topography (see Van der Molen et al. [2007] and Chapter D3.5).

Another error source is the limited precision and accuracy of the instrumentation. The measurement error for CO_2 is targeted to be 0.1 ppm, whereas model errors are in the order of several ppm. Therefore the models dominate the total error [Gerbig et al., 2009]. Nevertheless, a negative bias in the measurement would correspond directly to a sink in the inferred flux field. Small deviations can have a large impact on the global scale (a bias of 0.1 ppm corresponds to 0.2 PgC), but the error is reduced with increasing number of statistically independent measurement sites.

To incorporate the knowledge of the error sources into the transport inversion model, the uncertainty of continental stations is assumed to be constant over time with σ = 3.0 ppm for CO_2 and is included as a diagonal element σ^2 in the error covariance matrix $\mathbf{Q_m}$ [Rödenbeck, 2005]. This number comprises all measurement and transport errors, as the transport itself is otherwise assumed to be perfect in the inversion system. The errors between the different stations are supposed to be uncorrelated (no off-diagonal elements in the covariance matrix). This is an acceptable approximation, because the distance between the stations (700-900 km) is much longer than the observed correlation lengths of 20-100 km in the CO_2 concentration fields [Lauvaux et al., 2009b].

The previous chapter described the advantages of tall tower data that may allow the usage of measurements over a longer period of the day than just the well-mixed afternoon data. Because ZOTTO is not high enough to be unaffected by the nocturnal boundary layer (Figure 24), the nighttime measurements ideally would be included in the model system with an increased error during night, and less error during day – according to an increased weight of afternoon data. But the option of time-dependent errors is not yet implemented in the Jena inversion system. As an inspiration for further developments, the difference in mixing ratios between different tower levels or the mismatch between the 301 m tower level and an independent transport model, e.g. WRF in Chapter D3.5, may be helpful to scale the magnitude of this error.

Finally, the uncertainty of the flux fields needs attention. For the CO_2 inversion, the uncertainty of the regional a-priori flux estimates are scaled down from the global flux fields to the regional domain (further discussed in Rödenbeck et al. [2009]; variable *shapeFact* in the parameter files).

The global CH_4 inversion model underlies ongoing development, which includes the chemistry model. Therefore, the a-priori flux uncertainties of the ZOTTO region are not directly coupled to the global fields and are estimated to have 100 % relative error for each pixel [U. Karstens, personal communication, 2011].

The basic idea of the Bayesian inversion is to use the information of the atmospheric mixing ratios to narrow down the uncertainties of the a-priori flux for the posterior flux estimate (Figure 38). Mathematically, the posterior flux uncertainties and correlations can be calculated in the a-posteriori covariance matrix (equation 24 in [Rödenbeck, 2005]). In fact, this operation includes the matrix inversion of the transport matrix, measurement covariance matrix and a-priori covariance matrix. If the calculation is done for the full spatial and temporal resolution of the flux field, the inversion of those huge matrices is computationally too costly. For this reason the posterior error estimates are restricted in this work to the annual mean for the year 2009 and one single subregion. To achieve a meaningful result, it has been decided that the extensions of this subregion match the boreal forests cover in the West Siberian plain. Thus, the rectangular area of this region set *"WSIBplain"* is limited by the Ural mountains 59°E and the Yenisei River at 90°E, and is confined by the extension of the boreal forests from 56°N to 66°N, which is given by the land cover map SYNMAP [Jung et al., 2006] (Figure 48).
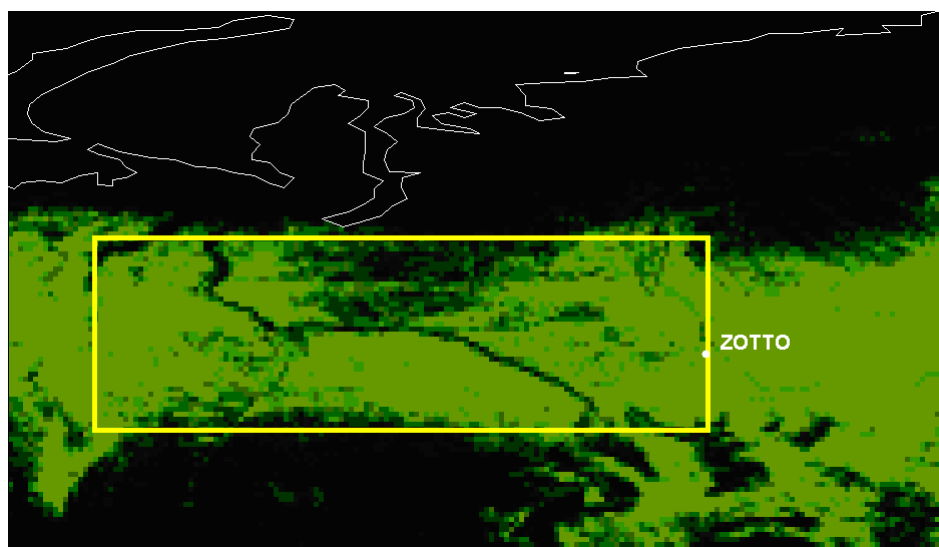
Figure 48 *Fractional forest cover in the ZOTTO domain; black ~ no forest, green color ~ fraction of all land cover types including the life form tree, given by SYNMAP indices 1-36*

The flux uncertainty calculation using the posterior covariance matrix strictly holds on all simplifying assumptions made when the model framework was constructed and takes all parameter settings for granted. Another approach to estimate the uncertainty of the inversion model is to compare model results with different initial settings. Exemplarily, the variation of the correlation lengths in the flux field will lead to an altered model result. The spread in a comprehensive model ensemble allows the assessment of probable model errors.

E3 Results and discussion

E3.1 Synthetic experiments for an optimized model setup

The whole inversion is an ill-posed problem, because it has much more degrees of freedom in the fluxes than can be calculated from the atmospheric mixing ratio observations. To simplify the calculation, the flux field with 188x108 pixel and 2920 time steps is transformed with the help of equation (21) to a less dimensional parameter vector. Different pixels are connected by each other via a shape function and exponential coherency functions $g_i^{time}(t)$ and $g_i^{space}(x, y)$, which are characterized by their correlation lengths. The true values of the correlation length in time and space are not known, because the real fine resolved flux patterns are unknown. The correlation lengths are disputed in the literature and also depend on the design of the inversion system. It is important to note, that the spatial and temporal correlations of the fluxes are not directly related to the atmospheric transport and cannot be inferred from the footprint calculations (e.g. Figure 40).

To optimize the correlation lengths for the Jena inversion system, a synthetic experiment was designed to test the ability of the model system to reconstruct an a-priori known flux field ("known-truth") from atmospheric data by starting with a different prior flux field.

The "known-truth" is given by the CO_2 prior data of the standard inversion in Table 8. A forward run of the STILT model simulated the transport of this flux field to the measurement stations and resulted in artificial data series of CO_2 mixing ratios at the place and time of the real measurement station ZOTTO. This ensures that the inversion with synthetic data uses the same amount of information as the targeted one with the real data. When the inversion was started with the full flux field of the "known-truth", the result stays identical, thus, the system is self-consistent. Now the model system can be started for further investigations with a modified prior flux field, which includes e.g. only spatial or temporal averages. The only information about the variability of the "known-truth" flux field is given by the synthetic concentration series.

The inversion is done with the full data time series, including day and night values. As the transport is the same for the "known-truth" and the synthetic experiments, transport model errors are nonexistent in these synthetic experiments. Therefore, there would not be any advantage by choosing afternoon data only. The full flux field – including nighttime fluxes – would still contribute to the modeled mixing ratios, because air that has traveled several hours had seen this nighttime signal before.

At first, the temporal correlation length is examined. Therefore, the biospheric prior flux field has been simplified by averaging over time. As the inversion is not able to reconstruct high frequencies in the fluxes like the diurnal cycle (standard time correlation length is 2 weeks), a high-pass filter was applied on the known-truth to still allow for diurnal to weekly variations (time filter '-Filt52.0Txax', see [Rödenbeck,

2005]). Figure 49 illustrates the operation principle. The inversion system "knows" the true (synthetic) concentration at ZOTTO (green dashed line). In contrast, the time averaged prior flux would result in the blue dotted concentration data without any seasonal cycle. Now the inversion model solves for a better flux distribution that simulates a concentration time series as close to the "known-truth" as possible. The final posterior concentration simulation (blue solid line) does already show the seasonal cycle again and follows the smaller scale variability, especially in winter. The posterior concentration does not match the synthetic "truth" completely, which demonstrates the restrictions of the Jena inversion system, which are necessary to allow a solution for the otherwise ill-posed problem.
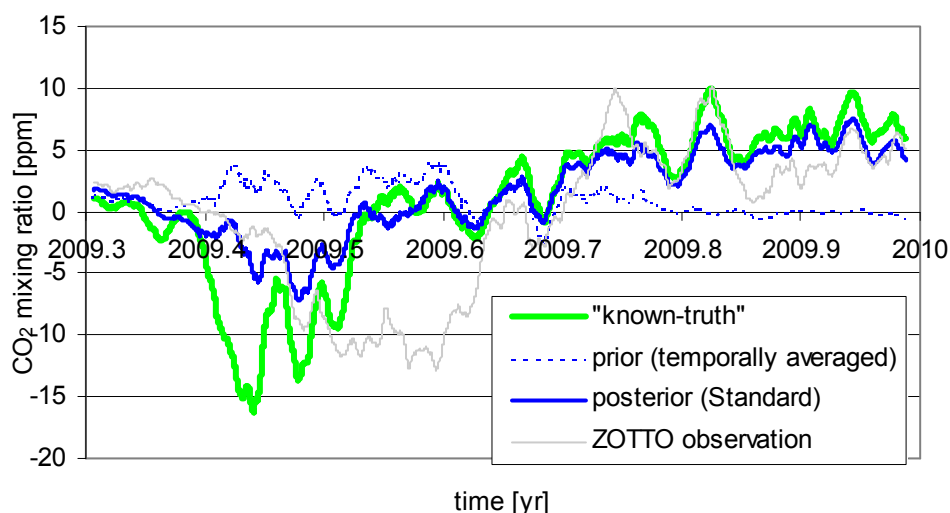
Figure 49 *Simulated CO_2 concentration time series shown as weekly averages: with flux field of the "known-truth", temporally smoothed prior and resulting posterior flux field*

It is worthwhile to note that the synthetic "known-truth" does not match the truly observed values at the ZOTTO station (grey in Figure 49). The summer minimum is shifted by almost two months.

The model experiment has been repeated with different multipliers on the temporal correlation length of the standard setting of 2 weeks (SLOW3x, Standard, FAST2x, FAST5x, FAST30x), corresponding to correlation times of 6, 2, 1 week, 3 days, and 12 hours.

Additionally, the experiment has been repeated for the different spatial correlation lengths. The biospheric prior flux has been averaged over the whole domain for each individual time step. Figure 50 illustrates that this flat prior conserves the seasonal cycle in the modeled concentration time series (orange dotted line). After the inversion, the posterior flux field came closer to the "known-truth". This spatial experiment was also repeated for several multipliers of the standard correlation length (LONG3x, Standard, SHORT3x, SHORT10x, SHORT30x), starting from several thousand kilometers down to tens of kilometers.

E   Regional flux estimation with the Jena inversion system for Central Siberia
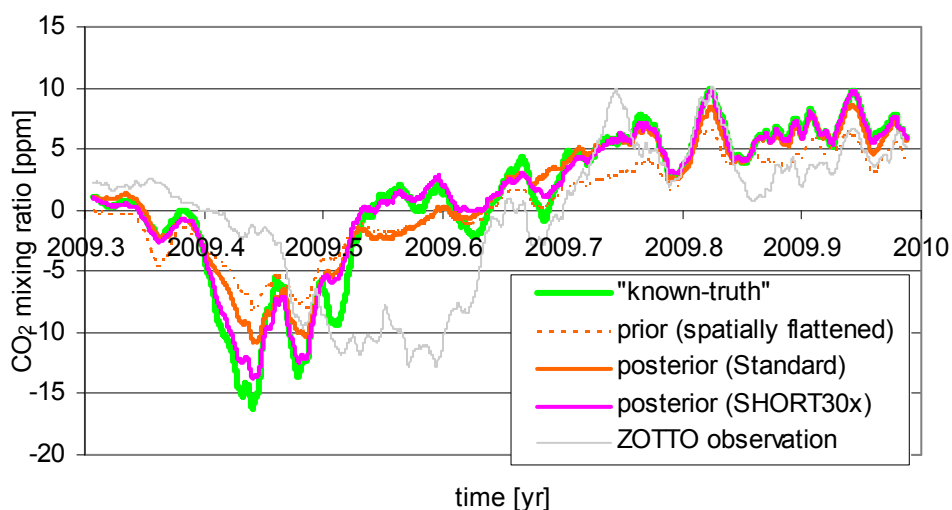
Figure 50 *Simulated CO_2 concentration time series shown as weekly averages: with flux field of the "known-truth", spatially flattened prior and resulting posterior flux field*

As expected, Figure 50 demonstrates that the mismatch in the concentration time series decreases strongly with shorter spatial correlation length. To investigate whether this signal corresponds to a flux field that is closer to the "known-truth", the flux time series are plotted in Figure 51.
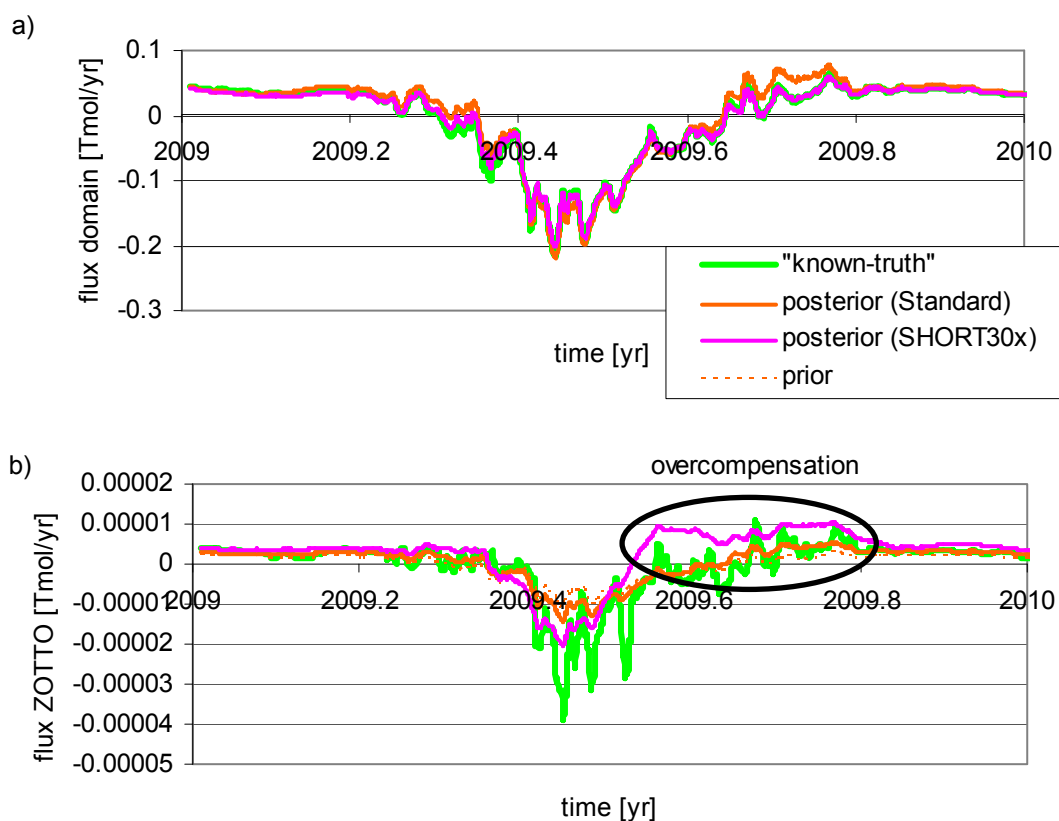
Figure 51 *CO_2 flux time series (aggregated daily) in the synthetic experiments:* **a)** *averaged over the whole domain,* **b)** *at the pixel of ZOTTO*

E   Regional flux estimation with the Jena inversion system for Central Siberia

The total flux in the domain (Figure 51a) does also improve with shorter spatial correlation length. The analysis of the spatial adjustments of the fluxes reveals a speckled pattern with too short correlation lengths (Figure 52). Since it does not falsify the total budget by large alternations in the near-field, it can be interpreted as a good sign of the robustness of the inversion system.
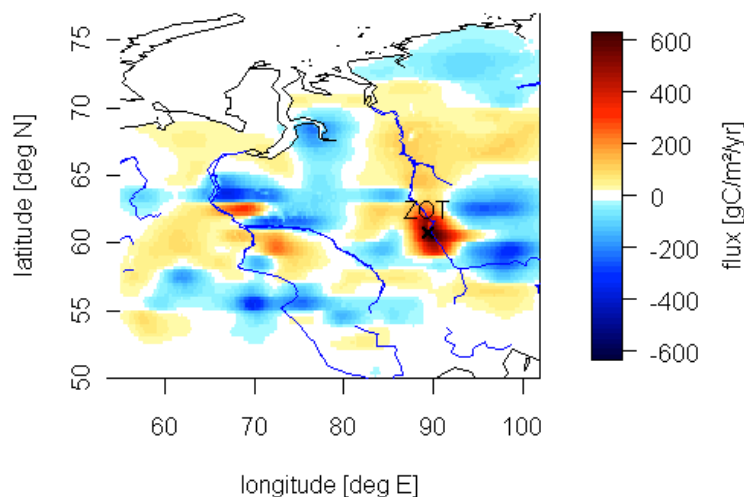
Figure 52 *Spatial distribution of the CO$_2$ flux adjustment (posterior – prior) for an underestimated correlation length of ~ 50 km (SHORT30x) for the period of July-September 2009*

Figure 51b and Figure 52 illustrate the costs of a too short spatial correlation length. While mixing ratios and total flux match the "known-truth" better with shorter correlation length, the convergence is reached by an overcompensation of the flux around the station. The increased degrees of freedom allow the near flux field to vary almost freely to counterbalance the unadjusted signals from the far field. The correlation between "known-truth" and posterior near-field flux decreases.

In summary, shorter correlation lengths match the mixing ratio time series and the total fluxes better, but for the cost of unrealistic near-field adjustments. To specify the best correlation length for the inversion system, the mismatch of all synthetic model experiments can be compared to the "known-truth" in the ZOTTO flux pixel. Therefore all experiments are summarized in Taylor plots in Figure 53. The Taylor plots illustrate the match between modeled and true flux data (ZOTTO pixel) in terms of their correlation (angle), their standard correlation (radius) and the root mean square error (distance from "true" point) in a polar diagram. The "known-truth" is marked on the abscissa by an open circle and is the target for a perfect model.
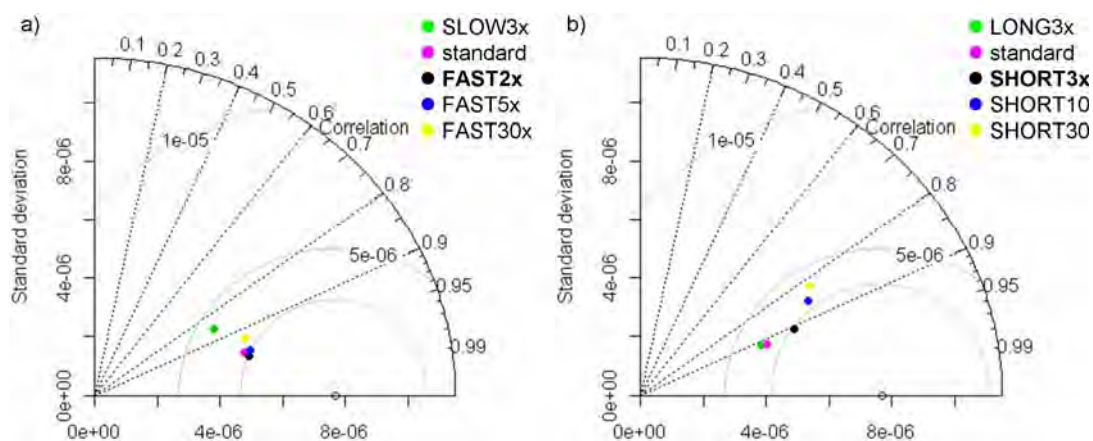
Figure 53 *Taylor plots of the results of the synthetic experiments for different settings (colored dots) in comparison to the "known truth" (given as an open circle):* **a)** *prior flux ~ mean in time to capture best temporal correlation length;* **b)** *prior flux = mean in space to capture best spatial correlation length*

By summing up all simulation results, the optimal inversion setup can be chosen. The lowest distance to the "known-truth" is achieved with the inversion setting SHORT3x and FAST2x. The optimal setting corresponds to a temporal correlation length of one week. The spatial correlation length differs for different components of the fluxes and for different geographical directions: in west-east direction, the inter-annual long-term components correlate on about 500 km scale, the seasonal component on 1200 km, and the fossil fuel emissions on 2100 km scale. The correlation in north-south direction is a factor of two smaller. In general, Figure 53 illustrates that a shorter correlation length increases the variability of the result, but the correlation does not increase further.

All results refer to an inversion setting with the scaling factor $\mu = 0.25$ (see equation (23)), which increases the prior flux uncertainty by a factor of two. In turn, the weighting of the atmospheric data is increased, as it should be the essential driver of the flux adjustments. The dependence on μ of the overall result for the optimal correlation length is small, with a weak preference for smaller spatial correlation lengths for larger μ.

The optimization of the spatial correlation lengths is performed with fixed temporal correlation lengths of two weeks. The optimization of the temporal correlation lengths is done for a fixed spatial correlation length of 1000 km. All other combinations have not been tested because of high computational costs (each test requires 2 days running time). But a test with the final optimal setting allows the assumption of a marginal cross sensitivity.

The result of the synthetic experiment depends on the choice of the prior flux field. Since the real flux is unknown, this experiment can give a first guess only. A look into the literature supports the results. 10 days temporal and 1000 km spatial averaging is necessary on a posterior flux to fit the "known truth" in Carouge et al. [2010a; 2010b]. An inversion with real data [Peylin et al., 2005] uses 500 km correlation length in the standard case, and suggests that the extreme case of 2000 km

E Regional flux estimation with the Jena inversion system for Central Siberia

correlation length overestimates the uncertainty reduction of the flux fields. Gerbig et al. [2006] investigated the flux uncertainty reduction vs. covariance lengths. The result implies preferring larger correlation lengths. In detail, the resulting flux uncertainty increases less, if the estimated correlation length is overestimated. If the correlation length is underestimated, the posterior flux uncertainty is substantially increased. This finding underlines the conservative choice of the setting SHORT3x, compared to the shorter correlation length that the $\mu = 1$ experiment may also tolerate.

The real data can now be used to estimate the real flux fields of the year 2009 with the optimized inversion setup.

E3.2 CO$_2$ flux fields

A 2-step Jena inversion system was run. The first step is the global inversion, which is refined in the second step to the Siberian domain. The regional inversion has been run with the optimized setup (named as *"Reg1.0"*), which has been found in the synthetic experiments. The result for the total CO$_2$ flux for the entire year 2009 is given in Figure 54, and includes the biosphere, fossil and forest fires, and ocean fluxes.
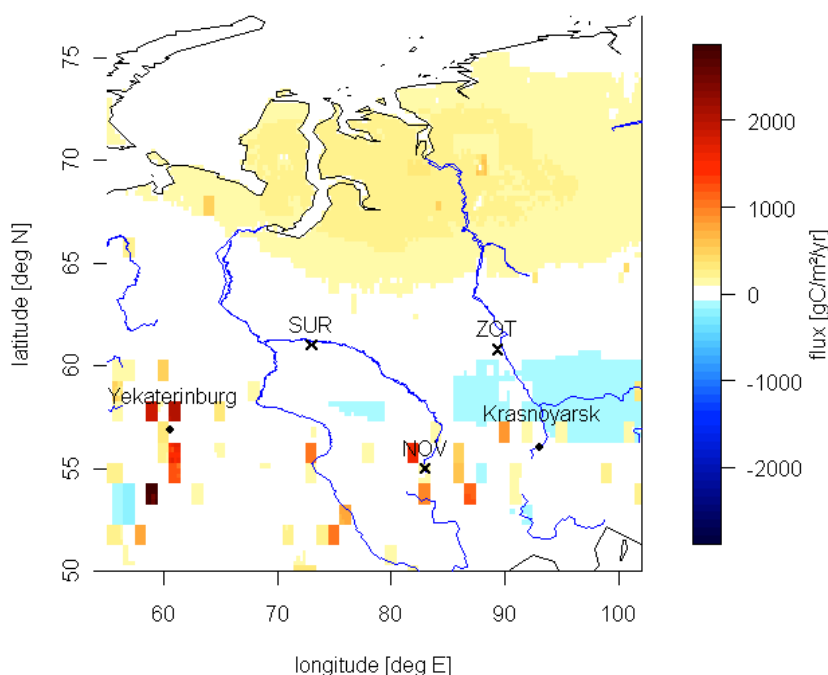
Figure 54 *Total CO$_2$ flux for the year 2009 (regional inversion setting "Reg1.0")*

The result for the total fluxes is dominated by fossil fuel sources. Because the fossil fuel emissions are assumed to be well-known in comparison to all other flux components, the fossil fuel emissions are fixed in the model. In case the fossil fuel emissions are wrongly estimated, the flux adjustment can only be compensated in the biospheric flux component. Therefore, for the visualization of the inversion results, only the biosphere flux is shown. To illustrate the seasonal variations, the results are

split up into three-monthly periods in Figure 55. The winter months are characterized by CO_2 emissions from plant respiration and possibly from increased fossil fuel emissions, which has not been accounted for in the fixed fossil fuel prior fields. In the summer months the photosynthetic activity fixes atmospheric CO_2 in the plants. Consequently, the area covered by boreal forests gets visible as a widespread sink.
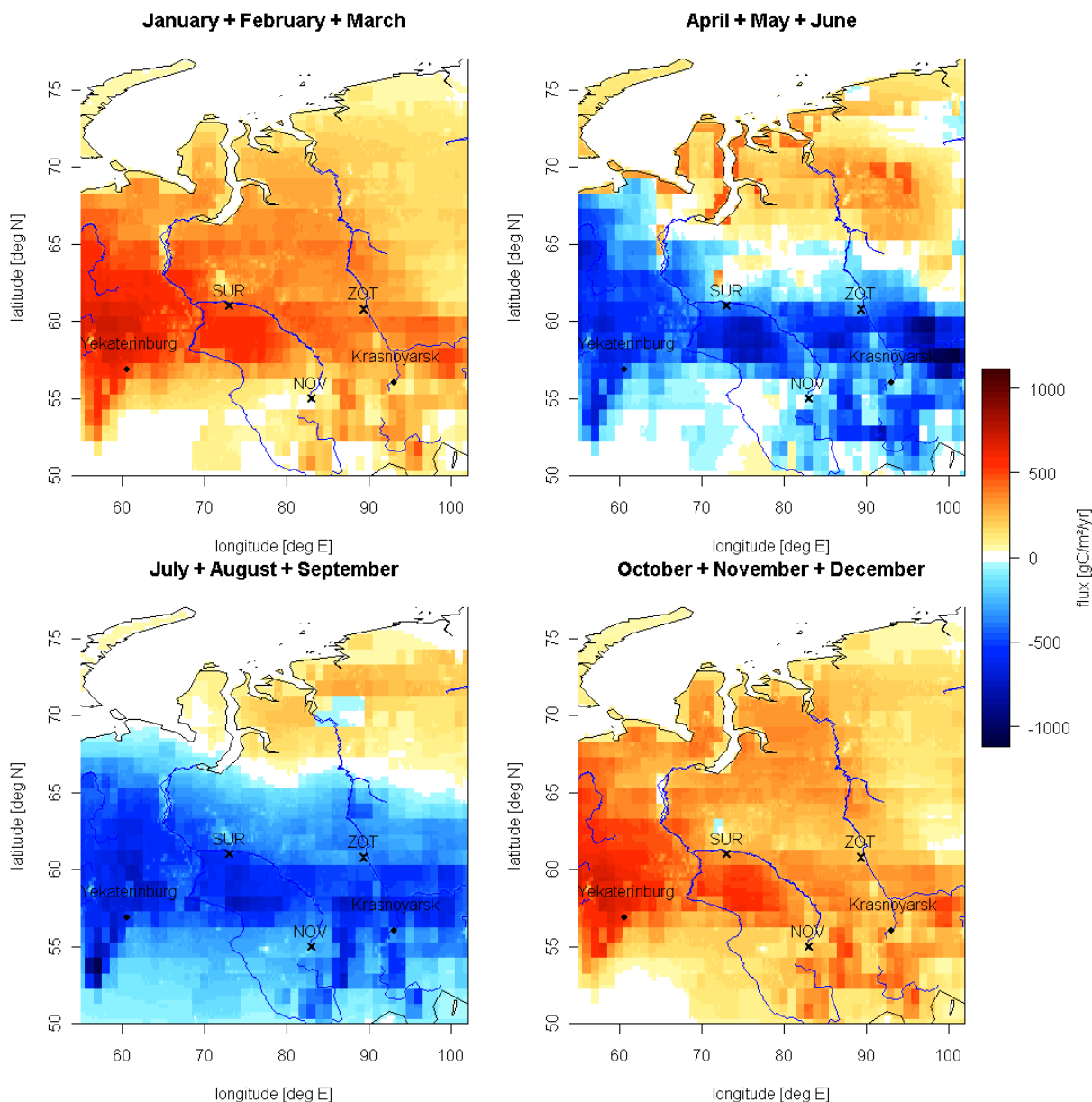
Figure 55 *Biospheric CO₂ flux for each quarter of the year 2009 ("Reg1.0")*

To analyze the behavior of the inversion system, Figure 56 illustrates the changes in the flux fields, when the posterior flux is compared to the prior knowledge. The inversion results indicate a robust behavior, because the flux fields show neither small scale dipoles nor bull-eye effects where the measurement stations are located (as in Figure 52). The positive flux adjustment in April to June is compensated by a stronger sink in the late summer July to September. It implies a shift in the seasonal cycle of the optimized fluxes compared to the prior ones, as it has already become

visible when comparing the observed CO_2 seasonal cycle at ZOTTO to the prior biosphere fluxes in Chapter E3.1. Moreover, the positive adjustments in the industrialized area around Yekaterinburg during winter indicate higher fossil fuel emissions than is given by the prior fluxes.
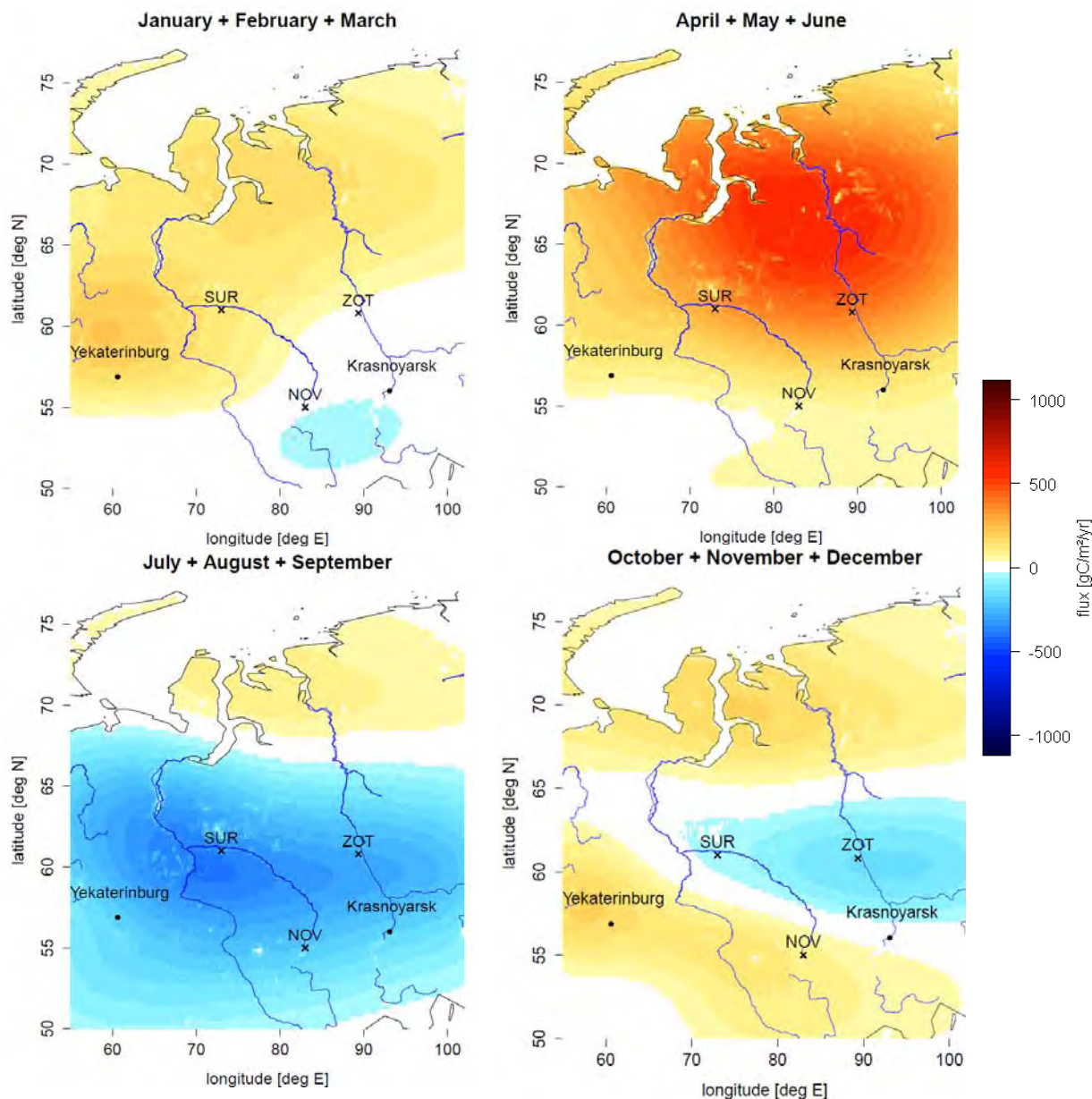
Figure 56 *Difference of CO_2 posterior flux to the prior flux for each quarter of the year 2009 ("Reg1.0")*

The inversion with the optimized setup (Reg1.0) gives a total biospheric flux of -0.01 PgC in the boreal forest region *"WSIBplain"* for the whole year 2009. To achieve this number, the posterior flux field is iteratively optimized pixel by pixel and time step by time step before finally integrating to the region of interest and the whole year. To estimate the according error, the posterior covariance is calculated additionally. This covariance calculation optimizes the fluxes only in the region of interest and only for a certain time filter (here: *"Filt2.0g"*) to make the matrix inversion

computationally feasible (Chapter E2.7). As a consequence, the flux integration is done before solving the matrix equations iteratively; thus, the size of the biospheric flux from the a-posteriori covariance matrix calculation deviates from the first result and gives -0.07 ± 0.11 PgC/yr for the boreal forest region *"WSIBplain"* in 2009. In comparison to the prior flux of the BIOME-BGC model and its a-priori uncertainty of -0.06 ± 0.21 PgC/yr, the uncertainty reduction is 45 %. For all variants, the fluxes from fossil fuel burning and forest fires account for further 0.05 PgC flux per year.

When the inversion model framework was set up (Chapter E2.1), some assumptions have been formulated and parameterized. As the correct parameter settings are not intrinsically given, they have been varied within a reasonable range. Additionally, each regional inversion comprises not only the second step of the inversion framework, but it is also based on a global first step (see Chapter E2.2). The global step of the regional inversion *"Reg1.0"* does not yet include CO_2 observations from the stations in the ZOTTO domain to guarantee full statistical independence of both runs. Following another argumentation line, the use of the sites within the regional domain is tolerated, because the second step is interpreted as a finer resolved continuation of the global first step (*"Reg.glob"*). Table 11 gives an overview about all the different runs done and the according results for the total budget of the region *"WSIBplain"* in the western Siberian plain (including fuel and fire emissions).

Table 11 *Overview of the CO_2 inversion settings*

Name	Inver-sion type	Prior data	Day/night data	Observation used globally[1]	μ	Temporal corr.	Spatial corr.	Flux in *"WSIBplain"* [PgC/yr]
Reg1.0	regional	Biome-BGC	day	No	1.0	FAST2x	SHORT3x	+0.04 ± 0.11
Reg0.25	regional	Biome-BGC	day	No	0.25	FAST2x	SHORT3x	+0.22
Reg4.0	regional	Biome-BGC	day	No	4.0	FAST2x	SHORT3x	-0.23
Reg.a	regional	Biome-BGC	all	No	1.0	FAST2x	SHORT3x	-0.23
Reg.glob	regional	Biome-BGC	day	Yes	1.0	FAST2x	SHORT3x	-0.06
Reg.glob.a	regional	Biome-BGC	all	Yes	1.0	FAST2x	SHORT3x	-0.11
Reg.old	regional	Biome-BGC	day	No	1.0	Std.	Std.	+0.002
Reg.CT	regional	CarbonTracker	day	No	1.0	FAST2x	SHORT3x	+0.09
Glob.no	global	Biome-BGC	-	No	1.0	Std.	Std.	-0.19
Glob	global	Biome-BGC	day	yes	1.0	Std.	Std.	-0.04
Glob.a	global	Biome-BGC	all	yes	1.0	Std.	Std.	-0.06
		Biome-BGC		prior data	-0.06 PgC (biosphere)	+0.05 PgC (burning)	-0.01 (total)	
		CarbonTracker		prior data	-0.14 PgC (biosphere)	+0.04 PgC (burning)	-0.11 (total)	

[1] describes, if the data from the regional domain have been used in the first step global inversion

All CO_2 inversions apart from the optimum setup *"Reg1.0"* give an average ensemble flux for the region *"WSIBplain"* of 0.01 ± 0.11 PgC/yr. This standard deviation of the different inversions of 0.11 PgC gives an independent assessment of the model error. It is nice to see that it perfectly matches the statistical error estimate

from the posterior covariance calculations of the *"Reg1.0"* setup, although the statistical error already comprises to a certain extent the model errors. Unfortunately, it is unknown to which amount exactly. Thus, it can only be stated that a combination of both error distributions would finally give the true error estimate – no less than 0.11 PgC.

Instead of using the full regional 2-step inversion setup, the global inversion alone allows estimating regional flux budgets. All three global runs *"Glob.no"*, *"Glob"*, and *"Glob.a"* give a flux estimate ± standard deviation of -0.10 ± 0.08 PgC in the region *"WSIBplain"*. The results agree within their error bounds with the regional budget. By including the regional CO_2 observations (*"Glob"*, *"Glob.a"*), the magnitude of the boreal sink gets reduced in comparison to a global inversion without CO_2 measurement sites in Central Siberia (*"Glob.no"*).

The posterior covariance calculations for the global inversion allow a conclusion about the importance of the Siberian data stream. The global inversion gains an uncertainty reduction of 56 % for the boreal region *"WSIBplain"*, when all data series are included (*"Glob.a"*). Without the data inside this domain (ZOT, SUR, NOV) the uncertainty reduction is reduced to 37 % only (*"Glob.no"*). This confirms the importance of setting up measurement stations in this region to better constrain the carbon budget.

The regional simulations match the CO_2 observations better than the global ones (see Figure 39), although the global inversion achieves a tighter constraint on the flux for a whole region through additional stations and longer time series. The standard deviation of simulation minus data gives 4.9 ppm for the regional inversion *"Reg1.0"*, but 6.0 ppm on global scale *"Glob"*.

Additionally, the realization of eight different regional inversion runs allows for a spatially better resolved analysis. The second column in Figure 57 visualizes the standard deviation σ of all runs for each pixel and the four three-months-periods. The largest uncertainties occur from April to June in the boreal regions. One reason is that a small relative change of large fluxes produces large absolute changes, thus, the spread for different settings increases with flux size. Moreover, the inversions allow for the largest flux modification, where the station footprints are localized. Finally, errors in the fossil fuel inventory can be adjusted by the inversion by increasing the biospheric emissions only, which seems to be the case in the industrialized areas in the western part of the domain.

The third column in Figure 57 shows the seasonal shift of biospheric fluxes from April-June to the period July-September, as it has been already seen in Figure 56 for the optimal inversion setting *"Reg1.0"*. The spatial distribution of the flux adjustments is generally quite homogeneous without disturbing bull-eye effects (as in Figure 52).
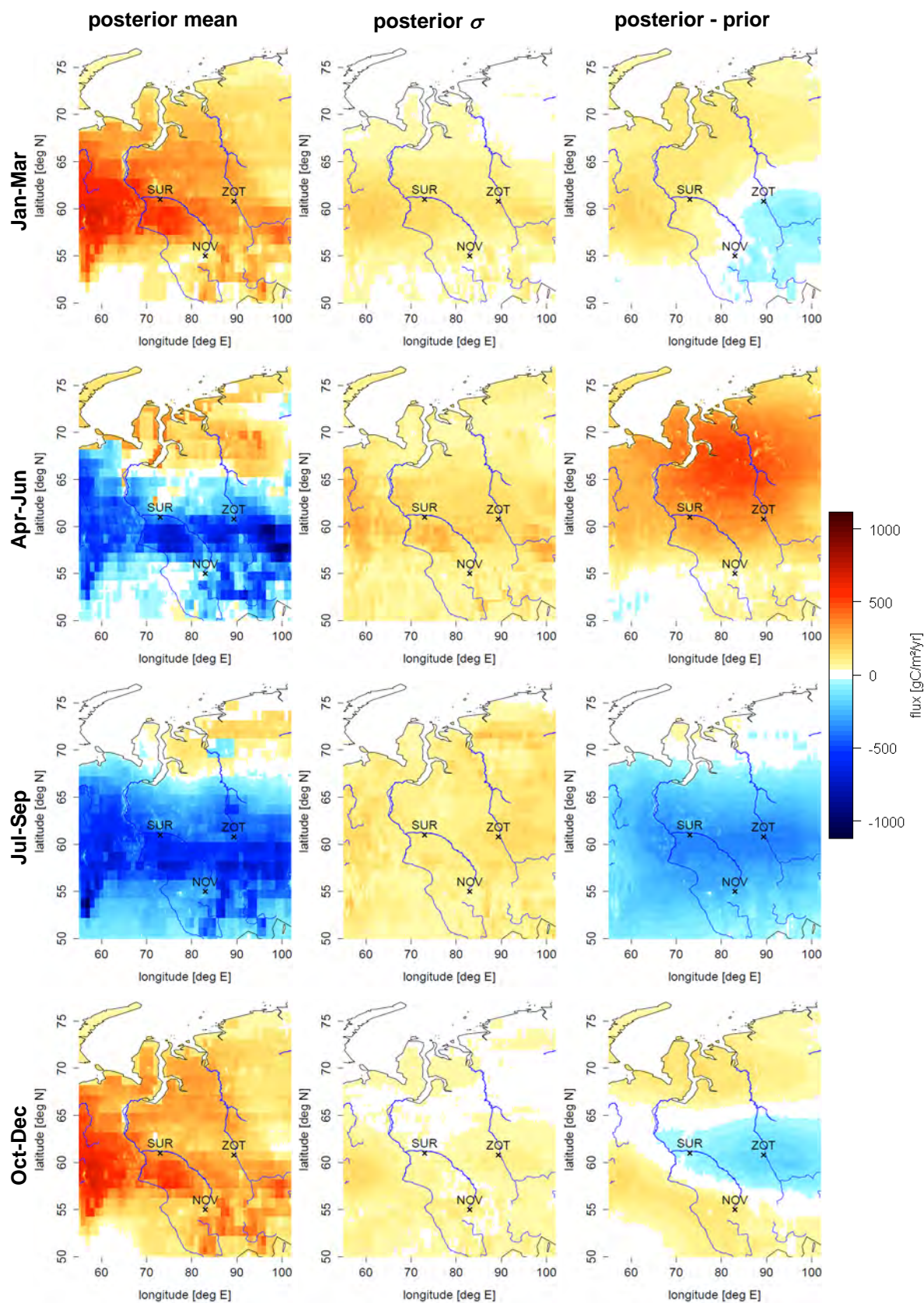
Figure 57 *Biospheric CO$_2$ fluxes for each quarter of the year 2009 (average of all regional inversions): 1st column: Posterior fluxes, 2nd column: Standard deviation of ensemble fluxes, 3rd column: difference of posterior fluxes to prior estimates.*

E   Regional flux estimation with the Jena inversion system for Central Siberia

The results of the inversion compare well with other recently published investigations. Pan et al. [2011] specify the carbon flux of the Asian boreal forests to -0.26 PgC/yr in 2000-2007. Given the fact that the region *"WSIBplain"* covers about one third to one half of this area, the total flux agrees well. Moreover, the summer photosynthetic uptake of the plants of -800 gC/m²/yr (Figure 55) is in line with bottom-up estimates and inventories; Peregon et al. [2008] give an average net primary production (NPP) in West Siberia of -790 gC/m²/yr, spreading from -354 gC/m²/yr in the northern Taiga to -1970 gC/m²/yr in the southern Taiga. A result of -800 gC/m²/yr from Figure 55 implies -200 gC/m² uptake in a three month period. This number matches the outcome of a regional high-resolution carbon flux inversion over North America for 2004 [Schuh et al., 2010], where typical values of -200 gC/m² occur in the boreal zone within the same period July to September.

E3.3 CO$_2$ flux time series

Apart from the spatial analysis, the inversion results can be analyzed for their temporal behavior. Figure 58 summarizes the cycle of carbon flux in *"WSIBplain"* throughout the year for all model settings in Table 11. The most remarkable feature is the outlier in February 2009. The setting *"Reg0.25"* has an increased data weighting. As the observation in ZOTTO did not start before May 2009, there is almost no further data constraint in February and March, the error in one footprint can allocate a flux signal to a wrong region, thus may falsify the flux of the whole domain. This irregular variation is expected to vanish in the following years, when a continuous data stream from the ZOTTO station is available for the entire year.
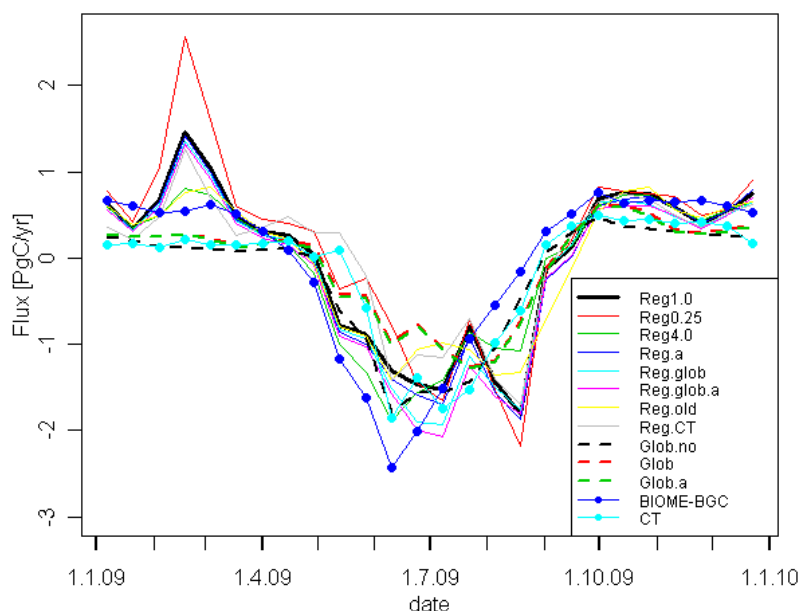
Figure 58 *Seasonal cycle of CO$_2$ fluxes from all individual inversions and prior data (2 week averages)*

Figure 58 also reveals a shift in the seasonal cycle. While the BIOME-BGC prior data peaks in the beginning of June, the regional inversions indicate a less distinct sink in June to July, but a second biospheric sink in August. This was already

indicated in Figure 49, when the ZOTTO CO_2 observations showed a significant shift in the seasonal cycle when compared to the BIOME-BGC prior data.
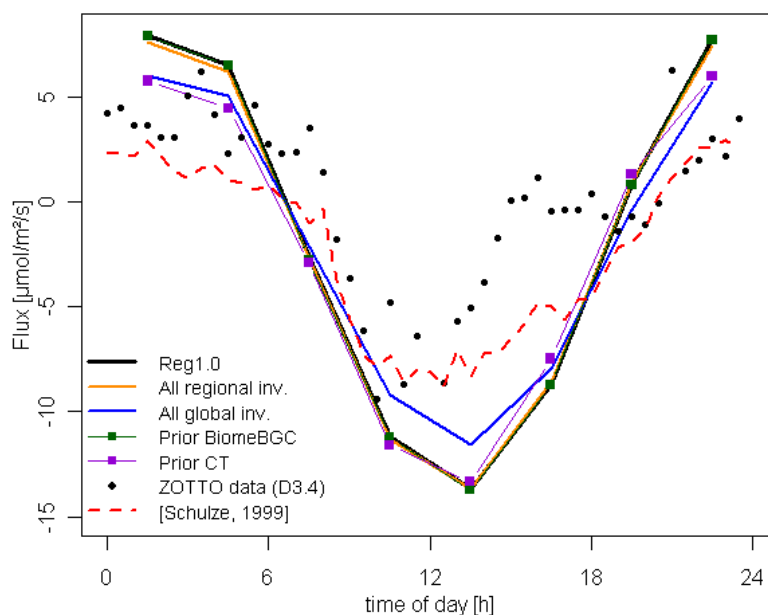
Figure 59 *Diurnal cycle of CO_2 fluxes for July 2009 from different data sources*

The diurnal cycle has also been extracted from the flux time series and is shown in Figure 59. Compared to the measurement data from Chapter D3.4 and the data from July 1996 [Schulze et al., 1999], the modeled cycle has a higher amplitude. A possible reason might be that the impact of the solar radiation is overestimated and the restriction by water is not fully included in the prior biospheric models. The inversion does not allow adaptations in the diurnal cycle from the prior fluxes to the data, because the temporal correlation length is too long. Therefore, the diurnal cycle of the posterior fluxes almost coincides with the one of the prior fluxes. For future inversions, the diurnal cycle of the ZOTTO data set may help to better constrain the biospheric models for an improved prior flux field.

E3.4 CH_4 flux fields

The CH_4 flux inversion is set up in full analogy to the CO_2 flux inversions. Nevertheless, the synthetic experiments (Chapter E3.1) for the correlation lengths have not been repeated for the CH_4 fields. It is known that the spatial correlation for CH_4 is smaller than for CO_2, e.g. other CH_4 inversion use correlation lengths of 100 to 300 km [Bergamaschi et al., 2010]. The Jena inversion system for CH_4 was set up with a correlation length of 212 km independent from the direction in space, and two weeks in time (*"Reg1.0", "Reg.a"*). The setting *"Reg.old"* covers longer correlation lengths: 530 km in east-western direction, and 320 km from north to south; the temporal correlation is monthly. All runs that have been performed are summarized in Table 12.

Table 12 *Overview of the CH₄ inversion settings*

Name	Inver-sion type	Day/night data	Observa-tion used globally[1]	μ	Temporal corr.	Spatial corr.	Flux in WSIBplain [TgC/yr]
Reg1.0	regional	Day	no	1.0	2 weeks	212 km	+ 8.4 ± 1.1
Reg.a	regional	All	no	1.0	2 weeks	212 km	+ 8.2
Reg.old	regional	Day	no	1.0	monthly	530 km E-W 320 km N-S	+ 9.6
Prior data							+ 5.2

[1] **describes, if the data from the regional domain have been used in the first step global inversion**

The result of the CH₄ inversion is summarized for the entire year 2009 in Figure 60. The flux is dominated by human emissions close to the cities and the wetland emissions in the west Siberian plains. The amount of CH₄ emissions that is contributed by forest fires is a factor of 250 smaller than for CO_2 [van der Werf et al., 2010], thus, they are not discernible in the annual budget.
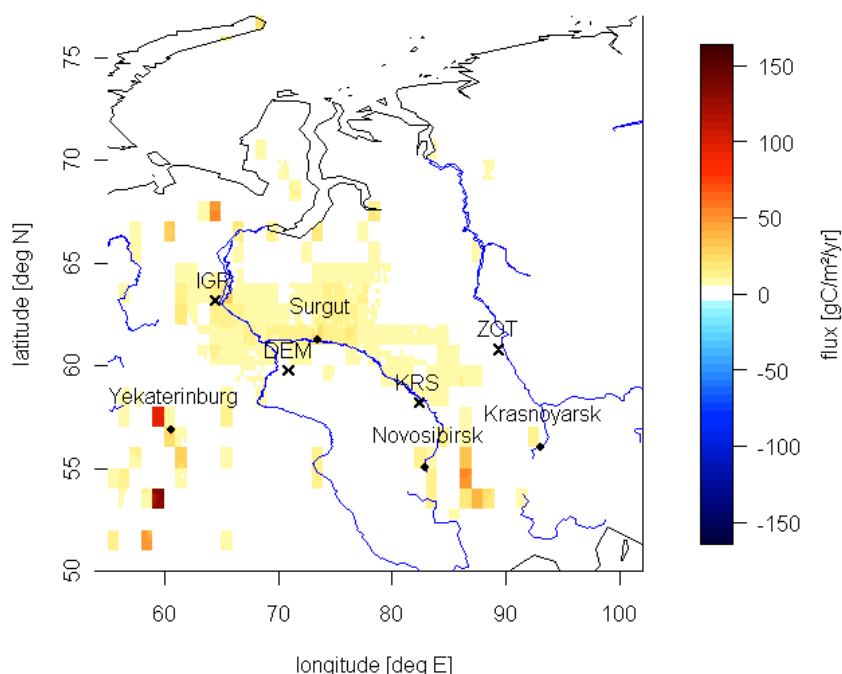
Figure 60 *Total CH₄ flux in the year 2009 (regional inversion setting "Reg1.0")*

The calculation of the posterior covariance matrix for the boreal region *"WSIBplain"* reveals an annual budget of 8.4 ± 1.1 TgC/yr (*"Reg1.0"*). The prior flux is given by 5.2 ± 1.3 TgC/yr, which equals an uncertainty reduction of 18 %.

The spatial distribution of the inversion adjustment posterior minus prior fluxes is shown in Figure 61. Since the prior uncertainty is proportional to the emissions, the inversion adjustments have the similar small-scale pattern as the prior fluxes, but weighted by the station footprints and adjusted at scales larger than the prior correlation length.
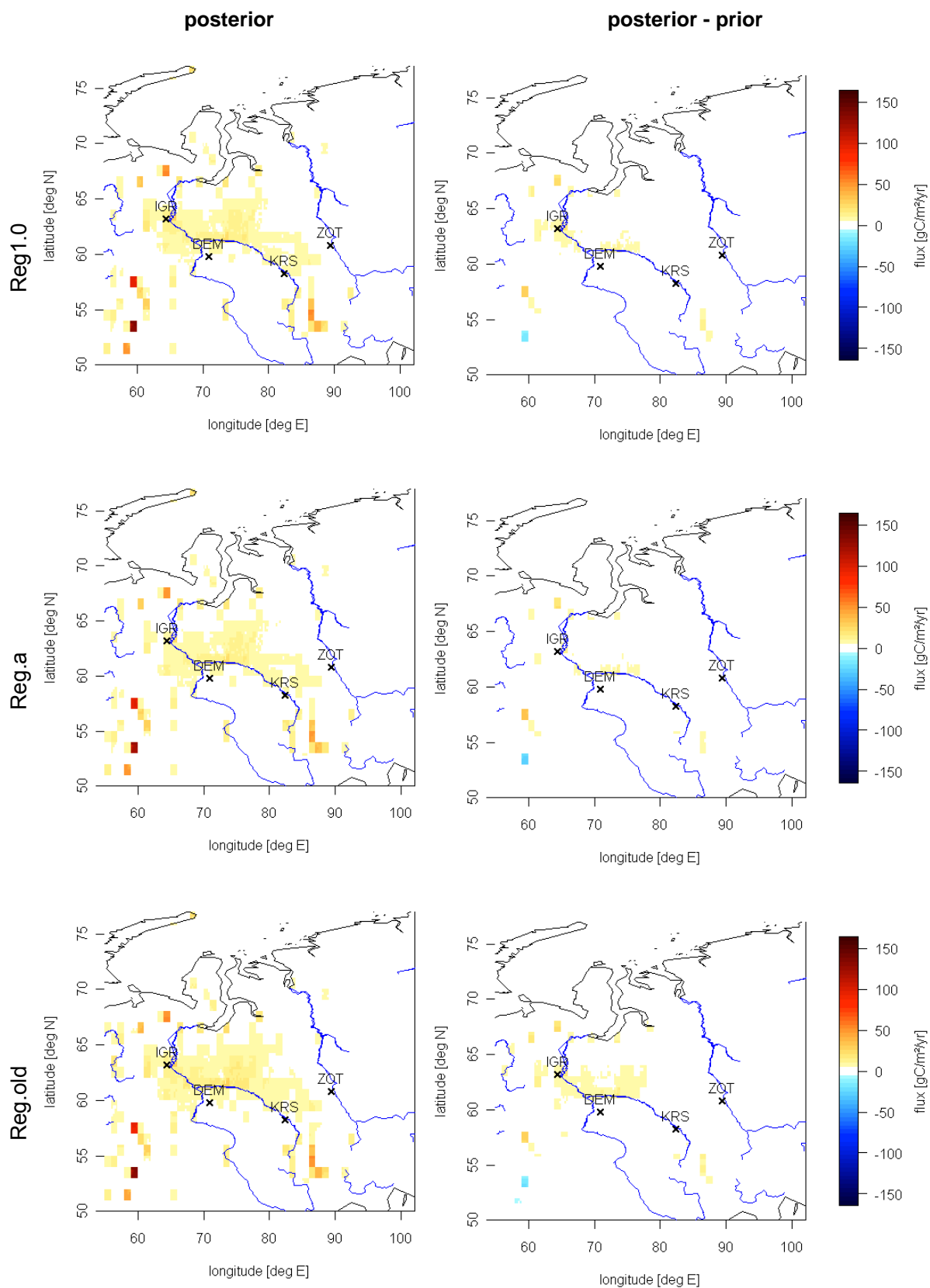
Figure 61 *Posterior CH₄ flux fields (left) and difference to the prior flux (right) for each regional inversion setting:* **top:** *"Reg1.0"* **middle:** *"Reg.a"* **bottom:** *"Reg.old"*

E   Regional flux estimation with the Jena inversion system for Central Siberia

The temporal evolution of the posterior and prior flux integrated over the boreal region *"WSIBplain"* is plotted in Figure 62. The largest fluxes in summer are mainly driven by the seasonal maximum in wetland CH_4 emissions. The inversions show a significant increase of the CH_4 budget, when comparing to the prior data.
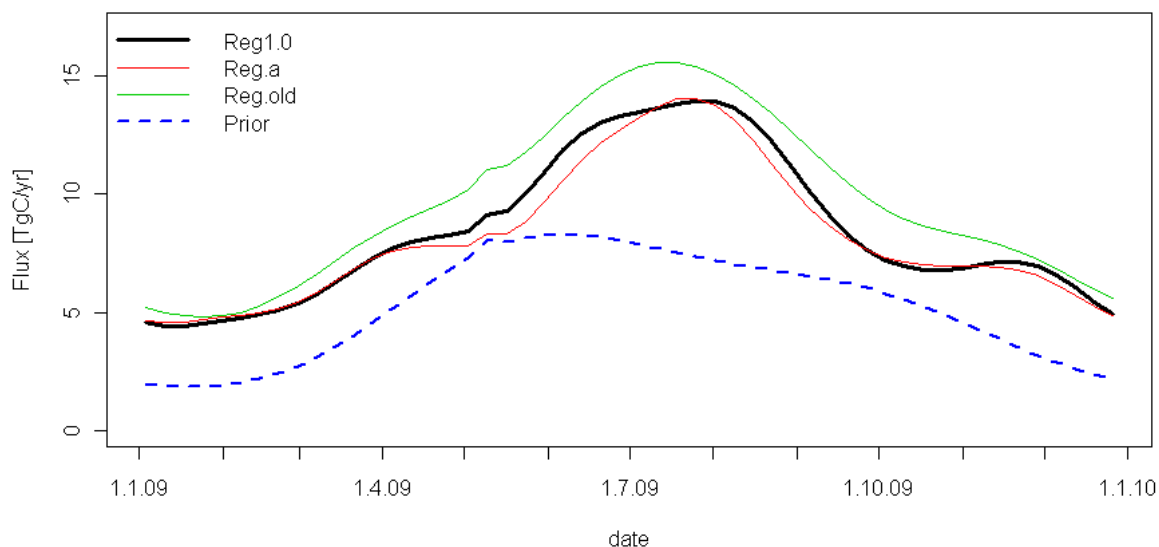
Figure 62 *Seasonal cycle of the CH_4 flux in "WSIBplain" for different inversion settings in the year 2009 (weekly averaged)*
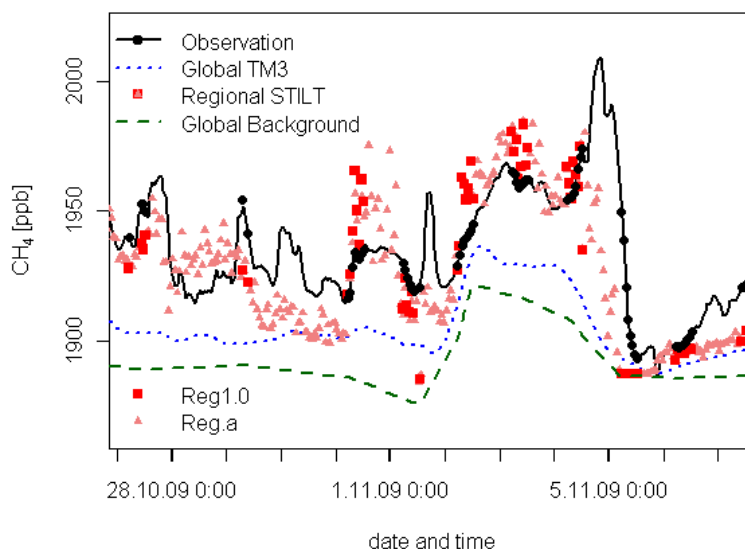
Figure 63 *CH_4 time series at ZOTTO from observation, global and regional inversion results (black dots and red squares mark afternoon data)*

The posterior flux fields allow the transport model to simulate the mixing ratio at the measurement stations. There is an improvement from the coarse grid global model TM3 with a standard deviation 44.0 ppb for CH_4 between model and data towards the regional model with 27.8 ppb (*"Reg1.0"*, ZOT). The other stations are not as representative as the 301 m tall tower station ZOTTO; the standard deviation in the regional model is 59 ppb for Demyanskoe (DEM), 106 ppb for Igrim (IGR), and

E   Regional flux estimation with the Jena inversion system for Central Siberia

52 ppb for Karasevoe (KRS). An individual snapshot of the model capabilities and how they represent the ZOTTO observations is presented in Figure 63. The global background concentration $c_{coarse,trans}$ (compare Figure 39 for CO_2) is lower than the observed values, because the CH4 flux fields do only have sources in the ZOTTO domain. The regional STILT model allows much larger diurnal variations than the global TM3 model, because of the finer resolved transport and flux fields.

A literature search did not yet reveal a regional CH_4 inversion in the boreal region. A global inversion by Bergamaschi et al. [2009] gives a magnitude in the boreal wetland fluxes that are similar to the present work, but it does not show further regional details. Bergamaschi et al. use a similar setup with the same priors, but without the data series that are used here, and their posterior fluxes are slightly reduced compared to the prior flux estimates for 2004. In the contrary to these results, the present inversion result has positive adjustments, because the observations from all stations are in average higher than the model simulations (13 ppb for ZOTTO, 35-45 ppb for the others). Even when daytime data only is used ("Reg1.0"), this offset is due to peaks of the measurement data, which last several hours. Outliers above 2500 ppb, which happen to appear throughout the year, are not represented by the model system, since they are most likely driven by local sources. This assumption of local contaminations is supported by the fact that the representation problems are less with the ZOTTO data than with the shorter towers DEM, IGR, and KRS. This insight may advance future work with CH_4 inversions: emission maps need further improvement of the spatial and temporal resolution, and the amount of tall tower data should be increased.

E3.5 Sensitivity to permafrost

The northern location of ZOTTO asks the question of whether changes in permafrost can be detected by the CO_2 or CH_4 observations. Even though ZOTTO itself is not in the permafrost region, portions of the detected air originate from the region of interest. To quantify the possible impact, a thought experiment can be done. A publication by Schuur et al. [2008] gives all necessary background information.

Future global permafrost emissions are estimated up to 1 PgC/yr [Schuur et al., 2008]. Assuming a uniform distribution in the global permafrost regions, about 10 % of the total is released in the ZOTTO domain. For the record, this amount of 8.3 TmolC/yr would lead to a global increase of 47 ppb/yr carbon-containing gases (mainly CO_2) in the atmosphere. The oceanic uptake would further weaken this signal.

Another assumption is that the release takes place in the region of discontinuous permafrost from 62° to 66°N latitude, where a temperature increase would have the highest impact. The average flux in this $\sim 10^{+12}$ m² wide region would be 0.3 µmol/m²/s. Given the average footprint of ZOTTO in this region with 1.2 ppm/(µmol/m²/s) (similar to Figure 13), the permafrost emissions would give a

305 ppb/yr increase in the ZOTTO mixing ratios. This number implies a six-fold higher sensitivity of the ZOTTO station to permafrost emission in the ZOTTO domain compared to a background station that measures the global average. Nevertheless the measured signal would be small. The partitioning of CO_2:CH_4 emissions of 120:1 [Schuur et al., 2008] suggests an increase of 0.3 ppm CO_2 and 2.5 ppb CH_4 per year. These numbers only marginally exceed the measurement uncertainties.

In summary, the thought experiment reveals only small measurement signals at the ZOTTO station, although all calculations are done with the tendency to prefer high emission estimates. Nevertheless, measurements stations in this region are sensitive to the permafrost gas releases. With regard to the hitherto ignored seasonality of the signal, the signals might be enhanced during the thawing period. Moreover, the usage of various stations further constrains the origin of the CH_4 emissions. Additionally, isotopic measurements and the correlation of diverse trace gases and climate signals can help to gain information about the permafrost releases. Finally, the ZOTTO data series gets the more valuable and sensitive the longer the record continues.

E4 Conclusions

The Jena inversion system has been successfully used to calculate carbon flux budgets in western and central Siberia. The two-step regional inversion allows a fine resolution of the source fields and improves the quality of the simulated mixing ratio series compared to the measurements. The data from Siberian stations, especially the highly representative ZOTTO data, allowed for constraining the total carbon budget for CO_2 and CH_4 for the area of the boreal forest in the west Siberian plains. The CO_2 budget is almost balanced by its sinks and sources with a net flux of 0.04 ± 0.11 PgC/yr. The CH_4 emissions of 8.4 ± 1.1 TgC/yr are likely to be underestimated by their prior flux estimates.

For future work, several measures can be recommended. The well known problem of how to find the optimal inversion settings about a-priori flux covariances and correlation lengths is closely related to the knowledge of the true flux distribution. The usage of satellite data (meteorology, plant phenology) may improve the knowledge of the flux fields temporally and spatially, e.g. with the Vegetation Photosynthesis and Respiration Model VPRM [Mahadevan et al., 2008] or the Simple Diagnostic Photosynthesis and Respiration Model [Badawy, 2011]. Furthermore, these biospheric models might be combined with the information of the global Fluxnet database (http://www.fluxnet.ornl.gov/, e.g. [Beer et al., 2010]) to achieve a higher spatial resolution of the a-priori flux fields.

Nevertheless the most important drivers of the atmospheric inversion models are the atmospheric concentration data. Since direct satellite measurements of CO_2 and CH_4 still have large uncertainties, for now the increasing duration of the time series

and the increasing number of stations will improve the results. The expansion of the current network looks promising, e.g. the 9-tower network in Siberia [Arshinov et al., 2009a; Sasakawa et al., 2010], and the global greenhouse gas network proposed by Earth Networks (http://www.earthnetworks.com).

All these suggestions give confidence that the carbon budget can be constrained even better in the near future. The growing ZOTTO time series will already enable calculations for a longer time period, which will reduce artifacts in the beginning and ending of the simulations. Therefore, the value of the regional atmospheric inversion for Central Siberia will increase with time alone.

E   Regional flux estimation with the Jena inversion system for Central Siberia

F Summary and outlook

"Because things are the way they are, things will not stay the way they are."
Bertolt Brecht (1898-1956)

In summary, this PhD thesis studied atmospheric CO_2 and CH_4 measurements in boreal Siberia. Based on numerous intensive laboratory tests, a high precision measurement system has been developed. The operation of a newly available cavity ring down analyzer renders the measurement of wet sample air possible. Thus, ZOTTO is the first system in the global atmospheric network at WMO precision level without an air drying system. In combination with the low amount of calibration gases, the system requires low maintenance efforts, an optimal feature to run a system on such a remote place as Central Siberia. The deployment of air buffer volumes in each of the six sample lines allows the continuous measurement of all six heights with only a single instrument.

The time series have been analyzed for long-term trends and average diurnal cycles since spring 2009. The intense seasonal cycle amplitude at this continental site emphasizes the active role of the boreal forests with its large carbon sink capacities to balance the carbon cycle.

The gradients in the mixing ratios along the tower have been analyzed for a further understanding of the local CO_2 and CH_4 sources and sinks. The stored amount of carbon within the monitored 301 m ground layer was corrected by the turbulent flux component, which dominates the daytime. Despite the fact that direct measurements for the carbon eddy covariance flux are not available, it was possible to estimate this turbulent flux component from three dimensional anemometer data by assuming the same transport characteristic for trace gases and heat.

A regional atmospheric transport inversion model was employed to identify CO_2 and CH_4 sources and sinks in the Central Siberian region. The model system has been adapted to the region of interest and a test was developed to optimize the parameter settings. By also including data from other available stations, the total flux in the boreal zone of the West Siberian plain was calculated to be 0.04 ± 0.11 PgC for CO_2 and 8.4 ± 1.1 TgC for CH_4 in the year 2009.

―――

Numerous tasks remain for the future. The ZOTTO measurement system needs surveillance to guarantee the stability of the calibration tanks and the water

correction function. It is necessary to improve the wind measurements during freezing periods. A reliable heating system would allow for flux estimates of the ZOTTO area throughout the year to close the annual carbon budget. The planning of additional flux measurements in the vicinity of the station makes confident that further information about local sources and sinks can be provided in the near future. The data set would be a good reference for the local flux estimates done so far.

The heat wave and forest fire anomaly in the CO_2 data in the year 2010 invites further investigations, e.g. looking at other trace gases like CO. For enhanced comparability to the CO_2 and CH_4 data and for less maintenance efforts, it might be worth considering additional trace gas analyzers, which are based on the same technology, to join the installed ZOTTO system. This might also improve the understanding of the cold winter events, which could be further explored through an aircraft or balloon campaign.

Not only the interpretation of short-term events, but also the comprehensive transport inversion frame-work can be improved, if in-situ measurements of the boundary layer height would be available. Exemplarily, this would ease the automated detection of the well-mixed periods, which otherwise could be inferred from a very comprehensive analysis of the mixing ratios from different tower levels only. Given that the well-mixed periods can be reliably detected, these individual data points could be given a stronger weight for constraining the flux fields. This approach would imply that the weighting for individual data points would be implemented in the inversion system. Apart from this, the inversion model framework can be enhanced by increasing the spatial resolution to 0.25 ° for all a-priori flux components. Currently, satellite remote sensing products are under development and might give additional information in the future. Moreover, the comparison of the Jena inversion system to the setups of other scientific groups can help to improve the algorithms and to better constrain the regional fluxes.

Beside the technical improvements, the data set may encourage further scientific studies. From a meteorological point of view it is interesting to know if the transport models could represent the strong temperature inversions during winter and the larger scale circulations in the Yenisei river basin during summer.

Investigations of the carbon cycle may start with a further analysis of the local flux estimates. For example, if these estimates are split up into night and daytime periods, nocturnal respiration fluxes can be inferred and be analyzed for their temperature sensitivity. This dependency would allow an extrapolation of the respiration fluxes to daytime and therefore would reveal the Gross Ecosystem Productivity (*GEP*) as difference to the *NEE* fluxes. The carbon fluxes can be correlated to their drivers, e.g. temperature, radiation, precipitation, soil temperature and humidity, heat fluxes, and wind patterns. This knowledge can be incorporated into process studies for a better

understanding and quantification of the climate sensitivity of the boreal forests and soils around ZOTTO.

On larger scale, the CO_2 seasonal cycle and its anomalies can tell about changes in the seasonal behavior of whole ecosystems [Randerson et al., 1999]. One example was already observed, when the 2010 European heat wave considerably modified the ZOTTO seasonal cycle. The model framework that has been used in the present work can help to quantify those drought impacts, if it is extended in time to the year 2010 and possibly in space to the European part of Russia. Moreover, the comparison of the CO_2 observations with the CO and aerosol data can help to calculate the contribution of forest fires to the signal.

The large interannual variability in the CO_2 signal that is characteristic for continental sites like ZOTTO has an advantage: a distinct signal can be easily attributed to the possible reason of the anomaly. As an illustration, the varying length of the growing season through shifting thaw cycles and soil freezing dates [Smith et al., 2004] will leave a detectable fingerprint on the seasonal cycle at ZOTTO.

On the long term, the importance of the measurements will grow, because climatic changes are related to time scales of 30 years and longer. In the coming years, the regional atmospheric inversion model can monitor future developments of the carbon pools in the vegetation and wetlands. The calculated carbon fluxes across Siberia can be compared with other satellite products, e.g. the shift in the growing season. Because the largest temperature changes of the future climate are predicted for Siberia, this region acts as an early indicator for other ecosystems: here, the strengths of climate feedbacks can be studied first. As the atmospheric inversion model gives the total budget, it will be possible to tell which process is dominating in a warmer and CO_2 richer environment: either the increased productivity of the forests [Nemani et al., 2003], or the enhanced soil and litter decomposition, exemplarily shown recently for the tropics by Sayer et al. [2011]. Changes in temperature and precipitation will additionally modify the wetland and permafrost extent, fire regimes, and ecosystem composition [Tchebakova et al., 2009]. Associated feedbacks on the greenhouse gas concentrations can be explored.

The thawing of permafrost links CO_2 and CH_4 observations. Both, in combination with their isotopic composition (from the flask series), may help to detect particularly vulnerable permafrost areas, as it is a common source region. On shorter time scale, the ZOTTO CH_4 data and coupled flux field calculations may already contribute to the solution of the current "enigma" of the recent methane budget [Heimann, 2011], whether changes in fossil fuel emissions [Aydin et al., 2011] or in rice agriculture [Kai et al., 2011] are responsible for recent reduction in the CH_4 growth rate.

Finally, each additional measurement station will further develop the greenhouse gases network (Earth Networks, Integrated Carbon Observing System (ICOS), satellite missions) and add information for the understanding of the carbon cycle

functioning. Ultimately, each model is only as representative as the data allows. The extra knowledge can further help to quantify the human influence on the earth system today, and may enable researchers to predict the potential future consequences of our actions.

F Summary and outlook

G References

"In every walk with nature one receives far more than he seeks."

John Muir (1838-1914)

Acevedo, O. C., Moraes, O. L. L., Da Silva, R., Fitzjarrald, D. R., Sakai, R. K., Staebler, R. M., and Czikowsky, M. J.: *Inferring nocturnal surface fluxes from vertical profiles of scalars in an Amazon pasture*, Global Change Biology, 10(5), 886-894, 2004.

Adachi, Y., Kawamura, K., Armi, L., and Keeling, R. F.: *Diffusive separation of the lower atmosphere*, Science, 311(5766), 1429-1429, doi:10.1126/science.1121312, 2006.

Ahmadov, R., Gerbig, C., Kretschmer, R., Korner, S., Rodenbeck, C., Bousquet, P., and Ramonet, M.: *Comparing high resolution WRF-VPRM simulations and two global CO_2 transport models with coastal tower measurements of CO_2*, Biogeosciences, 6(5), 807-817, 2009.

Allan, D. W.: *Time and Frequency (Time-Domain) Characterization, Estimation, and Prediction of Precision Clocks and Oscillators*, IEEE Transactions on Ultrasonics Ferroelectrics and Frequency Control, 34(6), 647-654, 1987.

Allison, C. E., and Francey, R. J.: *Verifying Southern Hemisphere trends in atmospheric carbon dioxide stable isotopes*, Journal of Geophysical Research-Atmospheres, 112(D21304), doi:10.1029/2006jd007345, 2007.

Arshinov, M., Belan, B., Davydov, D., Inouye, G., Krasnov, O., Maksyutov, S., Machida, T., Fofonov, A., and Shimoyama, K.: *Spatial and temporal variability of CO_2 and CH_4 concentrations in the surface atmospheric layer over West Siberia*, Atmospheric and Oceanic Optics, 22(1), 84-93, doi:10.1134/S1024856009010126, 2009a.

Arshinov, M., Belan, B., Davydov, D., Inouye, G., Maksyutov, S., Machida, T., and Fofonov, A.: *Vertical distribution of greenhouse gases above Western Siberia by the long-term measurement data*, Atmospheric and Oceanic Optics, 22(3), 316-324, doi:10.1134/S1024856009030087, 2009b.

Aubinet, M., Berbigier, P., Bernhofer, C. H., Cescatti, A., Feigenwinter, C., et al.: *Comparing CO_2 storage and advection conditions at night at different carboeuroflux sites*, Boundary-Layer Meteorology, 116(1), 63-94, 2005.

Aubinet, M.: *Eddy covariance CO_2 flux measurements in nocturnal conditions: An analysis of the problem*, Ecological Applications, 18(6), 1368-1378, doi:10.1890/06-1336.1, 2008.

Aubinet, M., Feigenwinter, C., Heinesch, B., Bernhofer, C., Canepa, E., et al.: *Direct advection measurements do not help to solve the night-time CO_2 closure problem: Evidence from three different forests*, Agricultural and Forest Meteorology, 150(5), 655-664, doi:10.1016/j.agrformet.2010.01.016, 2010.

Aydin, M., Verhulst, K. R., Saltzman, E. S., Battle, M. O., Montzka, S. A., Blake, D. R., Tang, Q., and Prather, M. J.: *Recent decreases in fossil-fuel emissions of ethane and methane derived from firn air*, Nature, 476(7359), 198-201, doi:10.1038/nature10352, 2011.

Bacastow, R. B.: *Modulation of atmospheric carbon dioxide by the Southern Oscillation*, Nature, 261(5556), 116-118, 1976.

Badawy, B.: *Quantifying carbon processes of the terrestrial biosphere in a global atmospheric inversion based on atmospheric mixing ratio, remote sensing and meteorological data*, Technical Report Vol. 21, ISSN 1615-7400, Max-Planck-Institut für Biogeochemie, Jena, 151pp, 2011.

Bakwin, P. S., Tans, P. P., Hurst, D. F., and Zhao, C. L.: *Measurements of carbon dioxide on very tall towers: results of the NOAA/CMDL program*, Tellus, 50B(5), 401-415, doi:10.1034/j.1600-0889.1998.t01-4-00001.x, 1998.

Bakwin, P. S., Davis, K. J., Yi, C., Wofsy, S. C., Munger, J. W., and Haszpra, L.: *Regional carbon dioxide fluxes from mixing ratio data*, Tellus, 56B(4), 301-311, 2004.

Baldocchi, D., Finnigan, J., Wilson, K., Paw U, K. T., and Falge, E.: *On Measuring Net Ecosystem Carbon Exchange Over Tall Vegetation on Complex Terrain*, Boundary-Layer Meteorology, 96(1), 257-291, 10.1023/a:1002497616547, 2000.

Baldocchi, D. D., Hincks, B. B., and Meyers, T. P.: *Measuring Biosphere-Atmosphere Exchanges of Biologically Related Gases with Micrometeorological Methods*, Ecology, 69(5), 1331-1340, 1988.

Barkley, M. P., Monks, P. S., Hewitt, A. J., Machida, T., Desai, A., et al.: *Assessing the near surface sensitivity of SCIAMACHY atmospheric CO2 retrieved using (FSI) WFM-DOAS*, Atmospheric Chemistry and Physics, 7(13), 3597-3619, doi:10.5194/acp-7-3597-2007, 2007.

Barriopedro, D., Fischer, E. M., Luterbacher, J., Trigo, R. M., and García-Herrera, R.: *The Hot Summer of 2010: Redrawing the Temperature Record Map of Europe*, Science, doi:10.1126/science.1201224, 2011.

Bedritsky, A. I., Blinov, V. G., Gershinkova, D. A., Golitsyn, G. S., Dymnikov, V. P., et al.: *Assessment Report on Climate Change and its Consequences in Russian Federation - General Summary*, Federal Service for Hydrometeorology and Environmental Monitoring (Roshydromet), Moscow, 24, 2008.

Beer, C., Reichstein, M., Tomelleri, E., Ciais, P., Jung, M., et al.: *Terrestrial Gross Carbon Dioxide Uptake: Global Distribution and Covariation with Climate*, Science, science.1184984, 10.1126/science.1184984, 2010.

Bergamaschi, P., Frankenberg, C., Meirink, J. F., Krol, M., Dentener, F., et al.: *Satellite chartography of atmospheric methane from SCIAMACHY on board ENVISAT: 2. Evaluation based on inverse model simulations*, Journal of Geophysical Research-Atmospheres, 112(D2), 2007.

Bergamaschi, P., Frankenberg, C., Meirink, J. F., Krol, M., Villani, M. G., et al.: *Inverse modeling of global and regional CH4 emissions using SCIAMACHY satellite retrievals*, J. Geophys. Res., 114(D22), D22301, 10.1029/2009jd012287, 2009.

Bergamaschi, P., Krol, M., Meirink, J. F., Dentener, F., Segers, A., et al.: *Inverse modeling of European CH4 emissions 2001-2006*, J. Geophys. Res., 115(D22), D22309, doi:10.1029/2010jd014180, 2010.

Bian, H., Kawa, S. R., Chin, M., Pawson, S., Zhu, Z., Rasch, P., and Wu, S.: *A test of sensitivity to convective transport in a global atmospheric CO2 simulation*, Tellus B, 58(5), 463-475, 10.1111/j.1600-0889.2006.00212.x, 2006.

Bohn, T. J., Lettenmaier, D. P., Sathulur, K., Bowling, L. C., Podest, E., McDonald, K. C., and Friborg, T.: *Methane emissions from western Siberian wetlands: heterogeneity and sensitivity to climate change*, Environmental Research Letters, 2(4), 2007.

Bonner, W. D.: *Climatology of the Low Level Jet*, Monthly Weather Review, 96(12), 833-850, doi:10.1175/1520-0493(1968)096<0833:COTLLJ>2.0.CO;2, 1968.

Businger, J. A.: *Evaluation of the Accuracy with Which Dry Deposition Can Be Measured with Current Micrometeorological Techniques*, Journal of Climate and Applied Meteorology, 25(8), 1100-1124, doi:10.1175/1520-0450(1986)025<1100:EOTAWW>2.0.CO;2, 1986.

Butler, M. P., Davis, K. J., Denning, A. S., and Kawa, S. R.: *Using continental observations in global atmospheric inversions of CO2: North American carbon sources and sinks*, Tellus B, 62(5), 550-572, doi:10.1111/j.1600-0889.2010.00501.x, 2010.

Canadell, J. G., Le Quere, C., Raupach, M. R., Field, C. B., Buitenhuis, E. T., et al.: *Contributions to accelerating atmospheric CO2 growth from economic activity, carbon intensity, and efficiency of natural sinks*, Proceedings of the National Academy of Sciences of the United States of America, 104(47), 18866-18870, 2007.

Cao, M. K., Marshall, S., and Gregson, K.: *Global carbon exchange and methane emissions from natural wetlands: Application of a process-based model*, Journal of Geophysical Research-Atmospheres, 101(D9), 14399-14414, 1996.

Carouge, C., Bousquet, P., Peylin, P., Rayner, P. J., and Ciais, P.: *What can we learn from European continuous atmospheric CO2 measurements to quantify regional fluxes - Part 1: Potential of the 2001 network*, Atmospheric Chemistry and Physics, 10(6), 3107-3117, doi:10.5194/acp-10-3107-2010, 2010a.

Carouge, C., Rayner, P. J., Peylin, P., Bousquet, P., Chevallier, F., and Ciais, P.: *What can we learn from European continuous atmospheric CO2 measurements to quantify regional fluxes - Part 2: Sensitivity of flux accuracy to inverse setup*, Atmospheric Chemistry and Physics, 10(6), 3119-3129, doi:10.5194/acp-10-3119-2010, 2010b.

Chen, H., Winderlich, J., Gerbig, C., Hoefer, A., Rella, C. W., et al.: *High-accuracy continuous airborne measurements of greenhouse gases (CO2 and CH4) using the cavity ring-down spectroscopy (CRDS) technique*, Atmos. Meas. Tech., 3(2), 375-386, doi:10.5194/amt-3-375-2010, 2010.

Chen, J. M., Chen, B. Z., and Tans, P.: *Deriving daily carbon fluxes from hourly CO2 mixing ratios measured on the WLEF tall tower: An upscaling methodology*, Journal of Geophysical Research-Biogeosciences, 112(G1), -, 2007.

G References

Ciais, P., Canadell, J. G., Luyssaert, S., Chevallier, F., Shvidenko, A., et al.: *Can we reconcile atmospheric estimates of the Northern terrestrial carbon sink with land-based accounting?*, Current Opinion in Environmental Sustainability, 2(4), 225-230, 2010a.

Ciais, P., Rayner, P., Chevallier, F., Bousquet, P., Logan, M., Peylin, P., and Ramonet, M.: *Atmospheric inversions for estimating CO2 fluxes: methods and perspectives*, Climatic Change, 103(1), 69-92, doi:10.1007/s10584-010-9909-3, 2010b.

Crosson, E. R.: *A cavity ring-down analyzer for measuring atmospheric levels of methane, carbon dioxide, and water vapor*, Applied Physics B-Lasers and Optics, 92(3), 403-408, doi:10.1007/s00340-008-3135-y, 2008.

Da Costa, G., and Steele, L. P.: Cape Grim's new low flow, high precision, in situ CO2 analyser system - Development status and results from four month's operation at Aspendale, WMO 10. Meeting of Experts on CO2 Measurements, Stockholm, 1999.

Daube Jr., B. C., Boering, K. A., Andrews, A. E., and Wofsy, S. C.: *A High-Precision Fast-Response Airborne CO2 Analyzer for In Situ Sampling from the Surface to the Middle Stratosphere*, Journal of Atmospheric and Oceanic Technology, 19, 1532-1543, doi:10.1175/1520-0426(2002)019<1532:AHPFRA>2.0.CO;2, 2002.

Davis, K. J., Bakwin, P. S., Yi, C. X., Berger, B. W., Zhao, C. L., Teclaw, R. M., and Isebrands, J. G.: *The annual cycles of CO2 and H2O exchange over a northern mixed forest as observed from a very tall tower*, Global Change Biology, 9(9), 1278-1293, 2003.

Denman, K. L., Brasseur, G., Chidthaisong, A., Ciais, P., Cox, P. M., et al.: *Couplings Between Changes in the Climate System and Biogeochemistry. In: Climate Change 2007: The Physical Science Basis. Contribution of Working Group I to the Fourth Assessment Report of the Intergovernmental Panel on Climate Change*, Cambridge University Press, Cambridge, United Kingdom and New York, NY, USA, 2007.

Dlugokencky, E. J., Myers, R. C., Lang, P. M., Masarie, K. A., Crotwell, A. M., Thoning, K. W., Hall, B. D., Elkins, J. W., and Steele, L. P.: *Conversion of NOAA atmospheric dry air CH4 mole fractions to a gravimetrically prepared standard scale*, Journal of Geophysical Research-Atmospheres, 110(D18), D18306, doi:10.1029/2005JD006035, 2005.

Dlugokencky, E. J., Bruhwiler, L., White, J. W. C., Emmons, L. K., Novelli, P. C., et al.: *Observational constraints on recent increases in the atmospheric CH4 burden*, Geophys. Res. Lett., 36(18), L18803, 10.1029/2009gl039780, 2009.

EDGAR: Emission Database for Global Atmospheric Research, European Commission, Joint Research Centre (JRC)/Netherlands Environmental Assessment Agency (PBL), release version 4.1: http://edgar.jrc.ec.europa.eu, access: 7.7.2011, 2010.

Eneroth, K., Kjellström, E., and Holmén, K.: *Interannual and seasonal variations in transport to a measuring site in western Siberia and their impact on the observed atmospheric CO2 mixing ratio*, J. Geophys. Res., 108(D21), 4660, 10.1029/2002jd002730, 2003.

Enting, I. G., and Mansbridge, J. V.: *Seasonal sources and sinks of atmospheric CO2 Direct inversion of filtered data*, Tellus B, 41B(2), 111-126, 10.1111/j.1600-0889.1989.tb00129.x, 1989.

FAO: Global Forest Resources Assessment 2005 - Progress towards sustainable forest management, FAO forestry paper 147, Food and Agriculture Organization of the United Nations, http://www.fao.org/docrep/008/a0400e/a0400e00.htm, ISBN 92-5-105481-9, Rome, 2006.

Feigenwinter, C., Bernhofer, C., and Vogt, R.: *The influence of advection on the short term CO2-budget in and above a forest canopy*, Boundary-Layer Meteorology, 113(2), 201-224, 2004.

Feigenwinter, C., Bernhofer, C., Eichelmann, U., Heinesch, B., Hertel, M., et al.: *Comparison of horizontal and vertical advective CO2 fluxes at three forest sites*, Agricultural and Forest Meteorology, 148(1), 12-24, 10.1016/j.agrformet.2007.08.013, 2008.

Finnigan, J.: *A comment on the paper by Lee (1998): "On micrometeorological observations of surface-air exchange over tall vegetation"*, Agricultural and Forest Meteorology, 97(1), 55-64, 1999.

Flessa, H., Rodionov, A., Guggenberger, G., Fuchs, H., Magdon, P., et al.: *Landscape controls of CH4 fluxes in a catchment of the forest tundra ecotone in northern Siberia*, Global Change Biology, 14(9), 2040-2056, 2008.

Friborg, T., Soegaard, H., Christensen, T. R., Lloyd, C. R., and Panikov, N. S.: *Siberian wetlands: Where a sink is a source*, Geophysical Research Letters, 30(21), 2129, doi:10.1029/2003GL017797, 2003.

Friedlingstein, P., Houghton, R. A., Marland, G., Hackler, J., Boden, T. A., et al.: *Update on CO2 emissions*, Nature Geoscience, 3(12), 811-812, doi:10.1038/ngeo1022, 2010.

G References

GAW Report No.161: 12th WMO/IAEA Meeting of Experts on Carbon Dioxide, Other Greenhouse Gases and Related Tracers Measurement Techniques, Toronto, Canada WMO TD No. 1275, 273 pp., 2003.

GAW Report No.186: 14th WMO/IAEA Meeting of Experts on Carbon Dioxide, Other Greenhouse Gases and Related Tracers Measurement Techniques, Helsinki, Finland WMO TD No. 1487, 145 pp., 2007.

Geels, C., Gloor, M., Ciais, P., Bousquet, P., Peylin, P., et al.: *Comparing atmospheric transport models for future regional inversions over Europe - Part 1: mapping the atmospheric CO2 signals*, Atmospheric Chemistry and Physics, 7(13), 3461-3479, 2007.

Gerbig, C., Lin, J. C., Wofsy, S. C., Daube, B. C., Andrews, A. E., Stephens, B. B., Bakwin, P. S., and Grainger, C. A.: *Toward constraining regional-scale fluxes of CO2 with atmospheric observations over a continent: 1. Observed spatial variability from airborne platforms*, Journal of Geophysical Research-Atmospheres, 108(D24), 4756, doi:10.1029/2002JD003018, 2003a.

Gerbig, C., Lin, J. C., Wofsy, S. C., Daube, B. C., Andrews, A. E., Stephens, B. B., Bakwin, P. S., and Grainger, C. A.: *Toward constraining regional-scale fluxes of CO2 with atmospheric observations over a continent: 2. Analysis of COBRA data using a receptor-oriented framework*, Journal of Geophysical Research-Atmospheres, 108(D24), 4757, doi:10.1029/2003JD003770, 2003b.

Gerbig, C., Lin, J. C., Munger, J. W., and Wofsy, S. C.: *What can tracer observations in the continental boundary layer tell us about surface-atmosphere fluxes?*, Atmospheric Chemistry and Physics, 6, 539-554, 2006.

Gerbig, C., Körner, S., and Lin, J. C.: *Vertical mixing in atmospheric tracer transport models: error characterization and propagation*, Atmospheric Chemistry and Physics, 8(3), 591-602, doi:10.5194/acp-8-591-2008, 2008.

Gerbig, C., Dolman, A. J., and Heimann, M.: *On observational and modelling strategies targeted at regional carbon exchange over continents*, Biogeosciences, 6(10), 1949-1959, 2009.

Glagolev, M. V., Golovatskaya, E. A., and Shnyrev, N. A.: *Greenhouse gas emission in West Siberia*, Contemporary Problems of Ecology, 1(1), 136-146, 2008.

GLOBALVIEW-CO2: Cooperative Atmospheric Data Integration, Project - Carbon Dioxide. CD-ROM, NOAA ESRL, Boulder, Colorado. : Available on Internet via anonymous FTP to ftp.cmdl.noaa.gov, Path: ccg/co2/GLOBALVIEW, access: 17.2.2011, 2010.

Gloor, M., Bakwin, P. S., Hurst, D. F., Lock, L., Draxler, R., and Tans, P. P.: *What is the concentration footprint of a tall tower?*, Journal of Geophysical Research, 106(D16), 17831-17840, 2001.

Göckede, M., Turner, D. P., Michalak, A. M., Vickers, D., and Law, B. E.: *Sensitivity of a subregional scale atmospheric inverse CO(2) modeling framework to boundary conditions*, Journal of Geophysical Research-Atmospheres, 115, doi:10.1029/2010JD014443, 2010.

Gourdji, S. M., Hirsch, A. I., Mueller, K. L., Yadav, V., Andrews, A. E., and Michalak, A. M.: *Regional-scale geostatistical inverse modeling of North American CO2 fluxes: a synthetic data study*, Atmospheric Chemistry and Physics, 10(13), 6151-6167, 10.5194/acp-10-6151-2010, 2010.

Groisman, P., and Soja, A. J.: *Ongoing climatic change in Northern Eurasia: justification for expedient research*, Environmental Research Letters, 4(4), 045002, 2009.

Grosse, G., Romanovsky, V. E., Jorgenson, T., Anthony, K. W., Brown, J., and Overduin, P. P.: *Vulnerability and feedbacks of permafrost to climate change*, Eos Trans. AGU, 92(9), 73-74, doi:10.1029/2011EO090001, 2011.

Gurney, K. R., Law, R. M., Denning, A. S., Rayner, P. J., Baker, D., et al.: *Towards robust regional estimates of CO2 sources and sinks using atmospheric transport models*, Nature, 415(6872), 626-630, doi:10.1038/415626a, 2002.

Haszpra, L., Barcza, Z., Bakwin, P. S., Berger, B. W., Davis, K. J., and Weidinger, T.: *Measuring system for the long-term monitoring of biosphere/atmosphere exchange of carbon dioxide*, J. Geophys. Res., 106(D3), 3057-3069, doi:10.1029/2000jd900600, 2001.

Haszpra, L., Barcza, Z., Davis, K. J., and Tarczay, K.: *Long-term tall tower carbon dioxide flux monitoring over an area of mixed vegetation*, Agricultural and Forest Meteorology, 132(1-2), 58-77, DOI 10.1016/j.agrformet.2005.07.002, 2005.

Heimann, M., and Körner, S.: *The global atmospheric tracer model TM3*, Max-Planck-Institut für Biogeochemie, Jena, 2003.

Heimann, M.: *TCOS Siberia - Final Report*, Max Planck Institute for Biogeochemistry, Jena, http://www.bgc-jena.mpg.de/bgc-systems/projects/web_TCOS/tcos/annual_report/TCOS_2005.pdf (last access: 24.01.2011), 185, 2005.

G References

Heimann, M., and Reichstein, M.: *Terrestrial ecosystem carbon dynamics and climate feedbacks*, Nature, 451(7176), 289-292, 2008.

Heimann, M.: *Atmospheric science: Enigma of the recent methane budget*, Nature, 476(7359), 157-158, doi:10.1038/476157a, 2011.

Heintzenberg, J., Birmili, W., and Theiss, D.: *The atmospheric aerosol over Siberia, as seen from the 300 m ZOTTO tower*, Tellus, 60B, 276-285, doi:10.1111/j.1600-0889.2007.00335.x, 2008.

Heintzenberg, J., Birmili, W., Otto, R., Andreae, M. O., Mayer, J. C., Chi, X., and Panov, A.: *Aerosol particle number size distributions and particulate light absorption at the ZOTTO tall tower (Siberia), 2006-2009*, Atmospheric Chemistry and Physics, 11(16), 8703-8719, doi:10.5194/acp-11-8703-2011, 2011.

Helliker, B. R., Berry, J. A., Betts, A. K., Bakwin, P. S., Davis, K. J., et al.: *Estimates of net CO2 flux by application of equilibrium boundary layer concepts to CO2 and water vapor measurements from a tall tower*, Journal of Geophysical Research-Atmosperes, 109(D20), -, 2004.

Höfer, A.: *Charakterisierung der Luftansaugleitung von Messtürmen (engl: Characterization of air inlet tubings of measurement towers)*, Diploma thesis, Physikalisch-Astronomische Fakultaet, Friedrich Schiller University, Jena, 58 pp., 2009.

Huntingford, C., Lowe, J. A., Booth, B. B. B., Jones, C. D., Harris, G. R., Gohar, L. K., and Meir, P.: *Contributions of carbon cycle uncertainty to future climate projection spread*, Tellus, 61B(2), 355-360, doi:10.1111/j.1600-0889.2009.00414.x, 2009.

Hurwitz, M. D., Ricciuto, D. M., Bakwin, P. S., Davis, K. J., Wang, W., Yi, C., and Butler, M. P.: *Transport of Carbon Dioxide in the Presence of Storm Systems over a Northern Wisconsin Forest*, Journal of the Atmospheric Sciences, 61(5), 607-618, doi:10.1175/1520-0469(2004)061<0607:TOCDIT>2.0.CO;2, 2004.

IPCC: Solomon, S., Qin, D., Manning, M., Alley, R. B., Berntsen, T., et al.: *Technical Summary, in: Climate Change 2007: The Physical Science Basis, Contribution of Working Group I to the Fourth Assessment Report of the Intergovernmental Panel on Climate Change*, edited by: Solomon, S., Qin, D., Manning, M., Chen, Z., Marquis, M., Averyt, K. B., Tignor, M., and Miller, H. L., Cambridge University Press, Cambridge, United Kingdom and New York, NY, USA, 2007.

Jacobson, A. R., Fletcher, S. E. M., Gruber, N., Sarmiento, J. L., and Gloor, M.: *A joint atmosphere-ocean inversion for surface fluxes of carbon dioxide: 1. Methods and global-scale fluxes (vol 21, art no GB1019, 2007)*, Global Biogeochemical Cycles, 21(2), Artn Gb2025, doi:10.1029/2007gb003012, 2007.

Jung, M., Henkel, K., Herold, M., and Churkina, G.: *Exploiting synergies of global land cover products for carbon cycle modeling*, Remote Sensing of Environment, 101(4), 534-553, 2006.

Kai, F. M., Tyler, S. C., Randerson, J. T., and Blake, D. R.: *Reduced methane growth rate explained by decreased Northern Hemisphere microbial sources*, Nature, 476(7359), 194-197, doi:10.1038/nature10259, 2011.

Kaplan, J. O.: *Wetlands at the Last Glacial Maximum: Distribution and methane emissions*, Geophysical Research Letters, 29(6), 2002.

Kaplan, J. O., Folberth, G., and Hauglustaine, D. A.: *Role of methane and biogenic volatile organic compound sources in late glacial and Holocene fluctuations of atmospheric methane concentrations*, Global Biogeochemical Cycles, 20(2), Artn: Gb2016, doi:10.1029/2005gb002590, 2006.

Karstens, U., Gloor, M., Heimann, M., and Rödenbeck, C.: *Insights from simulations with high-resolution transport and process models on sampling of the atmosphere for constraining midlatitude land carbon sinks*, Journal of Geophysical Research, 111(D12), D12301, doi:10.1029/2005JD006278, 2006.

Keeling, C. D.: *The Concentration and Isotopic Abundances of Carbon Dioxide in the Atmosphere*, Tellus, 12(2), 200-203, 1960.

Keeling, R. F., Manning, A. C., and Paplawsky, W. J.: *On the long-term stability of reference gases for atmospheric O2/N2 and CO2 measurements*, Tellus, 59B(1), 3-14, doi:10.1111/j.1600-0889.2006.00228.x, 2007.

Kiehl, J. T., and Trenberth, K. E.: *Earth's annual global mean energy budget*, Bulletin of the American Meteorological Society, 78(2), 197-208, doi:10.1175/1520-0477(1997)078<0197:EAGMEB>2.0.CO;2, 1997.

Kitzis, D., and Zhao, C. L.: CMDL/Carbon Cycle Grennhause Gases Group Standards Preparation and Stability, in, U.S. Department of Commerce - National Oceanic and Atmospheric Administration (NOAA) - Climate Monitoring and Diagnostics Laboratory - Carbon Cycle Greenhouse Gases Group, http://www.cmdl.noaa.gov/ccgg/refgases/airstandard.html, last access: March 2010, 1999.

G   References

Knorr, W.: *Is the airborne fraction of anthropogenic CO2 emissions increasing?*, Geophys. Res. Lett., 36, 10.1029/2009gl040613, 2009.

Körner, C.: *Slow in, rapid out - Carbon flux studies and Kyoto targets*, Science, 300(5623), 1242-1243, doi:10.1126/science.1084460, 2003.

Kozlova, E. A., Manning, A. C., Kisilyakhov, Y., Seifert, T., and Heimann, M.: *Seasonal, synoptic, and diurnal-scale variability of biogeochemical trace gases and O2 from a 300-m tall tower in central Siberia*, Global Biogeochemical Cycles, 22(GB4020), doi:10.1029/2008GB003209, 2008.

Kozlova, E. A., and Manning, A. C.: *Methodology and calibration for continuous measurements of biogeochemical trace gas and O2 concentrations from a 300-m tall tower in central Siberia*, Atmospheric Measurement Techniques, 2(1), 205-220, 2009.

Kraus, H., Malcher, J., and Schaller, E.: *A nocturnal low level jet during PUKK*, Boundary-Layer Meteorology, 31(2), 187-195, 10.1007/bf00121177, 1985.

Kurbatskiy, A., and Kurbatskaya, L.: *Modeling Of A Stable Boundary Layer With A Low-Level Jet*, Journal of Applied Mechanics and Technical Physics, 51(5), 655-662, doi:10.1007/s10808-010-0084-0, 2010.

Kurganova, I. N., Kudeyarov, V. N., and Lopes De Gerenyu, V. O.: *Updated estimate of carbon balance on Russian territory*, Tellus B, 62(5), 497-505, doi:10.1111/j.1600-0889.2010.00467.x, 2010.

Langenfelds, R. L., van der Schoot, M. V., Francey, R. J., Steele, L. P., Schmidt, M., and Mukai, H.: *Modification of air standard composition by diffusive and surface processes*, Journal of Geophysical Research, 110, D13307, doi:10.1029/2004JD005482, 2005.

Lauvaux, T., Uliasz, M., Sarrat, C., Chevallier, F., Bousquet, P., et al.: *Mesoscale inversion: first results from the CERES campaign with synthetic data*, Atmospheric Chemistry and Physics, 8(13), 3459-3471, 2008.

Lauvaux, T., Gioli, B., Sarrat, C., Rayner, P. J., Ciais, P., et al.: *Bridging the gap between atmospheric concentrations and local ecosystem measurements*, Geophys. Res. Lett., 36(19), L19809, 10.1029/2009gl039574, 2009a.

Lauvaux, T., Pannekoucke, O., Sarrat, C., Chevallier, F., Ciais, P., Noilhan, J., and Rayner, P. J.: *Structure of the transport uncertainty in mesoscale inversions of CO2 sources and sinks using ensemble model simulations*, Biogeosciences, 6(6), 1089-1102, 10.5194/bg-6-1089-2009, 2009b.

Le Quere, C., Raupach, M. R., Canadell, J. G., Marland, G., and et al.: *Trends in the sources and sinks of carbon dioxide*, Nature Geoscience, 2(12), 831-836, doi:10.1038/ngeo689, 2009.

Lee, X.: *On micrometeorological observations of surface-air exchange over tall vegetation*, Agricultural and Forest Meteorology, 91(1-2), 39-49, 1998.

Lin, J. C., Gerbig, C., Wofsy, S. C., Andrews, A. E., Daube, B. C., Davis, K. J., and Grainger, C. A.: *A near-field tool for simulating the upstream influence of atmospheric observations: The Stochastic Time-Inverted Lagrangian Transport (STILT) model*, Journal of Geophysical Research, 108(D16), 4493, doi:10.1029/2002JD003161, 2003.

Lloyd, J., Francey, R. J., Mollicone, D., Raupach, M. R., Sogatchev, A., et al.: *Vertical profiles, boundary layer budgets, and regional flux estimates for CO2 and its 13C/12C ratio and for water vapor above a forest/bog mosaic in central Siberia*, Global Biogeochemical Cycles, 15(2), 267-284, doi:10.1029/1999GB001211, 2001.

Lloyd, J. O. N., Langenfelds, R. L., Francey, R. J., Gloor, M., Tchebakova, N. M., et al.: *A trace-gas climatology above Zotino, central Siberia*, Tellus B, 54(5), 749-767, doi:10.1034/j.1600-0889.2002.01335.x, 2002a.

Lloyd, J. O. N., Shibistova, O., Zolotoukhine, D., Kolle, O., Arneth, A., Wirth, C., Styles, J. M., Tchebakova, N. M., and Schulze, E. D.: *Seasonal and annual variations in the photosynthetic productivity and carbon balance of a central Siberian pine forest*, Tellus B, 54(5), 590-610, doi:10.1034/j.1600-0889.2002.01487.x, 2002b.

Loescher, H. W., Law, B. E., Mahrt, L., Hollinger, D. Y., Campbell, J., and Wofsy, S. C.: *Uncertainties in, and interpretation of, carbon flux estimates using the eddy covariance technique*, J. Geophys. Res., 111(D21), D21S90, 10.1029/2005jd006932, 2006.

Luyssaert, S., Inglimaz, W. I., Jung, M., Richardson, A. D., Reichstein, M., et al.: *CO2 balance of boreal, temperate, and tropical forests derived from a global database*, Global Change Biology, 13, 2509-2537, 2007.

Luyssaert, S., Schulze, E. D., Borner, A., Knohl, A., Hessenmoller, D., Law, B. E., Ciais, P., and Grace, J.: *Old-growth forests as global carbon sinks*, Nature, 455(7210), 213-215, doi:10.1038/nature07276, 2008.

Magnani, F., Mencuccini, M., Borghetti, M., Berbigier, P., Berninger, F., et al.: *The human footprint in the carbon cycle of temperate and boreal forests*, Nature, 447(7146), 848-850, doi:10.1038/nature05847, 2007.

G   References

Mahadevan, P., Wofsy, S. C., Matross, D. M., Xiao, X. M., Dunn, A. L., et al.: *A satellite-based biosphere parameterization for net ecosystem CO2 exchange: Vegetation Photosynthesis and Respiration Model (VPRM)*, Global Biogeochemical Cycles, 22(2), Artn Gb2005, doi:10.1029/2006gb002735, 2008.

Mahecha, M. D., Reichstein, M., Carvalhais, N., Lasslop, G., Lange, H., et al.: *Global Convergence in the Temperature Sensitivity of Respiration at Ecosystem Level*, Science, science.1189587, 10.1126/science.1189587, 2010.

Mayer, J. C., Birmili, W., Heimann, M., Heintzenberg, J., Juergens, N., Kisilyakhov, Y., Panov, A., and Andreae, M. O.: *Long-Term Measurements of Carbon Monoxide and Aerosols at the ZOTTO tall tower, Siberia*, Eos Trans. AGU, 90(52), Fall Meet. Suppl., Abstract GC31A-0686, 2009.

McGrath-Spangler, E. L., and Denning, A. S.: *Impact of entrainment from overshooting thermals on land–atmosphere interactions during summer 1999*, Tellus B, 62(5), 441-454, doi:10.1111/j.1600-0889.2010.00482.x, 2010.

Mikaloff Fletcher, S. E., Gruber, N., Jacobson, A. R., Doney, S. C., Dutkiewicz, S., et al.: *Inverse estimates of anthropogenic CO2 uptake, transport, and storage by the ocean*, Global Biogeochemical Cycles, 20(2), Artn Gb2002, 2006.

Mikaloff Fletcher, S. E., Gruber, N., Jacobson, A. R., Gloor, M., Doney, S. C., et al.: *Inverse estimates of the oceanic sources and sinks of natural CO2 and the implied oceanic carbon transport*, Global Biogeochemical Cycles, 21(1), GB1010, 2007.

Moncrieff, J., Valentini, R., Greco, S., Seufert, G., and Ciccioli, P.: *Trace gas exchange over terrestrial ecosystems: Methods and perspectives in micrometeorology*, Journal of Experimental Botany, 48(310), 1133-1142, 1997.

Mu, M., Randerson, J. T., Van der Werf, G. R., Giglio, L., Kasibhatla, P., et al.: *Daily and hourly variability in global fire emissions and consequences for atmospheric model predictions of carbon monoxide*, J. Geophys. Res. (submitted), 2011.

Murphy, D. M., and Koop, T.: *Review of the vapour pressures of ice and supercooled water for atmospheric applications*, Quarterly Journal of the Royal Meteorological Society, 131(608), 1539-1565, doi:10.1256/qj.04.94, 2005.

Myneni, R. B., Dong, J., Tucker, C. J., Kaufmann, R. K., Kauppi, P. E., Liski, J., Zhou, L., Alexeyev, V., and Hughes, M. K.: *A large carbon sink in the woody biomass of Northern forests*, Proceedings of the National Academy of Sciences of the United States of America, 98(26), 14784-14789, doi:10.1073/pnas.261555198 2001.

Nakai, Y., Matsuura, Y., Kajimoto, T., Abaimov, A. P., Yamamoto, S., and Zyryanova, O. A.: *Eddy covariance CO2 flux above a Gmelin larch forest on continuous permafrost in Central Siberia during a growing season*, Theoretical and Applied Climatology, 93(3-4), 133-147, doi:10.1007/s00704-007-0337-x, 2008.

Nemani, R. R., Keeling, C. D., Hashimoto, H., Jolly, W. M., Piper, S. C., Tucker, C. J., Myneni, R. B., and Running, S. W.: *Climate-Driven Increases in Global Terrestrial Net Primary Production from 1982 to 1999*, Science, 300(5625), 1560-1563, 10.1126/science.1082750, 2003.

Pan, Y., Birdsey, R. A., Fang, J., Houghton, R., Kauppi, P. E., et al.: *A Large and Persistent Carbon Sink in the World's Forests*, Science, doi:10.1126/science.1201609, 2011.

Panofsky, H. A.: *Radiative cooling in the lowest layers of an atmophere warmer than the ground*, Journal of Meteorology, 4(1), 35-37, doi:10.1175/1520-0469(1947)004<0035:rcitll>2.0.co;2, 1947.

Paris, J.-D., Ciais, P., Nédélec, P., Stohl, A., Belan, B. D., Arshinov, M. Y., Carouge, C., Golitsyn, G. S., and Granberg, I. G.: *New Insights on the Chemical Composition of the Siberian Air Shed from the YAK-AEROSIB Aircraft Campaigns*, Bulletin of the American Meteorological Society, 91(5), 625-641, doi:10.1175/2009BAMS2663.1, 2010a.

Paris, J. D., Stohl, A., Ciais, P., Nédélec, P., Belan, B. D., Arshinov, M. Y., and Ramonet, M.: *Source-receptor relationships for airborne measurements of CO2, CO and O3 above Siberia: a cluster-based approach*, Atmospheric Chemistry and Physics, 10(4), 1671-1687, doi:10.5194/acp-10-1671-2010, 2010b.

Paw U, K. T., Baldocchi, D. D., Meyers, T. P., and Wilson, K. B.: *Correction Of Eddy-Covariance Measurements Incorporating Both Advective Effects And Density Fluxes*, Boundary-Layer Meteorology, 97(3), 487-511, 10.1023/a:1002786702909, 2000.

Peregon, A., Maksyutov, S., Kosykh, N. P., and Mironycheva-Tokareva, N. P.: *Map-based inventory of wetland biomass and net primary production in western Siberia*, Journal of Geophysical Research-Biogeosciences, 113(G1), -, 2008.

Peters, W., Jacobson, A. R., Sweeney, C., Andrews, A. E., Conway, T. J., et al.: *An atmospheric perspective on North American carbon dioxide exchange: CarbonTracker*, Proceedings of the National Academy of Sciences of the United States of America, 104(48), 18925-18930, 2007.

G References

Peters, W., Krol, M. C., Van Der Werf, G. R., Houweling, S., Jones, C. D., et al.: *Seven years of recent European net terrestrial carbon dioxide exchange constrained by atmospheric observations*, Global Change Biology, 16(4), 1317-1337, doi:10.1111/j.1365-2486.2009.02078.x, 2010.

Peylin, P., Rayner, P. J., Bousquet, P., Carouge, C., Hourdin, F., Heinrich, P., Ciais, P., and contributors, A.: *Daily CO2 flux estimates over Europe from continuous atmospheric measurements: 1, inverse methodology*, Atmospheric Chemistry and Physics, 5(12), 3173-3186, 2005.

Popa, M. E.: *Continuous tall tower multispecies measurements in Europe for quantifying and understanding land-atmosphere carbon exchange*, PhD thesis, Chemisch-Geowissenschaftliche Fakultaet, Friedrich Schiller University Jena, 237 pp., 2007.

Popa, M. E., Gloor, M., Manning, A. C., Jordan, A., Schultz, U., Haensel, F., Seifert, T., and Heimann, M.: *Measurements of greenhouse gases and related tracers at Bialystok tall tower station in Poland*, Atmos. Meas. Tech., 3(2), 407-427, doi:10.5194/amt-3-407-2010, 2010.

Randerson, J. T., Field, C. B., Fung, I. Y., and Tans, P. P.: *Increases in early season ecosystem uptake explain recent changes in the seasonal cycle of atmospheric CO2 at high northern latitudes*, Geophys. Res. Lett., 26(17), 2765-2768, doi:10.1029/1999gl900500, 1999.

Rask, H., Schoenau, J., and Anderson, D.: *Factors influencing methane flux from a boreal forest wetland in Saskatchewan, Canada*, Soil Biology and Biochemistry, 34(4), 435-443, 2002.

Rinne, J., Riutta, T., Pihlatie, M., Aurela, M., Haapanala, S., Tuovinen, J. P., Tuittila, E. S., and Vesala, T.: *Annual cycle of methane emission from a boreal fen measured by the eddy covariance technique*, Tellus B, 59(3), 449-457, 10.1111/j.1600-0889.2007.00261.x, 2007.

Rödenbeck, C., Houweling, S., Gloor, M., and Heimann, M.: *CO2 flux history 1982–2001 inferred from atmospheric data using a global inversion of atmospheric transport*, Atmospheric Chemistry and Physics, 3, 1919-1964, 2003.

Rödenbeck, C.: *Estimating CO2 sources and sinks from atmospheric concentration measurements using a global inversion of atmospheric transport.*, Technical Report Vol. 6, ISSN 1615-7400, Max-Planck-Institut für Biogeochemie, Jena, 2005.

Rödenbeck, C., Gerbig, C., Trusilova, K., and Heimann, M.: *A two-step scheme for high-resolution regional atmospheric trace gas inversions based on independent models*, Atmospheric Chemistry and Physics, 9(14), 5331-5342, doi:10.5194/acp-9-5331-2009, 2009.

Röser, C., Montagnani, L., Schulze, E. D., Mollicone, D., Kolle, O., et al.: *Net CO2 exchange rates in three different successional stages of the "Dark Taiga" of central Siberia*, Tellus B, 54(5), 642-654, doi:10.1034/j.1600-0889.2002.01351.x, 2002.

ROSHYDROMET Report on climate features in the Russian Federation for 2010 - Доклад об особенностях климата на территории Российской Федерации за 2010 год: http://www.meteorf.ru/default_doc.aspx?RgmFolderID=a4e36ec1-c49d-461c-8b4f-167d20cb27d8&RgmDocID=883032aa-9743-4fd0-bbf4-884fc840e23b (last access: 27.06.2011), 2011.

Sarmiento, J. L., Gloor, M., Gruber, N., Beaulieu, C., Jacobson, A. R., Mikaloff Fletcher, S. E., Pacala, S., and Rodgers, K.: *Trends and regional distributions of land and ocean carbon sinks*, Biogeosciences, 7(8), 2351-2367, 10.5194/bg-7-2351-2010, 2010.

Sarrat, C., Noilhan, J., Dolman, A. J., Gerbig, C., Ahmadov, R., et al.: *Atmospheric CO2 modeling at the regional scale: an intercomparison of 5 meso-scale atmospheric models*, Biogeosciences, 4(6), 1115-1126, 2007.

Sasakawa, M., Shimoyama, K., Machida, T., Tsuda, N., Suto, H., et al.: *Continuous measurements of methane from a tower network over Siberia*, Tellus B, doi:10.1111/j.1600-0889.2010.00494.x, 2010.

Sayer, E. J., Heard, M. S., Grant, H. K., Marthews, T. R., and Tanner, E. V. J.: *Soil carbon release enhanced by increased tropical forest litterfall*, Nature Clim. Change, 1(6), 304-307, doi:10.1038/nclimate1190, 2011.

Schaefer, K., Zhang, T., Bruhwiler, L., and Barrett, A. P.: *Amount and timing of permafrost carbon release in response to climate warming*, Tellus B, 63(2), 165-180, doi:10.1111/j.1600-0889.2011.00527.x, 2011.

Schimel, D. S., House, J. I., Hibbard, K. A., Bousquet, P., Ciais, P., et al.: *Recent patterns and mechanisms of carbon exchange by terrestrial ecosystems*, Nature, 414(6860), 169-172, doi:10.1038/35102500, 2001.

Schuh, A. E., Denning, A. S., Corbin, K. D., Baker, I. T., Uliasz, M., Parazoo, N., Andrews, A. E., and Worthy, D. E. J.: *A regional high-resolution carbon flux inversion of North America for 2004*, Biogeosciences, 7(5), 1625-1644, doi:10.5194/bg-7-1625-2010, 2010.

Schulze, E. D., Lloyd, J., Kelliher, F. M., Wirth, C., Rebmann, C., et al.: *Productivity of forests in the Eurosiberian boreal region and their potential to act as a carbon sink - a synthesis*, Global Change Biology, 5(6), 703-722, doi:10.1046/j.1365-2486.1999.00266.x 1999.

G   References

Schulze, E. D., Wirth, C., and Heimann, M.: *Climate change - managing forests after Kyoto*, Science, 289(5487), 2058-2059, 2000.

Schulze, E. D., Vygodskaya, N. N., Tchebakova, N. M., Czimczik, C. I., Kozlov, D. N., et al.: *The Eurosiberian Transect: an introduction to the experimental region*, Tellus B, 54(5), 421-428, doi:10.1034/j.1600-0889.2002.01342.x, 2002.

Schulze, E. D., Vaganov, E. A., Gloor, M., Verkhovets, S. V., Manning, A. C., et al.: *A tall tower station for monitoring atmospheric greenhouse-gas concentrations in Central Siberia*, Eos Trans. AGU (in preparation), 2011.

Schuur, E. A. G., Bockheim, J., Canadell, J. G., Euskirchen, E., Field, C. B., et al.: *Vulnerability of Permafrost Carbon to Climate Change: Implications for the Global Carbon Cycle*, BioScience, 58(8), 701-714, doi:10.1641/B580807, 2008.

Serreze, M., Kahl, J., and Schnell, R.: *Low-level temperature inversions of the Eurasian Arctic and comparisons with Soviet drifting station data*, Journal of Climate, 5(6), 615-629, doi:10.1175/1520-0442(1992)005<0615:LLTIOT>2.0.CO;2, 1992.

Shibistova, O., Lloyd, J. O. N., Evgrafova, S., Savushkina, N., Zrazhevskaya, G., Arneth, A., Knohl, A., Kolle, O., and Schulze, E. D.: *Seasonal and spatial variability in soil CO_2 efflux rates for a central Siberian Pinus sylvestris forest*, Tellus B, 54(5), 552-567, doi:10.1034/j.1600-0889.2002.01348.x, 2002.

Shvidenko, A. Z., Schepashchenko, D. G., Vaganov, E. A., and Nilsson, S.: *Net primary production of forest ecosystems of Russia: A new estimate*, Doklady Earth Sciences, 421(2), 1009-1012, Doi 10.1134/S1028334x08060330, 2008.

Sisterson, D. L., and Frenzen, P.: *Nocturnal boundary-layer wind maxima and the problem of wind power assessment*, Environmental Science & Technology, 12(2), 218-221, 10.1021/es60138a014, 1978.

Smith, N. V., Saatchi, S. S., and Randerson, J. T.: *Trends in high northern latitude soil freeze and thaw cycles from 1988 to 2002*, J. Geophys. Res., 109(D12), D12101, 10.1029/2003jd004472, 2004.

Sogachev, A., Menzhulin, G. V., Heimann, M., and Lloyd, J. O. N.: *A simple three-dimensional canopy - planetary boundary layer simulation model for scalar concentrations and fluxes*, Tellus B, 54(5), 784-819, doi:10.1034/j.1600-0889.2002.201353.x, 2002.

Stephens, B. B., Gurney, K. R., Tans, P. P., Sweeney, C., Peters, W., et al.: *Weak Northern and Strong Tropical Land Carbon Uptake from Vertical Profiles of Atmospheric CO_2*, Science, 316, 1732-1735, doi:10.1126/science.1137004, 2007.

Stull, R. B.: *An Introduction to Boundary Layer Meteorology*, Kluwer Academic Punlishers, Dordrecht, 1988.

Sturm, P., Leuenberger, M., Sirignano, C., Neubert, R. E. M., Meijer, H. A. J., Langenfelds, R. L., Brand, W. A., and Tohjima, Y.: *Permeation of atmospheric gases through polymer O-rings used in flasks for air sampling*, Journal of Geophysical Research, 109(D04309), doi:10.1029/2003JD004073, 2004.

Styles, J. M., Lloyd, J. O. N., Zolotukhin, D., Lawton, K. A., Tchebakova, N., et al.: *Estimates of regional surface carbon dioxide exchange and carbon and oxygen isotope discrimination during photosynthesis from concentration profiles in the atmospheric boundary layer*, Tellus B, 54(5), 768-783, doi:10.1034/j.1600-0889.2002.01336.x, 2002.

Tans, P. P., Fung, I. Y., and Takahashi, T.: *Observational Constraints on the Global Atmospheric CO_2 Budget*, Science, 247(4949), 1431-1438, doi:10.1126/science.247.4949.1431, 1990.

Tarantola, A.: *Inverse Problem Theory and Methods for Model Parameter Estimation*, Society for Industrial and Applied Mathematics, Philadelphia, 2005.

Tarasova, O., Houweling, S., Elansky, N., and Brenninkmeijer, C.: *Application of stable isotope analysis for improved understanding of the methane budget: comparison of TROICA measurements with TM3 model simulations*, Journal of Atmospheric Chemistry, 63(1), 49-71, 10.1007/s10874-010-9157-y, 2009.

Tarnocai, C., Canadell, J. G., Schuur, E. A. G., Kuhry, P., Mazhitova, G., and Zimov, S.: *Soil organic carbon pools in the northern circumpolar permafrost region*, Global Biogeochem. Cycles, 23, GB2023, doi:10.1029/2008gb003327, 2009.

Tchebakova, N. M., Parfenova, E., and Soja, A. J.: *The effects of climate, permafrost and fire on vegetation change in Siberia in a changing climate*, Environmental Research Letters, 4(4), 045013, doi:10.1088/1748-9326/4/4/045013, 2009.

Thompson, R. L., Manning, A. C., Gloor, E., Schultz, U., Seifert, T., Hänsel, F., Jordan, A., and Heimann, M.: *In-situ measurements of oxygen, carbon monoxide and greenhouse gases from Ochsenkopf tall tower in Germany*, Atmos. Meas. Tech., 2(2), 573-591, doi:10.5194/amt-2-573-2009, 2009.

G References

Tohjima, Y., Maksyutov, S., Machida, T., and Inoue, G.: *Airborne measurements of atmospheric methane over oil fields in western Siberia*, Geophys. Res. Lett., 23(13), 1621-1624, 10.1029/96gl01027, 1996.

Tohjima, Y., Katsumata, K., Morino, I., Mukai, H., Machida, T., Akama, I., Amari, T., and Tsunogai, U.: *Theoretical and experimental evaluation of the isotope effect of NDIR analyzer on atmospheric CO2 measurement*, Journal of Geophysical Research-Atmospheres, 114, D13302, doi:10.1029/2009JD011734, 2009.

Trusilova, K., and Churkina, G.: *The terrestrial ecosystem model GBIOME-BGCv1*, Technical Report Vol. 14, ISSN 1615-7400, Max-Planck-Institut für Biogeochemie, Jena, 2008.

Trusilova, K., Rödenbeck, C., Gerbig, C., and Heimann, M.: *Technical Note: A new coupled system for global-to-regional downscaling of CO2 concentration estimation*, Atmospheric Chemistry and Physics, 10(7), 3205-3213, 2010.

UNEP-WCMC: *Carbon and biodiversity: a demonstration atlas*, edited by: Kapos, V., Ravilious, C., Campbell, A., Dickson, B., Gibbs, H., Hansen, M., Lysenko, I., Miles, L., Price, J., Scharlemann, J. P. W., and Trumper, K., UNEP-WCMC, Cambridge, UK, 2008.

Valentini, R., Dore, S., Marchi, G., Mollicone, D., Panfyorov, M., Rebmann, C., Kolle, O., and Schulze, E. D.: *Carbon and water exchanges of two contrasting central Siberia landscape types: regenerating forest and bog*, Functional Ecology, 14(1), 87-96, doi:10.1046/j.1365-2435.2000.00396.x, 2000.

Van de Wiel, B. J. H., Moene, A. F., Steeneveld, G. J., Baas, P., Bosveld, F. C., and Holtslag, A. A. M.: *A Conceptual View on Inertial Oscillations and Nocturnal Low-Level Jets*, Journal of the Atmospheric Sciences, 67(8), 2679-2689, doi:10.1175/2010JAS3289.1, 2010.

van der Molen, M. K., and Dolman, A. J.: *Regional carbon fluxes and the effect of topography on the variability of atmospheric CO2*, Journal of Geophysical Research, 112, D01104, 2007.

van der Werf, G. R., Randerson, J. T., Giglio, L., Collatz, G. J., Mu, M., et al.: *Global fire emissions and the contribution of deforestation, savanna, forest, agricultural, and peat fires (1997-2009)*, Atmospheric Chemistry and Physics, 10(23), 11707-11735, doi:10.5194/acp-10-11707-2010, 2010.

Vasileva, A. V., Moiseenko, K. B., Mayer, J. C., Juergens, N., Panov, A., Heimann, M., and Andeae, M. O.: *Assessment of the regional atmospheric impact of wildfire emissions based on CO observations at the ZOTTO tall tower station in Central Siberia*, J. Geophys. Res., 116(D07301), doi:10.1029/2010JD014571, 2011.

Verma, S.: *Micrometeorological Methods for Measuring Surface Fluxes of Mass and Energy*, Remote Sensing Reviews, 5(1), 99-115, 1990.

Vermeulen, A. T.: *CHIOTTO Final Report*, ECN energy research Centre of the Netherlands, 2007.

Vermeulen, A. T., Hensen, A., Popa, M. E., van den Bulk, W. C. M., and Jongejan, P. A. C.: *Greenhouse gas observations from Cabauw Tall Tower (1992-2010)*, Atmospheric Measurement Techniques, 4(3), 617-644, doi:10.5194/amt-4-617-2011, 2011.

Vivchar, A. V., Moiseenko, K. B., Shumskii, R. A., and Skorokhod, A. I.: *Identifying anthropogenic sources of nitrogen oxide emissions from calculations of Lagrangian trajectories and the observational data from a tall tower in Siberia during the spring-summer period of 2007*, Izvestiya Atmospheric and Oceanic Physics, 45(3), 302-313, doi:10.1134/S0001433809030049, 2009.

Walter, B. P., Heimann, M., and Matthews, E.: *Modeling modern methane emissions from natural wetlands 1. Model description and results*, Journal of Geophysical Research, 106(D24), 34189-34206, 2001.

Wang, W. G., Davis, K. J., Cook, B. D., Yi, C. X., Butler, M. P., Ricciuto, D. M., and Bakwin, P. S.: *Estimating daytime CO2 fluxes over a mixed forest from tall tower mixing ratio measurements*, Journal of Geophysical Research-Atmospheres, 112, D10308, doi:10.1029/2006JD007770, 2007.

Wania, R.: *Modelling northern peatland land surface processes, vegetation dynamics and methane emissions*, PhD thesis, Department of Earth Sciences, University of Bristol, Bristol, 140 pp., 2007.

Werner, C., Davis, K., Bakwin, P. S., Yi, C., Hurst, D. F., and Lock, L.: *Regional-scale measurements of CH4 exchange from a tall tower over a mixed temperate/boreal lowland and wetland forest*, Global Change Biology, 9, 1251-1261, 2003.

Winderlich, J.: *Entwicklung und Test eines Probenahme- und Kalibriersystems für einen kontinuierlich messenden Hochpräzisions-CO2-Analysator zum Einsatz in kommerziellen Flugzeugen (engl: Development and Test of a Sample Conditioning and Calibration System for a High Accuracy Continuous CO2 Analyzer for Deployment in Commercial Aircrafts)*, Diploma thesis, Physikalisch-Astronomische Fakultaet, Friedrich Schiller University, Jena, 84 pp., 2007.

G References

Winderlich, J., Chen, H., Gerbig, C., Seifert, T., Kolle, O., Lavrič, J. V., Kaiser, C., Höfer, A., and Heimann, M.: *Continuous low-maintenance CO2/CH4/H2O measurements at the Zotino Tall Tower Observatory (ZOTTO) in Central Siberia*, Atmos. Meas. Tech., 3(4), 1113-1128, doi:10.5194/amt-3-1113-2010, 2010.

Winderlich, J., Gerbig, C., Kolle, O., and Heimann, M.: *Local flux estimates using CO2 and CH4 concentration profiles from Zotino Tall Tower Observatory (ZOTTO)*, Environmental Research Letters, NEESPI special issue(submitted), 2011.

Yi, C., Davis, K. J., Bakwin, P. S., Berger, B. W., and Marr, L. C.: *Influence of advection on measurements of the net ecosystem-atmosphere exchange of CO2 from a very tall tower*, J. Geophys. Res., 105(D8), 9991-9999, doi:10.1029/2000jd900080, 2000.

Zhao, C. L., and Tans, P. P.: *Estimating uncertainty of the WMO mole fraction scale for carbon dioxide in air*, Journal of Geophysical Research, 111(D08S09), doi:10.1029/2005JD006003, 2006.

G   References